)OT/FAA/SE-91/4
)OT-VNTSC-FAA-91-13

IAS System
:ngineering Service
Vashington, DC 20591

Multisensor Signal Processing Techniques

(Hybrid GPS/LORAN-C with RAIM)

Dr. Frank van Graas
Mark R. Kuhl

Ohio University
Athens, OH 45701

Final Report
September 1991

U.S. Department of Transportation
Federal Aviation Administration

Technical Report Documentation Page

1. Report No.	2. Government Accession No.	3. Recipient's Catalog No.
DOT/FAA/SE-91/4		

4. Title and Subtitle	5. Report Date
Multisensor Signal Processing Techniques (Hybrid GPS/LORAN-C with RAIM)	September 1991
	6. Performing Organization Code DTS-52
7. Author(s) Dr. Frank van Grass, Mark R. Kuhl*	8. Performing Organization Report No. DOT-VNTSC-FAA-91-13
9. Performing Organization Name and Address Avionics Engineering Center Ohio University Athens, OH 45701	10. Work Unit No. (TRAIS) FA160/A1074
	11. Contract or Grant No. DTRS-57-87-C-000006
12. Sponsoring Agency Name and Address U.S. Department of Transportation Federal Aviation Administration NAS System Engineering Service Washington, DC 20591	13. Type of Report and Period Covered Final Report August 1989 - October 1990
	14. Sponsoring Agency Code ASE-300

15. Supplementary Notes
*Under Contract to: U.S. Department of Transportation
Research and Special Programs Administration
John A. Volpe National Transportation Systems Center
Cambridge, MA 02142

16. Abstract

One of the major elements in alleviating existing problems in en route airspace is to allow more aircraft to traverse a given volume of airspace. Recent developments in navigation systems will support this effort by enabling user preferred routes and by offering more precise and reliable navigational capabilities.

Multisenor navigation system architectures are presented with the emphasis on signal processing techniques and receiver autonomous integrity monitoring (RAIM). This is followed by a detailed study of a hybrid navigation receiver based on the NAVSTAR Global Positioning System (GPS) and the Long Range Navigation System LORAN-C. The design, implementation and flight testing of a prototype hybrid GPS/LORAN receiver are presented, including the realtime simulation and detection of navigation signal malfunctions.

17. Key Words	18. Distribution Statement
Radionavigation System, Radio Determination System, Position Location, Global Positioning System, Long Range Navigation, Fault Detection	DOCUMENT IS AVAILABLE TO THE PUBLIC THROUGH THE NATIONAL TECHNICAL INFORMATION SERVICE, SPRINGFIELD, VIRGINIA 22161

19. Security Classif. (of this report)	20. Security Classif. (of this page)	21. No. of Pages	22. Price
UNCLASSIFIED	UNCLASSIFIED	96	

Form DOT F 1700.7 (8-72) Reproduction of completed page authorized

PREFACE

The work desscribed in this final report was performed in support of the Federal Aviation Administration. Jerry W. Bradley (ASE-300) is the sponsor's program manager.

This report is a deliverable under Task 2 of PPA No. FA-160. The work was performed by Assistant Professor Frank van Graas of Ohio University, Athens, Ohio. The PPA manager is M. J. Moroney (RSPA/VNTSC/DTS-52).

One of the major elements in alleviating existing problems in en route airspace is to allow more aircraft to traverse a given volume of airspace. Recent developments in navigation systems will support this effort by enabling user preferred routes and by offering more precise and reliable navigational capabilities. One develpment of specific interest is the integration of GPS and LORAN-C to acheive a sole means of navigation. This report addresses the capabilities offered by multisensor navigation systems in general with emphasis on signal processing techniques and receiver autonomous integrity monitoring (RAIM). In addition this report details the design, implementation, and flight testing of a protype hybrid GPS/LORAN navigation system.

A-1

METRIC / ENGLISH CONVERSION FACTORS

ENGLISH TO METRIC

LENGTH (APPROXIMATE)

1 inch (in) = 2.5 centimeters (cm)
1 foot (ft) = 30 centimeters (cm)
1 yard (yd) = 0.9 meter (m)
1 mile (mi) = 1.6 kilometers (km)

AREA (APPROXIMATE)

1 square inch (sq in, in^2) = 6.5 square centimeters (cm^2)
1 square foot (sq ft, ft^2) = 0.09 square meter (m^2)
1 square yard (sq yd, yd^2) = 0.8 square meter (m^2)
1 square mile (sq mi, mi^2) = 2.6 square kilometers (km^2)
1 acre = 0.4 hectares (he) = 4,000 square meters (m^2)

MASS - WEIGHT (APPROXIMATE)

1 ounce (oz) = 28 grams (gr)
1 pound (lb) = .45 kilogram (kg)
1 short ton = 2,000 pounds (lb) = 0.9 tonne (t)

VOLUME (APPROXIMATE)

1 teaspoon (tsp) = 5 milliliters (ml)
1 tablespoon (tbsp) = 15 milliliters (ml)
1 fluid ounce (fl oz) = 30 milliliters (ml)
1 cup (c) = 0.24 liter (l)
1 pint (pt) = 0.47 liter (l)
1 quart (qt) = 0.96 liter (l)
1 gallon (gal) = 3.8 liters (l)
1 cubic foot (cu ft, ft^3) = 0.03 cubic meter (m^3)
1 cubic yard (cu yd, yd^3) = 0.76 cubic meter (m^3)

TEMPERATURE (EXACT)

$[(x - 32)(5/9)]\ ^\circ F = y\ ^\circ C$

METRIC TO ENGLISH

LENGTH (APPROXIMATE)

1 millimeter (mm) = 0.04 inch (in)
1 centimeter (cm) = 0.4 inch (in)
1 meter (m) = 3.3 feet (ft)
1 meter (m) = 1.1 yards (yd)
1 kilometer (km) = 0.6 mile (mi)

AREA (APPROXIMATE)

1 square centimeter (cm^2) = 0.16 square inch (sq in, in^2)
1 square meter (m^2) = 1.2 square yards (sq yd, yd^2)
1 square kilometer (km^2) = 0.4 square mile (sq mi, mi^2)
1 hectare (he) = 10,000 square meters (m^2) = 2.5 acres

MASS - WEIGHT (APPROXIMATE)

1 gram (gr) = 0.036 ounce (oz)
1 kilogram (kg) = 2.2 pounds (lb)
1 tonne (t) = 1,000 kilograms (kg) = 1.1 short tons

VOLUME (APPROXIMATE)

1 milliliter (ml) = 0.03 fluid ounce (fl oz)
1 liter (l) = 2.1 pints (pt)
1 liter (l) = 1.06 quarts (qt)
1 liter (l) = 0.26 gallon (gal)
1 cubic meter (m^3) = 36 cubic feet (cu ft, ft^3)
1 cubic meter (m^3) = 1.3 cubic yards (cu yd, yd^3)

TEMPERATURE (EXACT)

$[(9/5)y + 32]\ ^\circ C = x\ ^\circ F$

QUICK INCH-CENTIMETER LENGTH CONVERSION

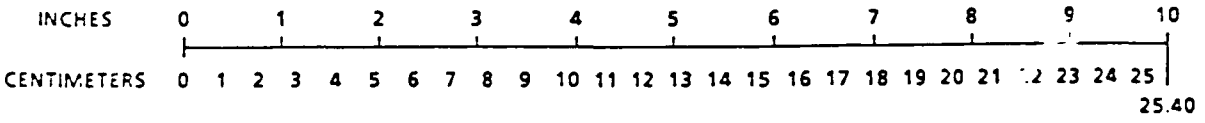

QUICK FAHRENHEIT-CELCIUS TEMPERATURE CONVERSION

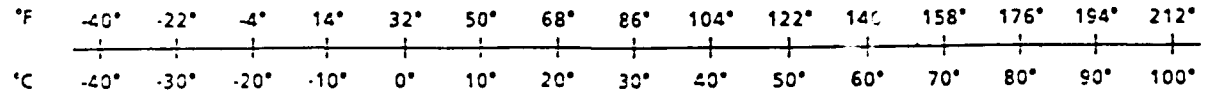

For more exact and/or other conversion factors, see NBS Miscellaneous Publication 286, Units of Weights and Measures. Price $2.50. SD Catalog No. C13 10 286.

TABLE OF CONTENTS

List of Figures

List of Tables

EXECUTIVE

The work described in this final report was performed in support of the Federal Aviation Administration. Jerry W. Bradley (ASE-300) is the sponsor's program manager.

This report is a deliverable under Task 2 of PPA No. FA-160. Assistant Professor Frank van Graas and Mr. Mark Kuhl of Ohio University, Athens, Ohio performed the work and are the authors of this report. The PPA manager is M. J. Moroney (RSPA/VNTSC/DTS-52).

One of the major elements in alleviating existing problems in en route airspace is to allow more aircraft to traverse a given volume of airspace. Recent developments in navigation systems will support this effort by enabling user preferred routes and by offering more precise and reliable navigational capabilities. One development of specific interest is the integration of GPS and LORAN-C to achieve a sole means of navigation. This report addresses the capabilities offered by multisensor navigation systems in general with emphasis on signal processing techniques and receiver autonomous integrity monitoring (RAIM). In addition this report details the design, implementation, and flight testing of a protype hybrid GPS/LORAN navigation system.

The first part of this report shows the derivation of the ordinary least squares (OLS) estimator from the linear model using the Projection Theorem. The performance of the OLS is subjected to a detailed error analysis which includes the effects of geometry and measurement errors, both bias and noise. Using similar procedures, the extended Ridge and Kalman filters are derived which are representative for the classes of biased and unbiased estimators, respectively. It is shown that in the presence of measurement bias errors, both estimators converge to the OLS inflation of the position error. It is therefore concluded that in the case of dominant measurement bias errors (e.g. GPS or LORAN), the integrity monitoring performance offered by the OLS estimator cannot be improved upon. It was also found that the Ridge estimator can be used to explain/optimize the performance of a mismatched Kalman filter. This provides a very helpful insight into the performance of the Kalman filter in the presence of unmodeled dynamics.

Based on the conclusion that the OLS estimator is sufficient to perform integrity monitoring, a general solution methodology is presented for a multisensor navigation system. The range residual integrity parameter was derived, again using the Projection Theorem.

The above results have been applied to a realtime prototype hybrid GPS/LORAN receiver. Two flight tests revealed that the hybrid GPS/LORAN receiver performs in accordance with its design. The course deviation indicator is responsive and the indicated course compares favorably with other area navigation equipment. Out of a total of fifteen simulated signal malfunctions, twelve malfunctions which would have caused unacceptable course deviations were detected by the range residual integrity algorithm.

Equal weighting of GPS and LORAN measurements is used for the flight

tests. Therefore, the accuracy of the hybrid system will be mostly determined by the LORAN measurements. Standard LORAN propagation models are used such that the achieved accuracies are representative for current LORAN receivers. Because of this, the accuracy of the hybrid system will not be as good as that provided by GPS; however, the availability and integrity of the hybrid system exceeds that of GPS by several orders of magnitude [4]. At the same time, the hybrid system accuracies were still found to be well within all current requirements as listed in Chapter 3. It is also concluded that the accuracy of hybrid GPS/LORAN can be improved upon significantly through LORAN calibration or by using a weighting matrix in the hybrid solution, see Section 6.1.

In summary, hybrid GPS/LORAN is a successful case study of fully hybrid, multisensor navigation. Similar performance characteristics may be anticipated for other multisensor systems based on sensors such as GPS, LORAN, GLONASS, Omega, and baro-altimeter.

1. INTRODUCTION

One of the major elements in alleviating existing problems in en route airspace is to allow more aircraft to traverse a given volume of airspace [1]. Recent developments in navigation systems will support this effort by enabling user preferred routes and by offering more precise and reliable navigational capabilities. Included in these developments are new satellite technologies such as the NAVSTAR Global Positioning System (GPS) and improvements of existing systems such as LORAN-C. One development of specific interest is the integration of GPS and LORAN-C to achieve a sole means of navigation. Hybrid GPS/LORAN is setting the stage for a next-generation of multisensor navigation systems which is anticipated to have a major impact on the safety, reliability, and efficiency of national and international transportation. A highly reliable multisensor navigation system will increase low-altitude, remote and offshore operations. Additionally, a multisensor navigation system could serve as the position sensor for automatic dependent surveillance (ADS) and Communication, Navigation, and Surveillance (CNS) services, thereby increasing the safety and operational efficiency of the Air Traffic Control (ATC) System.

The first part of this report, Chapters 2 through 6, addresses multisensor navigation systems in general, with emphasis on signal processing techniques and receiver autonomous integrity monitoring (RAIM). RAIM is recommended to be used as the integrity technique for a multisensor navigation system. The second part of this report, Chapters 7 through 10, details the design, implementation, and flight testing of a prototype hybrid GPS/LORAN navigation system. Chapters 11 and 12 contain conclusions and recommendations for future efforts, respectively.

2. PRINCIPLES OF POSITION FIXING

2.1 Path Delay Systems

Two basic methods exist for a vehicle to determine its position: dead reckoning and position fixing. Position determination using a dead reckoning method involves projecting a known position forward to some future time by keeping continuous track of velocity, accelerations, or both. Examples are Doppler and Inertial Reference Systems. A position fix method involves a vehicle sensing landmarks and determining an instantaneous position without reference to any former position. Landmarks are at known locations on or around the earth. Examples of landmarks are the Very High Frequency Omnidirectional Range (VOR) stations, the Global Positioning System (GPS) satellites, and stars (celestial fixes).

A vehicle can obtain range (ρ) or bearing (θ) information from the landmarks by measuring parameters such as phase delay and pulse time of arrival (TOA) delay. These make up what are called path delay systems (see Kelly and Cusick [2]). Extending the classifications presented by Kelly and Cusick, path delay systems may be of four different types: single path, multiple paths in three dimensions, multiple paths in four dimensions, and combinations. The four different types of path delay systems are shown in Figure 2.1.

Single path systems may be classified as either active or passive. An active single path system requires only one landmark to determine a range. The user in an active single path system transmits a signal to the landmark and listens for a reply. The range is then determined by multiplying half the round trip delay time by the speed of transmission of the signal. To measure the round trip delay time, the user clock needs only to be stable during the measurement time. A crystal oscillator is a sufficient frequency reference source for an active single path measurement. Examples of active single path systems include the Distance Measuring Equipment (DME) system and radio detecting and ranging (RADAR) systems. A receiver in a passive single path system measures path delay times (or ranges) with respect to known transmissions from landmarks. This method requires that the user clock be synchronized with the transmitter. Furthermore, both the user clock and the transmitter clock must be stable throughout the mission time. As an example, if one of the frequency reference sources drifts one part in 10^{11} (Rubidium standard), then after 1000 seconds the clock would have drifted 10 nanoseconds, which corresponds to a drift in the range measurement of approximately 10 feet. Passive single path systems are currently not used for vehicle navigation.

Three-dimensional multiple path systems measure differences in reception time (or compare the path delays) between at least two landmarks and the receiver, or use multiple range measurements. These systems may be classified as true hyperbolic, radial or spherical. True hyperbolic systems determine when time or frequency differences in the path delays are constant. This yields a hyperbolic line of position (LOP). When the time or frequency difference in the path delays are zero, a straight LOP will result. This is called a radial system. Examples of hyperbolic systems are LORAN-C and Omega, while an example of a radial system is VOR. An example of an active spherical system is multiple DME. Spherical systems reduce to a circular system if the altitude of the vehicle is known. An example of a passive two-path system is the two-station French LORAN-C chain [3].

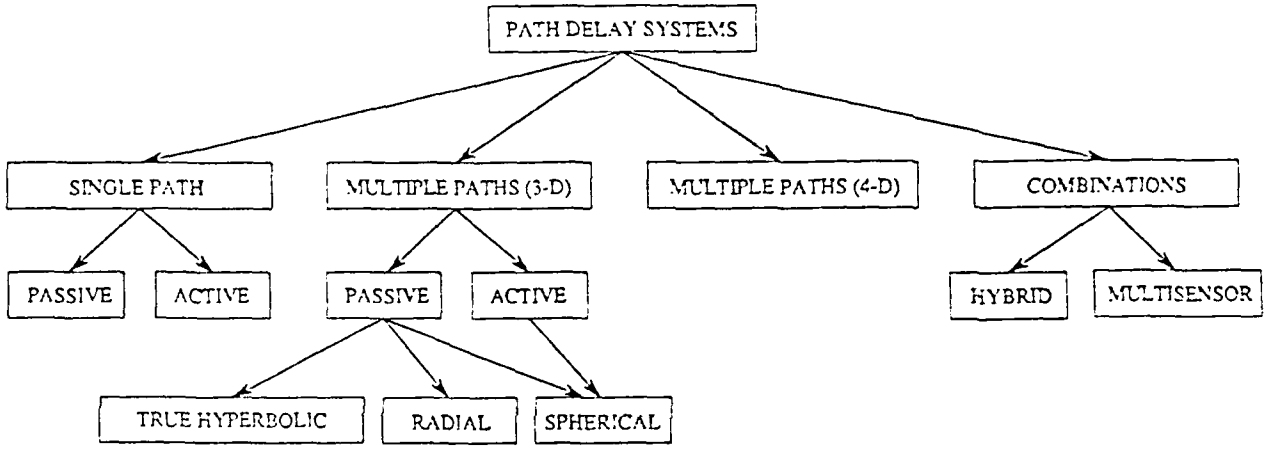

Figure 2.1 Types of path delay systems used for navigation (extended from the classifications presented in reference [2]).

Four-dimensional multiple path systems are similar to spherical systems without synchronized clocks. The passive measurements to the landmarks are called "pseudoranges" (or "pseudofrequencies") because the measurements contain an unknown clock phase (or frequency) offset. Therefore, the user must solve for its clock phase or frequency offset with respect to the landmarks. The unknown receiver clock phase or frequency adds another dimension to be solved for in the position solution. Examples of four-dimensional multiple path systems are the Global Positioning System (GPS) and the Global Navigation Satellite System (GLONASS). These two worldwide satellite systems are sponsored by the United States and the Soviet Union, respectively.

In order to improve accuracy, availability, reliability and integrity, the above path delay systems may be combined [4]. With the focus on aircraft positioning, combinations of the various path delay systems can be implemented in two ways:

(1) Multi-Sensor System
(2) Hybrid System

A multi-sensor system incorporates navigation data from landmarks which are selected by the system operator or by some type of automatic selection scheme. As specified in Federal Aviation Administration (FAA) Advisory Circular 20-130 [5], a multi-sensor system may be approved for instrument flight rules (IFR) enroute and terminal navigation within the conterminous United States (CONUS). But for instrument approaches, only navigation data from landmarks which are already individually approved for charted instrument approaches may be selected. Moreover, a sole means of navigation must be installed and operable at the same time [6].

A hybrid system uses navigation data from all landmarks that are available for all phases of flight (enroute, terminal and approach). For a hybrid system, no selection process is exercised. An example of a hybrid system may be GPS/LORAN-C. Alone, GPS and LORAN-C will not meet sole means requirements for navigation [7]. But by combining these two systems into a hybrid system, sole means requirements could be satisfied [8]. A "multisensor" hybrid system - or simply called a multisensor system - arises from the fact that many systems may be combined for navigation, i.e. a hybrid system consisting of GPS, GLONASS, DME, VOR, Omega and LORAN-C. Currently, navigation requirements have not been defined for hybrid systems, see Chapter 3.

2.2 Classification of Position Fix Methods

The way a vehicle determines a position fix from the information provided by the landmarks may be classified into several different methods:

(1) Triangulation Method
(2) Trilateration Method
(3) Polar Method
(4) Hyperbolic Method
(5) Combinations of Methods

These methods are discussed below for a two-dimensional (2-D) position fix.

(1) Triangulation Method (θ-θ)

Bearing information from two different landmarks may be used to obtain a position fix. This method is called triangulation and is depicted in Figure 2.2. The method proceeds as follows: Each of the two stations provides the vehicle with a certain bearing angle from true or magnetic North with respect to the station. These bearing angles will cross at only one location, giving a unique position fix. VOR stations are an example of a navigation system that transmits bearing information to the vehicle.

(2) Trilateration Method (ρ-ρ)

Range information from two different landmarks may be used to obtain a position fix. This method is called trilateration and is portrayed in Figure 2.2. The method proceeds as follows: A particular range is provided by each of the two stations. Each range defines a circle of positions on which a vehicle may be located. The two circles will cross at two locations - one being the correct vehicle position and the other being an ambiguous solution. The ambiguous solution may be eliminated by using prior information, additional information such as speed or heading, or a third station. DME stations are an example of a navigation system that provides range information to the vehicle. In three dimensions, the range from a DME station is called a slant range to take into account the altitude of the vehicle. Also, GPS and GLONASS are navigation systems from which a vehicle can determine a three-dimensional position fix based on ranges between the vehicle and four satellites in the system. (The fourth satellite is needed to resolve the receiver clock offset from the system clock.)

(3) Polar Method (ρ-θ)

Range and bearing information from a single landmark may also be used to acquire a position fix. This method is called the polar method and is shown in Figure 2.3. The method proceeds as follows: One station provides the vehicle with both a bearing angle and a range. As stated before, the range gives a circle of possible positions; and the bearing angle indicates where on that circle the vehicle is located. The VOR/DME stations and Tactical Air Navigation (TACAN) stations are examples of navigation systems that transmit both range and bearing information to the vehicle.

(4) Hyperbolic Method

Another method, called the hyperbolic method, uses lines of constant time difference (TD) between two pairs of landmarks to determine a position fix. The hyperbolic method is also depicted in Figure 2.3; and it requires three different landmarks (stations 1 and 2 make up one pair while stations 2 and 3 constitute the second pair). The method proceeds as follows: Station 1 transmits a signal which is received by the user at some later time. The same transmission is also received by station 2. Upon reception of the signal from station 1, station 2 transmits a signal. A constant difference between the time of arrivals of the signals from station 2 and station 1 define a hyperbolic LOP, on which the user is located. In the same way, a second pair of stations is used to determine another hyperbolic LOP. Where these two hyperbolic LOPs cross gives a position fix for the vehicle. LORAN-C and Omega are examples of navigation systems that employ time differencing for position fixing.

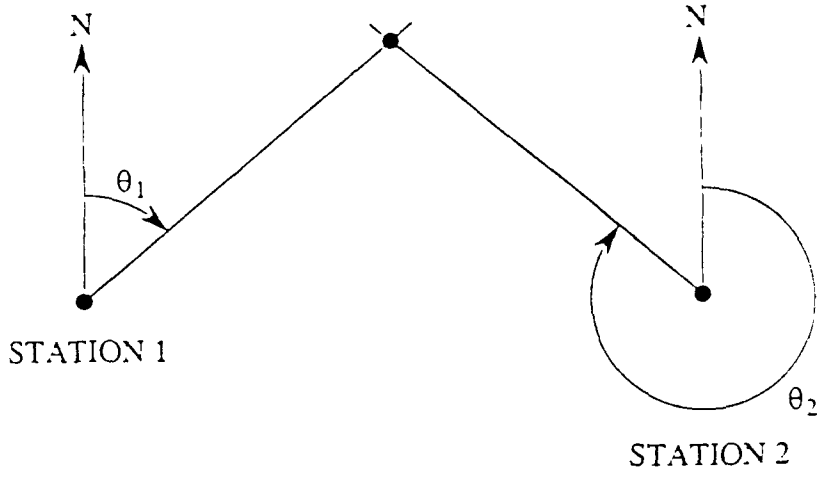

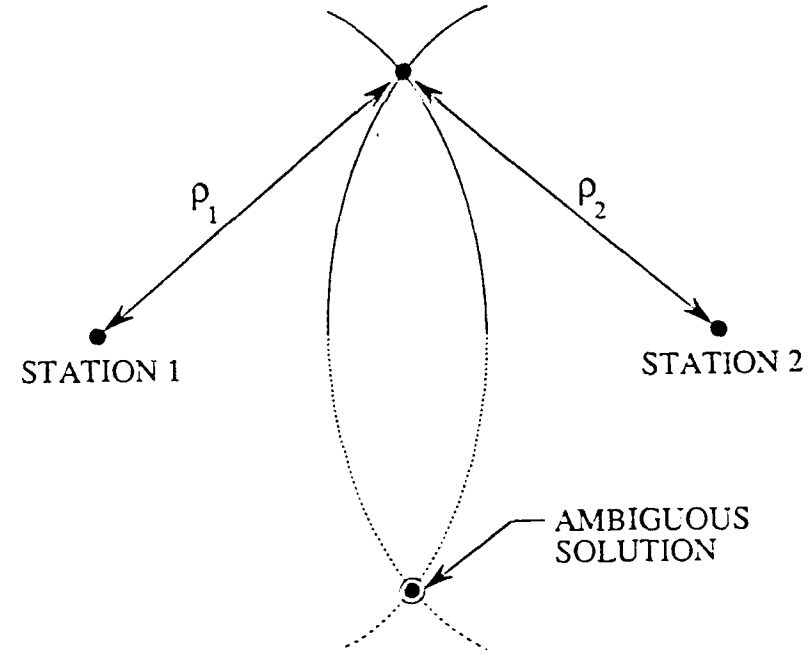

Figure 2.2 Triangulation and Trilateration position fix methods.

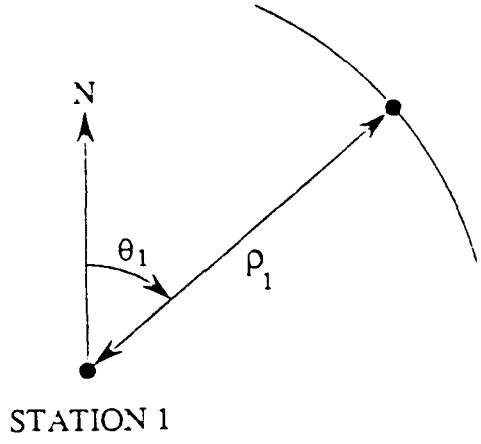

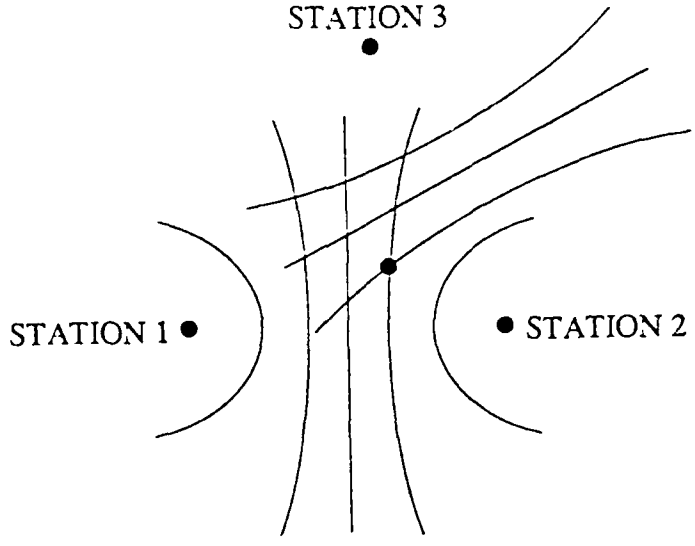

Figure 2.3 Polar and Hyperbolic position fix methods.

As a special note, LORAN-C may be used in the passive ranging mode as well as in the hyperbolic mode of operation.

(5) Combinations of Methods

The above methods may be combined in various ways to obtain a position fix. This gives rise to a multisensor navigation system: a vehicle may integrate information from all the available navigation systems to obtain an optimum position fix.

2.3 Position Fixing Accuracies of Current Path Delay Systems

Range and bearing measurements are subject to a variety of error sources, including measurement errors, noise sources (atmospheric and man-made), multipath, unmodeled ionospheric and tropospheric propagation delays, clock errors and landmark location uncertainty. (References [9] and [10] provide a detailed description of the error sources affecting the GPS in particular.)

Measurement errors propagate into position errors as a function of geometry and solution methods. Table 2.1 summarizes the accuracies of current U.S. radionavigation systems (compiled from the 1990 edition of the Federal Radionavigation Plan (FRP) [11]). These accuracies are 95% confidence level numbers, meaning that statistically at least 95% of the position estimates will be within the value listed. An exception to this accuracy level specification are the 2-D accuracies. The 2 drms (distance root mean square) numbers are used where 2-D accuracies are specified. As shown in reference [12], 2 drms numbers may have anywhere from a 95% to a 98% confidence level. (Two different accuracies are shown for the GPS in Table 2.1 because the GPS offers two navigation services: Precise Positioning Service (PPS) for military users and Standard Positioning Service (SPS) which anybody can use.) At this time, the accuracies for GLONASS are not clearly defined, although the system should have similar performance characteristics as the GPS.

Navigation System	Accuracy (95% confidence level)
VOR	± 1.4°
DME	185 meters
TACAN	± 1°, 185 meters
Radiobeacons	± 3 - 10°
Omega	3.7 - 7.4 kilometers
LORAN-C	460 meters
Transit	
single frequency	500 meters
dual frequency	25 meters
GPS	
SPS (civil)	100 meters (horizontal) 156 meters (vertical)
PPS (military)	17.8 meters (horizontal) 27.7 meters (vertical)

Table 2.1 Accuracies of current navigation systems as specified by the 1990 FRP [11].

3. REQUIREMENTS FOR AIRBORNE POSITION FIXING SYSTEMS

Two types of navigation systems must be considered when addressing the navigation requirements: 1. sole means of navigation systems, and 2. supplemental type navigation systems. The main difference between these two types of systems is that the sole means of navigation system must have some level of redundancy to allow for continued navigation in the presence of signal failures. Supplemental systems only have to announce the failure, upon which the pilot switches to a sole means of navigation. Therefore, differences in system requirements are mainly in the areas of integrity and availability.

Five major performance characteristics that must be satisfied are accuracy, availability, reliability, coverage and integrity (see reference [11, 13, 14] for additional requirements). Furthermore, the system must be compatible with the air traffic control system and the existing airspace structure, which is largely based on VOR/DME. Most of the requirements for sole means navigation are well understood and documented, except for availability and integrity requirements. The FAA is currently developing a regulation that will establish minimum standards under which a radionavigation system may be certified as the sole radionavigation system. The Advance Notice of Proposed rulemaking has been distributed [13].

The focus of this report is on the feasibility of receiver autonomous integrity monitoring schemes to supply the integrity information. In the case of a multisensor navigation system, many redundant measurements are available to determine the validity of the position solution.

For supplemental navigation, the performance requirements in the areas of accuracy and integrity are taken from reference [15], and are summarized in Table 3.1. The following notes are provided to explain some of the quantities in Table 3.1:

1. Detection probability is defined as a conditional probability; it is the probability of not detecting an out-of-tolerance condition given that an out-of-tolerance condition is present. The detection probability must be guaranteed at each space/time point. It is assumed that errors that are hard to detect are slowly growing bias errors (of order 2 m/s) and that these errors occur approximately once every two years for each satellite, which corresponds to a probability of occurrence of 10^{-6}. This then yields an overall detection probability of $1 - 10^{-9}$. Consequently, the alarm threshold would be exceeded with a probability of 10^{-9}. (The detection probability is on a per sample basis).

2. All accuracy specifications are on a 95% probability basis.

Phase of Flight / Performance	Enroute	Terminal	Nonprecision Approach
Position Fixing Radial Accuracy	0.124 nmi	0.124 nmi	0.124 nmi
Flight Technical Error (crosstrack)	1.00 nmi (2.00 oceanic)	1.00 nmi	0.50 nmi
Total Radial Accuracy	1.008 nmi (2.004 oceanic)	1.008 nmi	0.515 nmi
Radial Alarm Threshold	2.00 nmi	1.00 nmi	0.30 nmi
Maximum Allowable Alarm Rate	0.002/Hr	0.002/Hr	0.002/Hr
Time to Alarm	30 sec.	10 sec.	10 sec.
Minimum Detection Probability	.999	.999	.999

Table 3.1 Tentative accuracy and integrity requirements for supplemental GPS (from ref. [15]).

4. THEORY OF LINEAR REGRESSION

This section covers the general topic of estimating a vehicle position fix given range measurements with respect to landmarks. The ordinary least squares (OLS) estimator is presented; and it is shown that the OLS estimator results in an unbiased position solution. An error criterion, called the mean square error (MSE), is defined in order to analyze the performance of position estimators. Next, the effects of geometry on the position fix are addressed. Finally, a DME simulation is presented which provides insight into the performance of the OLS estimator under poor geometry conditions.

4.1 The General Linear Model

As stated in Section 2.1, all path delay systems provide either a range or bearing from which a vehicle can obtain a position fix. The position fix is an estimate because of errors in the measurement data. Since the data exhibit a significant degree of error or "noise", the strategy is to find a position fix that best represents the general trend of the data, which is accomplished through the use of regression theory [16].

For this section, assume that the measurement data consist of range measurements, which are related to a position fix by a nonlinear model. Since the relation is nonlinear, one must first linearize the relation by taking a Taylor series expansion around some given reference point (usually the initial estimate) [17], see Section 4.4.1. The general linear model is given by

$$\underline{Y} = H\underline{\beta} + \underline{\Delta B} + \underline{e} \tag{4.1}$$

where $\underline{Y}$ is the n x 1 data vector which consists of n range measurements, H is the known n x p design matrix which may include linearized terms which represent a nonlinear system and $\underline{\beta}$ is the p x 1 regressor vector to be estimated. For navigation, the elements of $\underline{\beta}$ may be position, velocity, acceleration and clock offset. ($\underline{\beta}$ is also known as the system state vector.) The $\underline{e}$ vector represents zero mean, uncorrelated, normally distributed noise on the range measurements, i.e. $\underline{e}$ - N(0,R) where R is the known covariance matrix of $\underline{e}$ and N signifies the normal distribution. The covariance matrix is determined as follows

$$R = E[\underline{e}\underline{e}^T] = \sigma^2 I \tag{4.2}$$

where E signifies the expected value, σ is the standard deviation of the measurement noise and I is the identity matrix (the off-diagonal elements of R are zero because the noise is uncorrelated). Bias errors, represented by the $\underline{\Delta B}$ vector, also exist on the range measurements. Bias errors are seen as constant and unknown to the estimator. In this section, the analysis of noise-only on the measurement data will be performed. Section 4.5 covers the case of both noise and bias errors. Without bias errors, the linear model is given by

$$\underline{Y} = H\underline{\beta} + \underline{e} \tag{4.3}$$

Many techniques have been developed to solve the above equation; the most straightforward being the ordinary least squares (OLS) estimator.

4.2 Ordinary Least Squares (OLS) Estimator

The OLS estimator is developed as follows. The residuals after estimating $\underline{\beta}$ in the linear model are given by

$$\underline{e}_R = \underline{Y} - H\hat{\underline{\beta}} = \underline{Y} - \hat{\underline{Y}} \tag{4.4}$$

where $\underline{e}_R$ is the residual vector, $\hat{\underline{\beta}}$ is an estimate of $\underline{\beta}$ and $\hat{\underline{Y}}$ is the estimated measurement vector. Using the Projection Theorem [18,19], project the measurements, $\underline{Y}$, from the measurement space onto the estimation space such that the distance between true $\underline{Y}$ and estimated $\hat{\underline{Y}}$ is a minimum. This is shown in Figure 4.1. Therefore, $\hat{\underline{Y}}$ is orthogonal to $\underline{e}_R$, or

$$\begin{aligned}
&\hat{\underline{Y}}^T\underline{e}_R = 0 \\
&(H\hat{\underline{\beta}})^T(\underline{Y} - H\hat{\underline{\beta}}) = 0 \\
&\hat{\underline{\beta}}^T H^T(\underline{Y} - H\hat{\underline{\beta}}) = 0 \\
&\hat{\underline{\beta}}^T(H^T\underline{Y} - H^T H\hat{\underline{\beta}}) = 0
\end{aligned} \tag{4.5}$$

The problem is to solve this equation for $\hat{\underline{\beta}}$. Since $\hat{\underline{\beta}}$ is usually not zero, the terms inside the parenthesis must be set to zero. This yields the OLS estimator

$$\begin{aligned}
&H^T\underline{Y} - H^T H\hat{\underline{\beta}} = 0 \\
&H^T\underline{Y} = H^T H\hat{\underline{\beta}} \qquad \rightarrow \text{called the "normal equation"} \\
&\hat{\underline{\beta}} = (H^T H)^{-1}H^T\underline{Y} = \hat{\underline{\beta}}_{OLS}
\end{aligned} \tag{4.6}$$

Substituting equation 4.3 into equation 4.6 gives

$$\begin{aligned}
&\hat{\underline{\beta}}_{OLS} = (H^T H)^{-1}H^T H\underline{\beta} + (H^T H)^{-1}H^T\underline{e} \\
&\hat{\underline{\beta}}_{OLS} = \underline{\beta} + (H^T H)^{-1}H^T\underline{e}
\end{aligned} \tag{4.7}$$

From equation 4.7 the expected value, or mean, of the OLS estimator is

$$\begin{aligned}
&E[\hat{\underline{\beta}}_{OLS}] = E[\underline{\beta} + (H^T H)^{-1}H^T\underline{e}] \\
&E[\hat{\underline{\beta}}_{OLS}] = \underline{\beta}
\end{aligned} \tag{4.8}$$

since the expected value of $\underline{e}$ is zero. Therefore, the OLS estimator is an unbiased estimator. The bias is zero, denoted by

$$BIAS[\hat{\underline{\beta}}_{OLS}] = 0 \tag{4.9}$$

The variance of the OLS estimator is

$$\begin{aligned}
&VAR[\hat{\underline{\beta}}_{OLS}] = E[\hat{\underline{\beta}}_{OLS}^2] - [E(\hat{\underline{\beta}}_{OLS})]^2 \\
&VAR[\hat{\underline{\beta}}_{OLS}] = \sigma^2 TRACE[(H^T H)^{-1}]
\end{aligned} \tag{4.10}$$

where σ is the standard deviation of the measurement noise and the TRACE operator is the sum of the diagonal elements of a matrix.

$$H = \begin{bmatrix} h_{11} & h_{12} \\ h_{21} & h_{22} \end{bmatrix} \quad \begin{matrix} H_1 & H_2 \\ \downarrow & \downarrow \end{matrix}$$

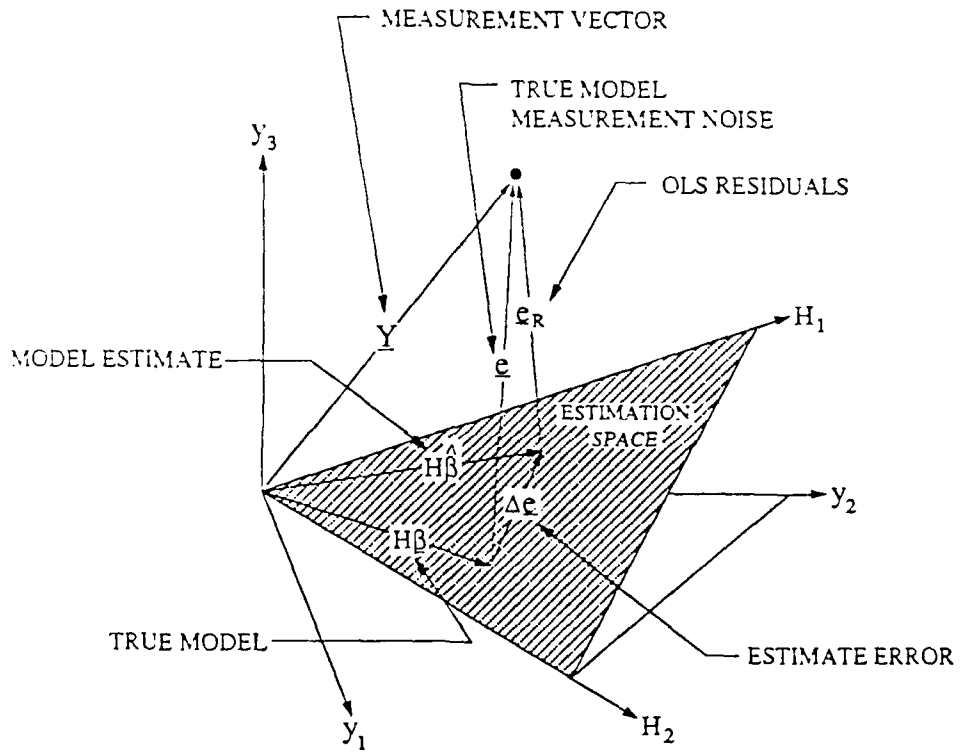

02X 029 / 005 E38

Figure 4.1 Measurement space and estimation space with Projection Theorem geometry (reference [19]).

4.3 Mean Square Error (MSE) Error Criterion

The OLS estimator minimizes the sum of the squares of the residuals, $SS(\underline{e}_R)$, which is given by

$$SS(\underline{e}_R) = (\underline{Y} - H\hat{\underline{\beta}})^T(\underline{Y} - H\hat{\underline{\beta}}) \tag{4.11}$$

where $\hat{\underline{\beta}} = \hat{\underline{\beta}}_{OLS}$ for minimum $SS(\underline{e}_R)$. However, for navigation purposes the appropriate error criterion is the mean square error (MSE). The MSE indicates how far off the estimated position is from the true position. It includes both bias errors in the solution as well as variance. For the OLS estimator, the MSE is given by

$$\begin{aligned} MSE[\hat{\underline{\beta}}_{OLS}] &= E[(\hat{\underline{\beta}}_{OLS} - \underline{\beta})^T(\hat{\underline{\beta}}_{OLS} - \underline{\beta})] \\ MSE[\hat{\underline{\beta}}_{OLS}] &= E[(\underline{\beta} + (H^TH)^{-1}H^T\underline{e} - \underline{\beta})^T(\underline{\beta} + (H^TH)^{-1}H^T\underline{e} - \underline{\beta})] \\ MSE[\hat{\underline{\beta}}_{OLS}] &= \sigma^2 TRACE[(H^TH)^{-1}] \end{aligned} \tag{4.12}$$

which is the same as the variance (given by equation 4.10). This should be expected since the OLS estimator is an unbiased estimator, no bias exists in the solution. Another way to determine the MSE is as follows

$$\begin{aligned} MSE[\hat{\underline{\beta}}_{OLS}] &= BIAS[\hat{\underline{\beta}}_{OLS}]^2 + VAR[\hat{\underline{\beta}}_{OLS}] \\ MSE[\hat{\underline{\beta}}_{OLS}] &= \quad 0 \quad\quad + VAR[\hat{\underline{\beta}}_{OLS}] \\ MSE[\hat{\underline{\beta}}_{OLS}] &= \sigma^2 TRACE[(H^TH)^{-1}] \end{aligned} \tag{4.13}$$

In the case of vehicle positioning, the OLS estimator minimizes the $SS(\underline{e}_R)$, not the MSE. Since the OLS estimator does not allow a bias to exist in the solution, it restricts the MSE to include only the variance term. This variance inflates significantly when a "poor geometry" condition arises among the landmarks and the vehicle. Geometry effects on position fixing will be discussed in the next section.

4.3.1 Geometry Effects on Position Fixing

For position fixing, the geometry of the landmarks with respect to the vehicle is a major factor in how accurate the position estimate will be in terms of the MSE. In order to illustrate what is meant by the term geometry, equation 4.12 is converted into its canonical coordinates using a singular value decomposition (SVD) of H

$$H^{nxp} = U^{nxn}\,\Sigma^{nxp}\,(V^T)^{pxp} \tag{4.14}$$

where U and V^T are defined as orthogonal transformation matrices that diagonalize H, and Σ is a diagonal matrix whose elements are the singular values of H. The singular values of H are equal to the square root of the eigenvalues of H ($\sqrt{\lambda_i}$). For a more in depth discussion of the SVD and how it relates to solving OLS problems, see reference [20]. Therefore, equation 4.12 transforms into

$$MSE[\hat{\underline{\beta}}_{OLS}] = \sigma^2 TRACE[\Sigma^T\Sigma]$$

$$MSE[\hat{\beta}_{OLS}] = \sigma^2 \sum_{i=1}^{p} \left[\frac{1}{\lambda_i} \right] \qquad (4.15)$$

where λ_i are the eigenvalues of H^TH. Note that as the eigenvalues become smaller, the MSE grows. Small eigenvalues represent an ill-conditioned (or nearly singular) H matrix. This gives rise to what is considered to be a poor geometry condition.

Figure 4.2 shows a physical interpretation of the relation between the eigenvalues and the position fix in two dimensions. When estimating a two-dimensional position (2-D), a statistical error ellipse is defined [21]. (the error ellipse will contain 95% to 98% of the position estimates, see reference [12].) This error ellipse is a function of the range measurement noise and the eigenvalues. Assuming that the measurement noise is fairly constant, the error ellipse will inflate when the eigenvalues become small. For the 2-D case, one of the two eigenvalues will obtain a small value as the crossing angle, γ, becomes small.

For example, $\gamma = 90^{\circ}$ is considered to be very good geometry while $\gamma = 1^{\circ}$ is considered to be very poor geometry. The crossing angle is also depicted in Figure 4.2. If the range measurements from the two DME stations in Figure 4.2 have a small crossing angle, λ_2 will be small; and this will inflate the error ellipse in the direction corresponding to λ_2.

"Near collinearity" is another term that is used for the case when a small crossing angle exists between the range measurements [22]. Nearly collinear range measurements inflate the range errors into a poor position estimate. This is what is meant by a poor geometry condition.

4.3.2 GDOP Factor Description

For navigation, the type of geometry condition that exists is portrayed by a statistical factor called the Geometric Dilution of Precision (GDOP). The GDOP is defined as follows

$$GDOP = \sqrt{TRACE(H^TH)^{-1}} \qquad (4.16)$$

Five different types of DOPs are defined below

GDOP = 3-D position and time dilution of precision
PDOP = 3-D position dilution of precision
HDOP = position dilution of precision in the horizontal plane
VDOP = position dilution of precision in the vertical direction
TDOP = time dilution of precision

For satellite navigation (GPS, GLONASS), GDOP is used to represent a 4-D geometry condition: 3-D position and time (X,Y,Z,T). In the context of navigation using the GPS, Jorgenson [23] states the following about GDOP

1) GDOP is, in effect, the amplification factor of pseudorange measurement errors into user errors due to the effect of satellite geometry.
2) GDOP is independent of the coordinate system employed.

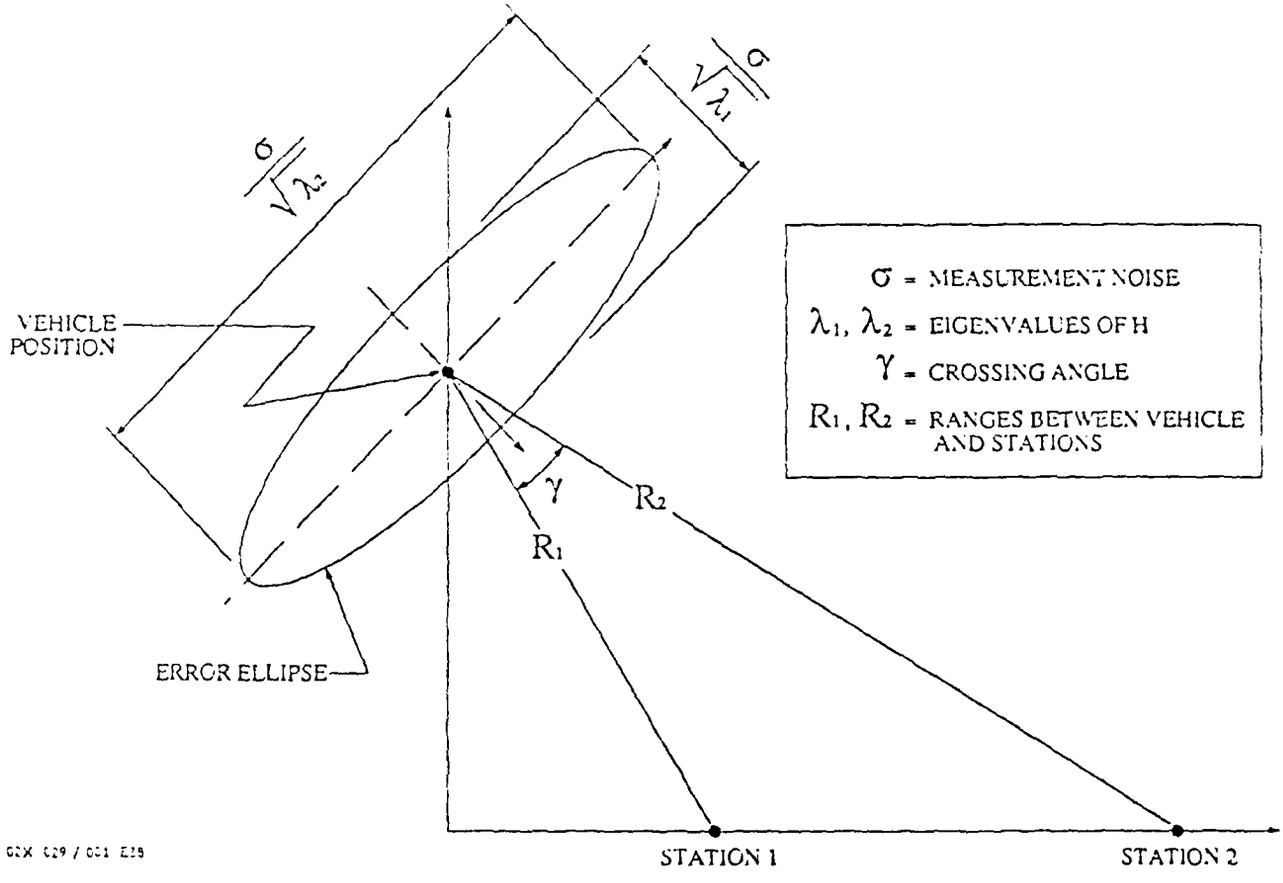

Figure 4.2 Relation between the eigenvalues of the data matrix H and the error ellipse.

3) GDOP is a criterion for designing satellite constellations.
4) GDOP is a means for user selection of the four best satellites from those that are visible.

PDOP is more useful in navigation than GDOP because it is the critical information needed to calculate position. Also, one may wish to calculate PDOP by finding the volume of a tetrahedron rather than implementing equation 4.16 [24]. As seen in reference [24], this saves processing time over the matrix inversion method of equation 4.16 when many possible combinations of satellites exist.

Furthermore, for aircraft, the vertical position information is obtained from the baro-altimeter. The good, relative accuracy of the baro-altimeter is the basis for the vertical separation of aircraft. Therefore, aircraft positioning using landmarks only requires 2-D information, and subsequently, HDOP is the parameter of interest. Note that HDOP is dependent on the coordinate system used as it involves the propagation of measurement errors into a user-defined horizontal plane.

4.4 DME Simulation Example

A DME simulation is presented to illustrate the points made above about geometry conditions and how they affect the OLS estimator. The simulation involves the estimation of an aircraft's position as it travels along a constant velocity flight path. Figure 4.3 shows the simulation set-up.

4.4.1 DME Simulation Set-Up

Range measurements from two different DME stations are needed to solve for a two-dimensional position (X,Y) as depicted in Figure 4.3. The equations are shown below

$$[(\hat{X}-X_i)^2 + (\hat{Y}-Y_i)^2]^{1/2} = R_i \qquad (4.17)$$

where R_i is the range measurement from the aircraft to DME station i, $(\hat{X},\hat{Y})$ is the estimated user position and (X_i,Y_i) are the coordinates for DME_i. Using these two equations, the aircraft estimates its position and velocity. One way to do this is to linearize the above equation by constructing a Taylor series expansion around an initial estimate and retaining only the first order terms.

$$R_i = R_{i0} + \left.\frac{\partial R_i}{\partial \hat{X}}\right|_{(\hat{X}_0,\hat{Y}_0)} \delta X + \left.\frac{\partial R_i}{\partial \hat{Y}}\right|_{(\hat{X}_0,\hat{Y}_0)} \delta Y \qquad (4.18)$$

where δX and δY are the corrections to the initial aircraft state estimate $(\hat{X}_0,\hat{Y}_0)$. R_{i0} is the initial estimated range to DME station i using the initial aircraft state estimate. This is shown below

$$[(\hat{X}_0-X_i)^2 + (\hat{Y}_0-Y_i)^2]^{1/2} = R_{i0} \qquad (4.19)$$

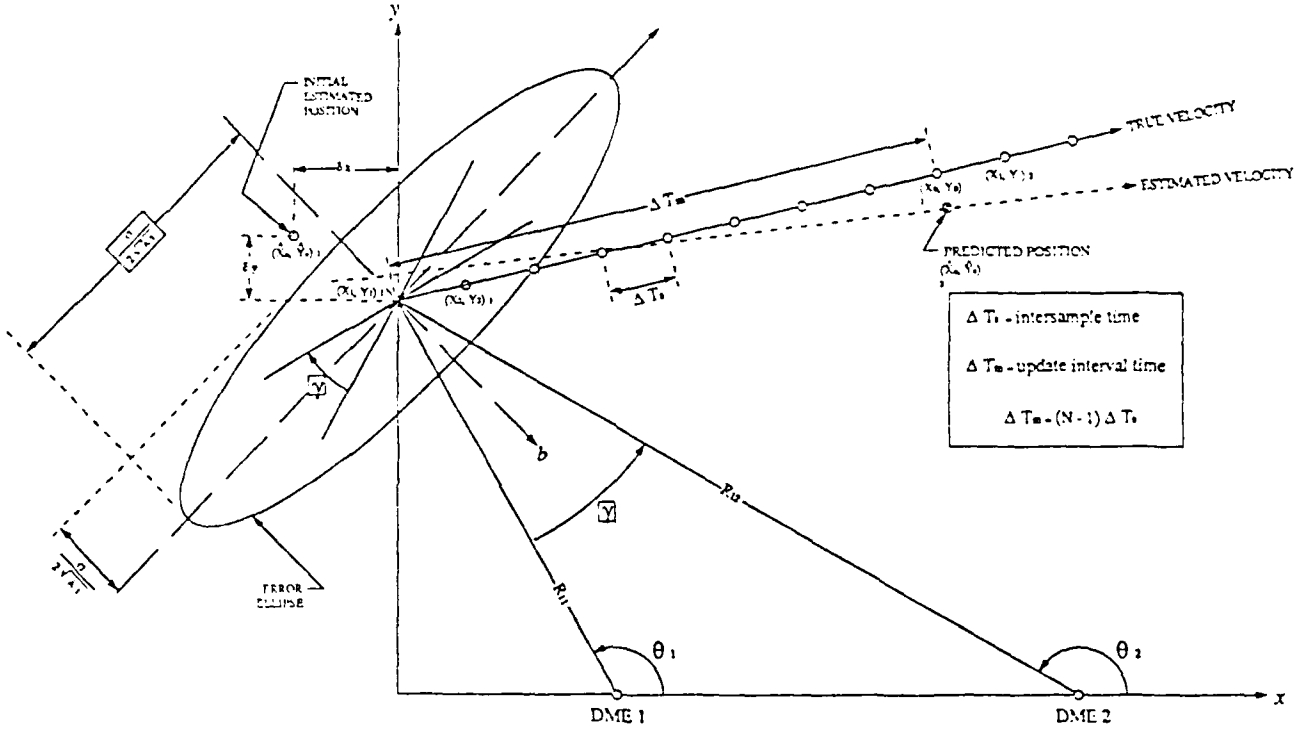

Figure 4.3 DME simulation geometry with a vehicle on a constant velocity flight path making range measurements to two DME stations.

The direction cosines, α_{ij}, are the cosines of the angles between the line-of-sight (LOS) vector from the aircraft to DME station i and its projection along the coordinate axes

$$\frac{\partial R_i}{\partial \hat{X}} = \frac{\hat{X} - X_i}{R_i} = \alpha_{i1}$$

$$\frac{\partial R_i}{\partial \hat{Y}} = \frac{\hat{Y} - Y_i}{R_i} = \alpha_{i2} \qquad (4.20)$$

The measurement model for a constant velocity flight path is given below for a batch of j measurement sets; j = 1, N. N is the number of range measurements in a batch interval (ΔT_m). See also Figure 4.3.

$$\begin{bmatrix} \delta R_{11} \\ \delta R_{21} \\ \hline \delta R_{12} \\ \delta R_{22} \\ \hline \vdots \\ \hline \delta R_{1N} \\ \delta R_{2N} \end{bmatrix} = \left[\begin{array}{cccc} \alpha_{11} & \alpha_{12} & 0 & 0 \\ \alpha_{21} & \alpha_{22} & 0 & 0 \\ \hline \alpha_{11} & \alpha_{12} & \Delta T_s\alpha_{11} & \Delta T_s\alpha_{12} \\ \alpha_{21} & \alpha_{22} & \Delta T_s\alpha_{21} & \Delta T_s\alpha_{22} \\ \hline \vdots & \vdots & \vdots & \vdots \\ \hline \alpha_{11} & \alpha_{12} & (N-1)\Delta T_s\alpha_{11} & (N-1)\Delta T_s\alpha_{12} \\ \alpha_{21} & \alpha_{22} & (N-1)\Delta T_s\alpha_{21} & (N-1)\Delta T_s\alpha_{22} \end{array}\right] \begin{bmatrix} \delta X \\ \delta Y \\ \hline V_X \\ V_Y \end{bmatrix} + \begin{bmatrix} e_{11} \\ e_{21} \\ \hline e_{12} \\ e_{22} \\ \hline \vdots \\ \hline e_{1N} \\ e_{2N} \end{bmatrix} \qquad (4.21)$$

$$\delta \underline{R} = H \underline{\beta} + \underline{e}$$

where i is the DME station number, j is the measurement set, V_X and V_Y is the aircraft velocity, and $\delta R_{ij} = R_{ij} - R_{i0}$. ΔT_s is the intersample time of the range measurements in a batch.

δX and δY <u>do not</u> represent the difference in position from one observation to the next. They represent the initial aircraft position <u>offset</u> from the start of the constant velocity flight path; or in other words, the error in the *a priori* estimate of the aircraft position ($\hat{X}_0$,$\hat{Y}_0$). The direction cosines are calculated every batch-interval using new estimates of X and Y ($\hat{X}$,$\hat{Y}$).

Based on one batch of measurements, the aircraft estimated state is updated at time t_k as follows

$$\begin{bmatrix} \hat{X}_k \\ \hat{Y}_k \end{bmatrix} = \begin{bmatrix} \hat{X}_0 \\ \hat{Y}_0 \end{bmatrix} + \begin{bmatrix} \delta\hat{X} \\ \delta\hat{Y} \end{bmatrix} + (N-1)\Delta T_s \begin{bmatrix} \hat{V}_X \\ \hat{V}_Y \end{bmatrix} \qquad (4.22)$$

where $\hat{V}_X$ and $\hat{V}_Y$ are the estimates of velocity.

4.4.2 Results of the OLS Estimator Using the DME Simulation

In order to evaluate the performance of the batch OLS estimator for navigation, two cases are analyzed:

(1) A good geometry situation: $\gamma = 90^\circ$ (HDOP = 1.4).
DME station 1 location, $[X_1 \; Y_1]$ = [-1.108e05 0] feet
DME station 2 location, $[X_2 \; Y_2]$ = [3.608e05 0] feet

(2) A poor geometry situation: $\gamma = 1^\circ$ (HDOP = 80).
DME station 1 location, $[X_1 \; Y_1]$ = [3.464e05 0] feet
DME station 2 location, $[X_2 \; Y_2]$ = [3.608e05 0] feet

Both cases have the following initial conditions:

true aircraft location, $[X_{TR} \; Y_{TR}]$ = [0 2.000e05] feet
measurement noise, σ = 60 feet
measurement bias, $\underline{\Delta B}$ = [0 0] feet
number of range measurements in a batch, N = 16
aircraft initial position offset, [δX δY] = [270 -370] feet

For batch estimation with measurement noise only, note that the position error inflation is effectively reduced by one over the square root of the number of measurements in a batch. Since a batch of 16 measurements is used in the simulation, the position error inflation above is reduced by a factor of 4.

For these two cases, a 1000 iteration Monte Carlo analysis is performed. For this simulation, the first iteration of the simulation process is repeated M times (M = 1000), and each time different measurement noise is used. The results for cases (1) and (2) are shown in Figures 4.4 and 4.5, respectively. Notice that the errors in Figure 4.4 are in a near circular formation. This is due to the fact that good geometry exists ($\gamma = 90^\circ$). Figure 4.5 depicts the position results of the OLS estimator when a poor geometry condition exists ($\gamma = 1^\circ$); the solution is still unbiased, but the errors form a rather large ellipse around the true solution. The MSE, which is the appropriate error criterion to try to minimize for navigation purposes, is given below in terms of the square root of the MSE (i.e. SQRT[MSE]) for each case:

(1) SQRT[MSE] = 20 feet (2) SQRT[MSE] = 1177 feet

From these results it can be seen that the OLS estimator's MSE and associated error ellipse is inflated significantly when a poor geometry situation exists. To see just when the MSE starts to inflate as the geometry becomes worse, the results from "small" Monte Carlo analyses for various crossing angles between the measurements are compiled. In order to obtain different crossing angles, the location of DME station 1 is moved in distinct steps from the good geometry location ([-1.108e05 0] feet) toward the DME station 2 location ([3.608e05 0] feet). Each step is 4716 feet in the X direction. At each step a 50 iteration Monte Carlo analysis is implemented and the SQRT[MSE] is recorded. The crossing angle versus the SQRT[MSE] is shown in Figure 4.6. From this figure it can seen that the SQRT[MSE] starts to increase rapidly when the crossing angle becomes less than 6°.

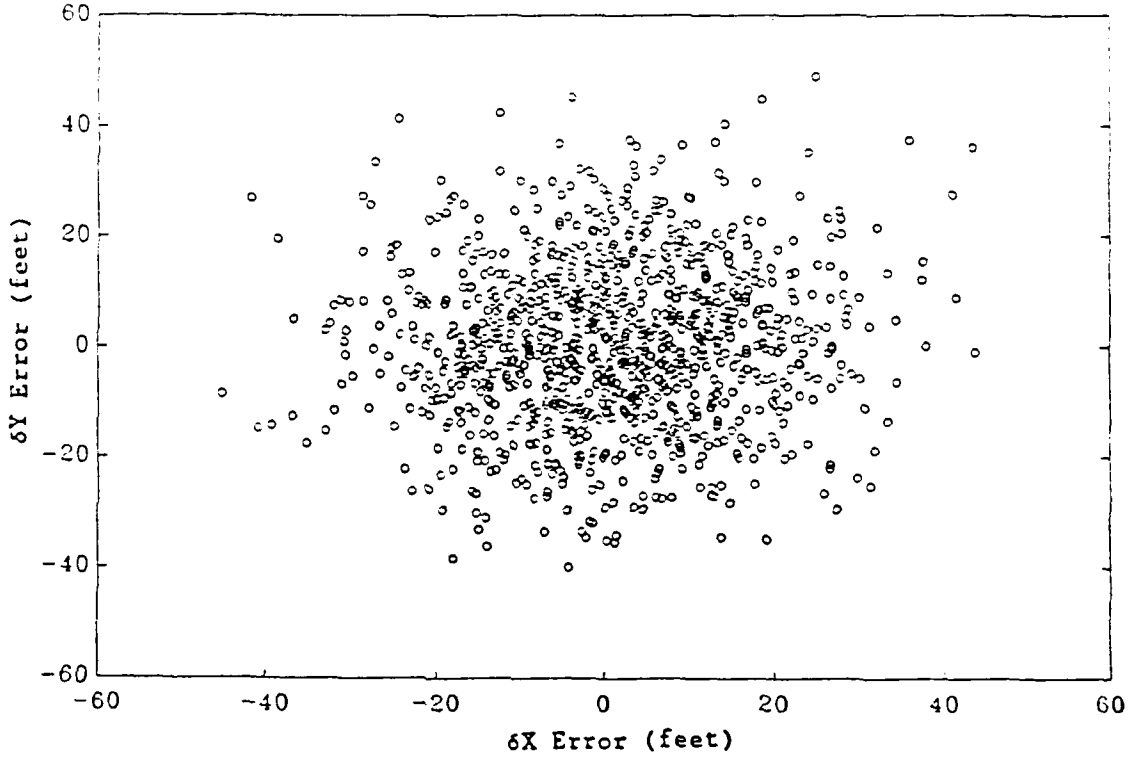

Figure 4.4 Monte Carlo analysis of the OLS estimator in a good geometry condition ($\gamma = 90^{\circ}$).

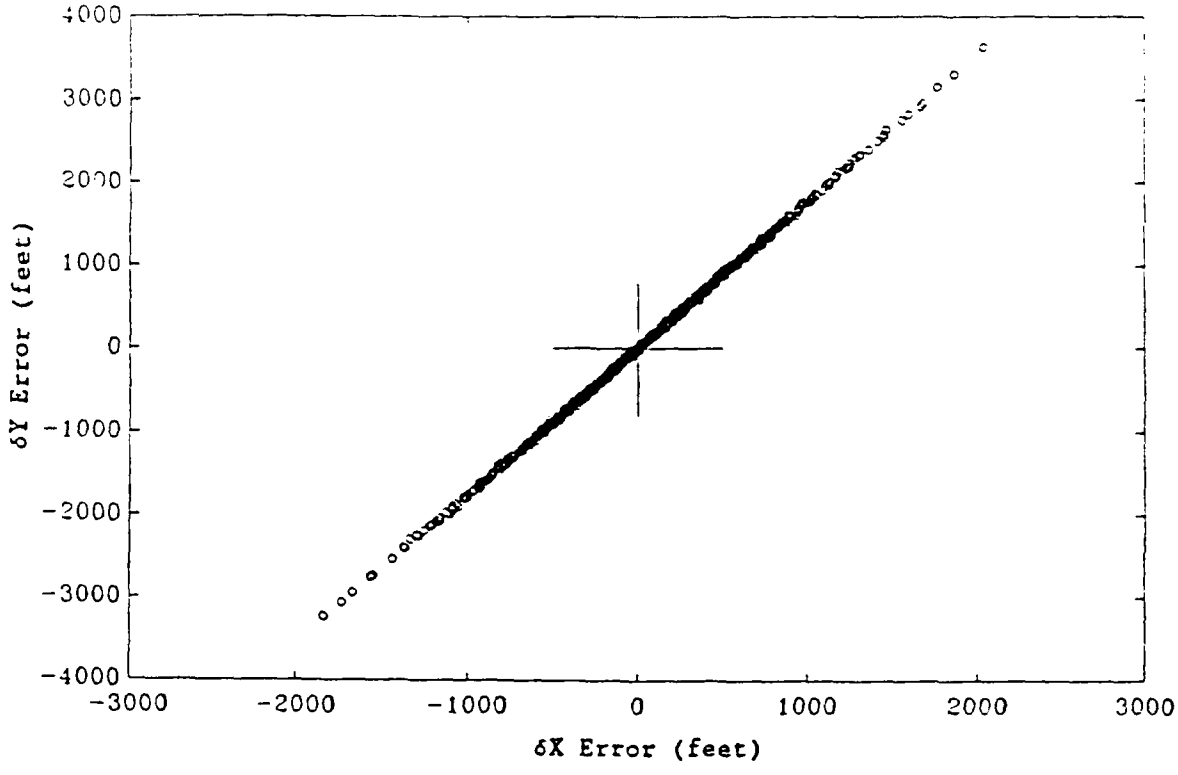

Figure 4.5 Monte Carlo analysis of the OLS estimator in a poor geometry condition ($\gamma = 1^{\circ}$).

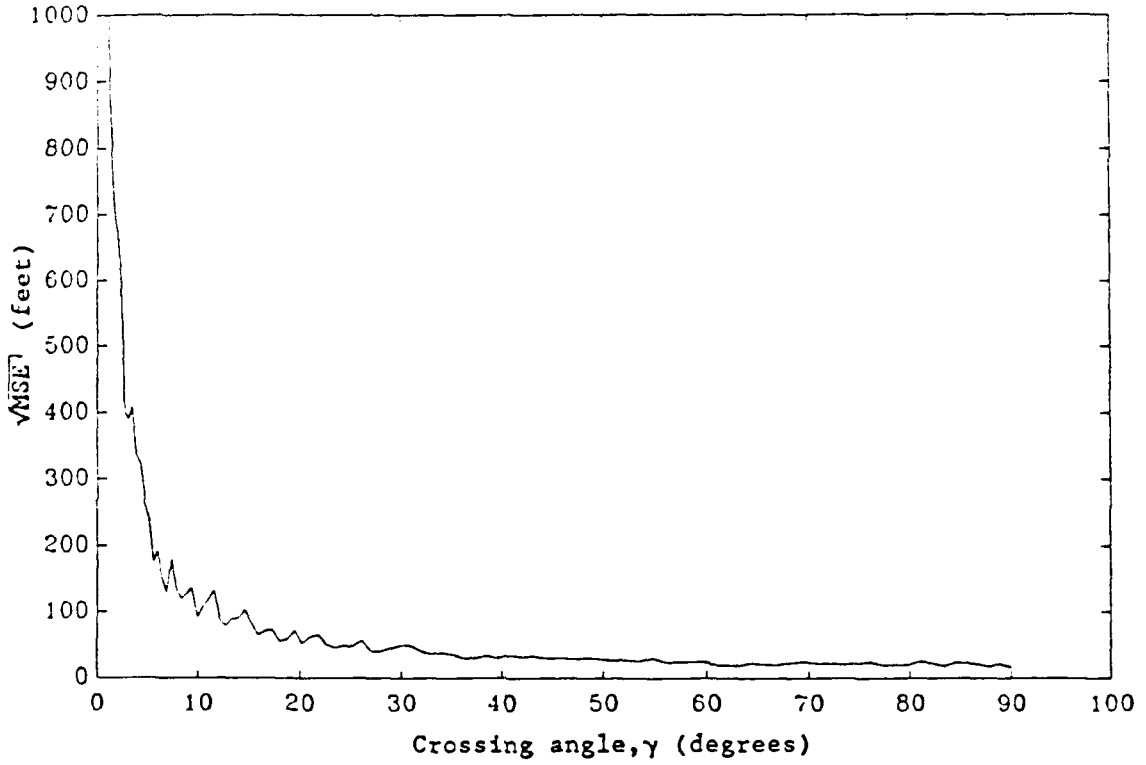

Figure 4.6 Relation between the crossing angle and the SQRT[MSE] for an OLS estimator.

4.5 OLS Estimator with Range Measurement Bias Errors

To complete the discussion on the OLS estimator, the MSE equation must be developed for the case of bias errors as well as noise existing on the range measurements. Start with the linear model given by equation 4.1

$$\underline{Y} = H\underline{\beta} + \underline{\Delta B} + \underline{e} \tag{4.23}$$

Recall that the OLS estimator is given by

$$\hat{\underline{\beta}}_{OLS} = (H^T H)^{-1} H^T \underline{Y} \tag{4.24}$$

Substituting the linear model into the OLS estimator yields

$$\hat{\underline{\beta}}_{OLS} = (H^T H)^{-1} H^T H\underline{\beta} + (H^T H)^{-1} H^T \underline{\Delta B} + (H^T H)^{-1} H^T \underline{e}$$
$$\hat{\underline{\beta}}_{OLS} = \underline{\beta} + (H^T H)^{-1} H^T \underline{\Delta B} + (H^T H)^{-1} H^T \underline{e} \tag{4.25}$$

From equation 4.23 the expected value, or mean, of the OLS estimator is

$$E[\hat{\underline{\beta}}_{OLS}] = E[\underline{\beta} + (H^T H)^{-1} H^T \underline{\Delta B} + (H^T H)^{-1} H^T \underline{e}]$$
$$E[\hat{\underline{\beta}}_{OLS}] = \underline{\beta} + (H^T H)^{-1} H^T \underline{\Delta B} \tag{4.26}$$

Therefore, the OLS estimator's solution bias is

$$BIAS[\hat{\underline{\beta}}_{OLS}] = (H^T H)^{-1} H^T \underline{\Delta B} \tag{4.27}$$

This shows that the bias of the OLS solution is only a function of the measurement bias errors. If no measurement bias errors exist, then the OLS solution would be unbiased, as was shown before in Section 4.2. The variance of the OLS estimator is the same as before

$$VAR[\hat{\underline{\beta}}_{OLS}] = E[\hat{\underline{\beta}}_{OLS}^2] - [E(\hat{\underline{\beta}}_{OLS})]^2$$
$$VAR[\hat{\underline{\beta}}_{OLS}] = \sigma^2 TRACE[(H^T H)^{-1}] \tag{4.28}$$

The MSE equation is then given by

$$MSE[\hat{\underline{\beta}}_{OLS}] = E[(\hat{\underline{\beta}}_{OLS} - \underline{\beta})^T (\hat{\underline{\beta}}_{OLS} - \underline{\beta})]$$
$$MSE[\hat{\underline{\beta}}_{OLS}] = E[(\underline{\beta} + (H^T H)^{-1} H^T \underline{\Delta B} + (H^T H)^{-1} H^T \underline{e} - \underline{\beta})^T$$
$$(\underline{\beta} + (H^T H)^{-1} H^T \underline{\Delta B} + (H^T H)^{-1} H^T \underline{e} - \underline{\beta})]$$

$$MSE[\hat{\underline{\beta}}_{OLS}] = \underline{\Delta B}^T H (H^T H)^{-1T} (H^T H)^{-1} H^T \underline{\Delta B} + \sigma^2 TRACE[(H^T H)^{-1}]$$

Since $(H^T H)^{-1}$ is symmetric, $(H^T H)^{-1T} = (H^T H)^{-1}$ and the MSE becomes

$$MSE[\hat{\underline{\beta}}_{OLS}] = \underline{\Delta B}^T H (H^T H)^{-2} H^T \underline{\Delta B} + \sigma^2 TRACE[(H^T H)^{-1}] \tag{4.29}$$

This completes the discussion on the OLS estimator, which will be used as the baseline estimation scheme to evaluate the performance of the Kalman filter and the Ridge regression signal processor presented in the next Section.

5. THE EXTENDED KALMAN AND RIDGE/KALMAN FILTERS

5.1 Theory of Kalman Filtering

This section moves from the previous discussions on batch processing to a recursive processing technique. The Kalman filter is presented, which can be shown to be just a recursive form of the ordinary least squares (OLS) estimator. For two key references, [25] portrays the inherent equivalence of OLS estimation and Kalman filter theory; and [26] shows that Kalman filter theory is essentially the same as random parameter linear regression theory.

5.1.1 Recursive versus Batch Processing

The performance of the batch and the recursive processor is equivalent. Batch processing gives a position estimate after averaging a group of measurements over a specified time interval. Usually, it is considered memoryless, since it only analyzes the measurement group over the given time interval; no weight is given to the measurements that were received before the time interval began. A batch processor may also incorporate some type of previous information (called *a priori* information), weighted appropriately, into the linear model [27]. On the other hand, a recursive processor employs a time-history of measurements received as the *a priori* information, and continuously updates the current position estimate (or state) with a combination of the newly received measurement data and the model estimate obtained from the previous measurement information.

Below it will be shown how the Kalman filter is developed from the model with *a priori* information. Next, issues are discussed involving the selection of the error covariance matrix (P_0) and system covariance matrix (Q).

5.1.2 Kalman Filter Development

In 1960, R. E. Kalman provided an alternative way of formulating the OLS estimator using state-space methods [28]. The result is what is known today as the Kalman filter. There are many ways to derive the Kalman filter including: the Bayesian approach, using the Projection Theorem, and from properties of Gaussian conditional probability densities. Below, the Bayesian approach is implemented to develop the Kalman filter from a model that includes *a priori* information. This will be shown to form the Kalman filter's updating step. Since the Kalman filter is a recursive estimator, its updating step will allow new information to be combined in some way with previously given measurement information at each time interval.

Assume that the linear model given by equation 4.1 in Section 4.1 has experimental data concerning β such that the average of all previous measurements equals β_0 with some uncertainty, $\underline{v}$. Using β_0 and $\underline{v}$, two equations now define the model: the initial conditions equation and the linear model equation

$$\beta = \beta_0 + \underline{v} \tag{5.1}$$

$$\underline{Y} = H\beta + \underline{\Delta B} + \underline{e} \tag{5.2}$$

Recall that $\underline{\Delta B}$ represents range measurement bias errors and $\underline{e} \sim N(0,R)$ defines the mean (which is 0) and covariance $R = [\underline{e}\underline{e}^T]$ of the normally distributed

range measurement noise ($\underline{e}$). $\underline{v}$ - WS(0,P_0) defines the mean (which is 0) and covariance (P_0) of $\underline{v}$ in the weaker form called wide sense (WS) which does not make any distributional assumptions. P_0 is known as the error covariance matrix and is given by

$$P_0 = E[\underline{v}\underline{v}^T] = E[(\underline{\beta} - \underline{\beta}_0)(\underline{\beta} - \underline{\beta}_0)^T] \tag{5.3}$$

Since the initial conditions are actually random variables, the system state ($\underline{\beta}$) cannot be propagated with certainty. Therefore, the state itself must be considered a random variable and the result is a stochastic process [29].

Following the Goldberger-Theil method given in [25], the idea is to use $\underline{\beta}_0$ as a measurement

$$\begin{bmatrix} \underline{\beta}_0 \\ \underline{Y} \end{bmatrix} = \begin{bmatrix} I \\ H \end{bmatrix} \underline{\beta} + \begin{bmatrix} -\underline{v} \\ \underline{e} \end{bmatrix} + \begin{bmatrix} 0 \\ \underline{\Delta B} \end{bmatrix} \tag{5.4}$$

Now, solving for $\underline{\beta}$ yields the Bayesian solution ($\hat{\underline{\beta}}_P$). As derived in reference [30], the Bayesian solution, which incorporates the *a priori* information into the linear model, is given by

$$\hat{\underline{\beta}}_P = [P_0^{-1} + H^T R^{-1} H]^{-1} [P_0^{-1}\underline{\beta}_0 + H^T R^{-1}\underline{Y}] \tag{5.5}$$

The linear recursive dynamic model is obtained by placing the estimate $\hat{\underline{\beta}}_k$ in the role of the *a priori* information $\underline{\beta}_0$.

Next, the goal is to rewrite equation 5.5 in a recursive form. The recursive state model is given by

$$\underline{\beta}_{k+1} = \Phi\underline{\beta}_k + \underline{w}_{k+1} \tag{5.6}$$

where Φ is the state transition matrix which represents how a dynamical system naturally evolves from one state to the next in the absence of a driving function. (Note that the system would be in a constant state if Φ equals the identity matrix.) Also, $\underline{w}_{k+1}$ represents the process noise with associated system covariance matrix, $Q = E[\underline{w}\underline{w}^T]$.

Following a procedure given by reference [26], equation 5.5 can be written as

$$\hat{\underline{\beta}}_k = (P_{k/k-1}^{-1} + H_k^T R^{-1} H_k)^{-1}(P_{k/k-1}^{-1}\hat{\underline{\beta}}_{k/k-1} + H_k^T R^{-1}\underline{Y}_k) \tag{5.7}$$

where $\hat{\underline{\beta}}_{k/k-1}$ is the predicted estimate of $\underline{\beta}_k$ based upon observations up to k-1, and $P_{k/k-1} = \text{cov}(\hat{\underline{\beta}}_{k/k-1} - \underline{\beta}_k)$. Equation 5.7 is the recursive form of the Bayesian estimator.

Equation 5.7 can then be transformed into the Kalman filter measurement update equation by using the Matrix Inversion Lemma (The Matrix Inversion Lemma is used to obtain the following relation: $[P^{-1} + H^T R^{-1} H]^{-1} = P - PH^T(HPH^T + R)^{-1}HP$ [18])

$$\hat{\underline{\beta}}_k = \hat{\underline{\beta}}_{k/k-1} + K_k(\underline{Y}_k - H_k\hat{\underline{\beta}}_{k/k-1}) \tag{5.8}$$

where $\underline{Y}_k$ are the new measurements, $H_k\hat{\underline{\beta}}_{k/k-1}$ are the predicted measurements based on the last k-1 estimates, and K_k is called the Kalman gain. $\hat{\underline{\beta}}_{k/k-1}$ represents the state estimate before the new measurements are available, while $\hat{\underline{\beta}}_k$ represents the state estimate after the new measurements are incorporated. The term $(\underline{Y}_k - H_k\hat{\underline{\beta}}_{k/k-1})$ forms what are called the innovations; it represents the part of $\underline{Y}_k$ that cannot be predicted from the previous measurement data. The innovations are the same as the residuals of the OLS estimator ($\underline{e}_R$) in the sense that the Kalman filter minimizes the error in the estimate by making the innovations white (i.e. zero mean and random).

Equation 5.8 may be interpreted as follows: the new "best" state estimate equals the previous "best" state estimate plus the new information that is received (the innovations) multiplied by a gain factor. The state estimates are the best in the sense that the sum of the squares of the errors are minimized. This makes the filter "matched" to the measurement data being processed by it. When the Kalman filter model is matched to the data, the best linear unbiased estimator (BLUE) is obtained [18].

Following reference [25], the gain factor is determined from

$$K_k = P_{k/k-1}H_k^T(H_kP_{k/k-1}H_k^T + R)^{-1} \tag{5.9}$$

And the error covariance is updated by

$$P_k = (I - K_kH_k)P_{k/k-1} \tag{5.10}$$

The error covariance is propagated by the following equation

$$P_{k+1/k} = \Phi P_k\Phi^T + Q \tag{5.11}$$

where Q represents the uncertainty in the state model. Figure 5.1, which emulates a figure given in reference [31], shows how equations 5.6, 5.8, 5.9, 5.10 and 5.11 interact with each other to form the Kalman filter.

Note that Φ, Q, and R are not time varying in the above equations (no "$_k$" follows them). This may not always be true. For example, the system dynamic model (Φ) may need to change with time, or the system covariance matrix (Q) may be updated by some type of adaptive scheme.

The major point of this section is that the Kalman filter is the same as an OLS estimator made into a recursive process by combining the incoming measurement data with some *a priori* information.

5.1.3 The Extended Kalman Filter (EKF)

Since the equations that relate the measurements to the state vector are usually nonlinear (i.e. the H matrix is nonlinear), an extended Kalman filter (EKF) is needed. Therefore, a linearization procedure is performed when deriving the Kalman filter equations. This is shown below.

First, the nonlinear discrete-time system model is as follows

$$\underline{Y}_k = g_k(\underline{\beta}_k) + \underline{\Delta B} + \underline{e} \tag{5.12}$$

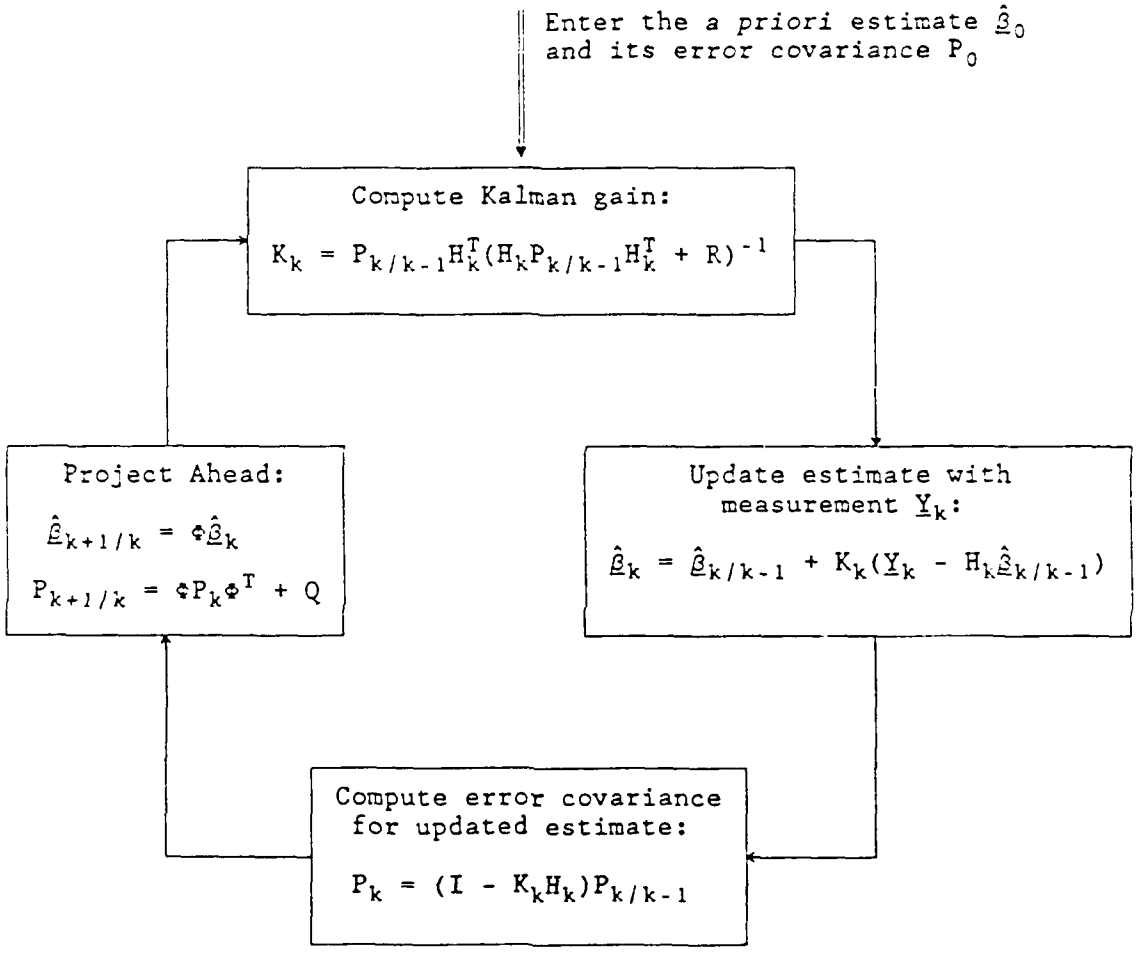

Figure 5.1 Kalman filter equations (from reference [31]).

where g_k is a nonlinear vector-valued function which relates the system state to the measurements (see reference [32]). Then, the linearized model is given by

$$\delta \underline{Y}_k = \left[\frac{\partial g_k(\hat{\underline{\beta}}_{k/k-1})}{\partial \underline{\beta}_k} \right] \delta \underline{\beta}_k + \underline{\Delta B} + \underline{e} \qquad (5.13)$$

The $g_k(\hat{\underline{\beta}}_{k/k-1})$ term signifies that the linearization is taking place around the estimate, $\hat{\underline{\beta}}_{k/k-1}$. Incorporate equation 5.12 into equation 5.7 to obtain the recursive update equation for the extended Kalman filter

$$\hat{\underline{\beta}}_k = \hat{\underline{\beta}}_{k/k-1} + (P^{-1}_{k/k-1} + H^T_k R^{-1} H_k)^{-1} (H^T_k R^{-1} \delta \underline{Y}_k) \qquad (5.14)$$

where $\delta \underline{Y}_k$ is the difference between the actual measurements and the predicted measurements (the innovations) as shown below

$$\delta \underline{Y}_k = \underline{Y}_k - g_k(\hat{\underline{\beta}}_{k/k-1}) \qquad (5.15)$$

And as given by reference [33]

$$H = \frac{\partial g_k(\hat{\underline{\beta}}_{k/k-1})}{\partial \underline{\beta}_k} \qquad (5.16)$$

As will be seen in Section 5.6, the extended Kalman filter's update equation as given by 5.14 is very useful when incorporating ridge regression theory into the Kalman filter.

5.1.4 Selection of the P_0 and Q Matrices in the Kalman Filter

An optimum unbiased estimator arises when both the model and the estimator match the process which generates the data. Kalman filter optimization techniques include the selection of P_0 and Q based upon past experience or by adaptively tuning the filter until its innovations (residuals) become white (i.e. zero mean and random). However, the selection of the proper Q matrix is usually not a very easy or straightforward task [31].

For example, the system covariance matrix Q is often set artificially high such that the Kalman filter can track the vehicle when it encounters dynamics such as turning-induced accelerations. Therefore, the Kalman filter allows more noise in the solution during periods of low dynamics. Although some methods exist for selecting Q adaptively [34], these are stochastic in nature.

Another problem arises when the Kalman filter is subjected to a poor geometry condition. In the case of inaccurate P_0 and Q matrices (a mismatched filter), the filter may become biased. The performance of a biased Kalman filter is not readily understood, as the Kalman filter is optimal and defined in a Gaussian environment only. Therefore, the performance of a Kalman filter for a deterministic maneuver in a poor geometry condition cannot be predicted from the regular Kalman filter equations. Furthermore, near

collinearity effects cannot be minimized by observing the innovations in the Kalman filter's update equation (equation 5.8), because these effects only appear in the estimator $\underline{\hat{\beta}}$. This is shown in reference [35].

In applying the Kalman filter to navigation, the MSE is the appropriate error criterion to be minimized. The MSE of a mismatched Kalman filter is not necessarily the smallest obtainable. Recall that the MSE is the sum of two components: the variance term and bias term squared. Since the Kalman filter is developed from the OLS estimator, it is inherently an unbiased estimator. This restricts the MSE equation to only one component - the variance term.

The next section presents a biased estimator derived from ridge regression theory. A biased estimator is purposely not matched to the process that generates the data in order to achieve a smaller MSE.

5.2 Theory of Ridge Regression

This section covers a biased estimation technique called ridge regression. First, the ridge estimator is analyzed with respect to the ordinary least squares (OLS) estimator through a comparison of mean square error (MSE) equations. Second, the effects of range measurement noise and bias errors on the ridge estimator's solution are addressed. Finally, a linearized recursive ridge processor is developed which explains the behavior of the extended Kalman filter (EKF).

5.2.1 Historical Perspective

The theory of ridge regression was developed by Arthur Hoerl and Robert Kennard in 1970 [36] based on some earlier work by Hoerl in 1959 on what he termed "ridge" analysis because the results he obtained formed what looked like ridges in the output data [37]. The purpose for the development of ridge regression was to combat the ill-effects of near collinearity when it arises in the predictor matrix of a linear regression model. In order to counter situations with near collinearity, ridge regression introduces a biasing parameter, κ. Statisticians have had much debate over the proper selection of this biasing parameter [38,39,40] (also see Oman [41] for a confidence bound approach to selecting κ), let alone the fact that many feel that a biasing parameter should not be added at all (see Efron [42] who points out the heated controversy among statisticians between biased and unbiased estimation). The biasing parameter in a sense "unbalances" the normal linear regression model and causes a bias to exist in the solution. This is in direct conflict with an unbiased estimator like the OLS estimator which minimizes the sum of the squares of the errors. (This was examined in Section 4.3.) Further, detailed information about ridge regression may be found in references [43,44,45].

In 1988, Robert Kelly introduced a ridge regression signal processor for navigation applications to combat the effects of nearly collinear range measurements [46]. Inaccuracies in the position solution become highly inflated when range measurements are nearly collinear. The term poor geometry is used for cases when range measurements are nearly collinear. In subsequent developments over the past two years [30,47,48,49], it has been determined that a proper selection of the biasing parameter can be made based on the geometry of the range measurements. Therefore, ridge regression may be used

to improve position estimates obtained from a navigation system in the presence of poor geometry.

5.2.2 Biased Estimation

Position fixing using any type of navigation system suffers a loss of accuracy when the range measurements are nearly collinear, i.e poor geometry. Under such conditions, the range measurement errors are propagated into position errors which are highly inflated (see Section 4.3.1). To improve estimation properties when several parameters are to be estimated, the ridge estimator deliberately induces biases in the solution. This results in a solution with a consistently smaller mean square error (MSE) than the ordinary least squares (OLS) solution.

Recall that the MSE consists of the sum of two components; MSE = Variance + Bias^2. The ridge estimator takes advantage of an extra degree of freedom, the bias term, which is not used by a OLS estimator. In effect, small biases induced by the ridge estimator decrease the variance term such that the overall MSE is smaller than the MSE obtained from an unbiased estimator, as illustrated in Figure 5.2.

For navigation, the most useful error criterion is the MSE. It expresses the deviation of the vehicle with respect to its intended path. The ridge estimator has the property that the MSE in the presence of poor geometry is much smaller than the MSE of a conventional OLS estimator as discussed above. It should be noted, however, that the ridge estimator cannot remove a steady-state bias in the estimator caused by measurement bias errors. This is shown in Section 5.2.5.1.

5.2.3 The Ridge Estimator

Following Kelly [48], who extends the ridge regression concept as developed by Hoerl and Kennard [44] for navigation applications, the linear model for a system with an unknown n x 1 measurement bias vector, $\underline{\Delta B}$, and a measurement noise vector, $\underline{e}$, is given by

$$\underline{Y} = H\underline{\beta} + \underline{\Delta B} + \underline{e} \tag{5.17}$$

where $\underline{Y}$ is the n x 1 range measurement vector, $\underline{\beta}$ is the p x 1 unknown system state vector (or parameter vector), and H is the n x p predictor (or design) matrix which relates the range measurement vector to the system state vector. Also, the measurement noise is uncorrelated; $\text{cov}(\underline{e} + \underline{\Delta B}) = [\underline{e}\underline{e}^T] = \sigma^2 I$, where I is the n x n identity matrix. Recall that the OLS estimate of equation 5.17 is

$$\hat{\underline{\beta}}_{OLS} = (H^T H)^{-1} H^T \underline{Y} \tag{5.18}$$

The corresponding ridge estimate of equation 5.17 is

$$\hat{\underline{\beta}}_R = (H^T H + P_R)^{-1} H^T \underline{Y} \tag{5.19}$$

where P_R is the ridge parameter matrix (which is formed from the chosen κ parameters as will be seen in Section 5.2.4). When P_R consists of zeros, the ridge estimator reduces to the OLS estimator. Adding a non-zero ridge

ORDINARY LEAST SQUARES (OLS)

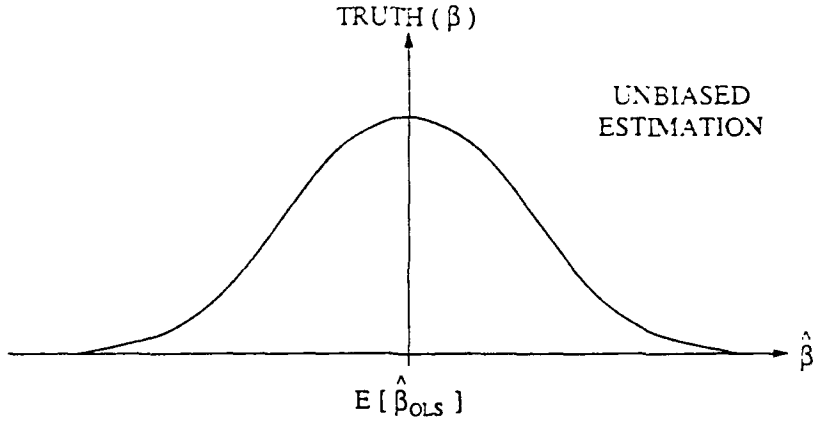

RIDGE REGRESSION

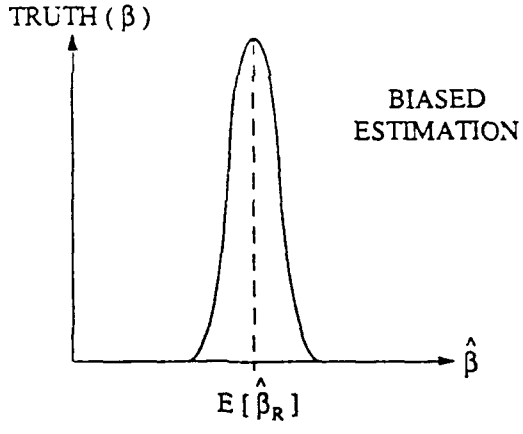

$$MSE = BIAS^2 + VARIANCE$$

02X 029 / 006 E38

Figure 5.2 Comparison of unbiased and biased solutions and definition of the MSE.

parameter matrix to H^TH purposely upsets the balance between the first and second moment components of $\hat{\underline{\beta}}$, thereby introducing a bias. Substituting equation 5.17 into equation 5.19 gives

$$\hat{\underline{\beta}}_R = G_\kappa H^T H\underline{\beta} + G_\kappa H^T\underline{\Delta B} + G_\kappa H^T\underline{e} \tag{5.20}$$

where $G_\kappa = (H^TH + P_R)^{-1}$. From equation 5.20 the expected value (or mean) of the ridge estimator is

$$E[\hat{\underline{\beta}}_R] = G_\kappa H^T H\underline{\beta} + G_\kappa H^T\underline{\Delta B} \tag{5.21}$$

The following relation is introduced

$$G_\kappa H^T H\underline{\beta} = \underline{\beta} - G_\kappa P_R\underline{\beta} \tag{5.22}$$

which will be used to rewrite equation 5.21. Equation 5.22 can be proven as follows

$$(G_\kappa H^TH)\underline{\beta} = (I - G_\kappa P_R)\underline{\beta}$$
$$H^TH = G_\kappa^{-1} - G_\kappa^{-1}G_\kappa P_R$$
$$H^TH = G_\kappa^{-1} - P_R$$
$$G_\kappa = (H^TH + P_R)^{-1}$$

Therefore, the expected value given by equation 5.21 may be rewritten as

$$E[\hat{\underline{\beta}}_R] = \underline{\beta} - G_\kappa P_R\underline{\beta} + G_\kappa H^T\underline{\Delta B} \tag{5.23}$$

Then, the ridge estimator's solution bias is seen to be

$$BIAS[\hat{\underline{\beta}}_R] = -G_\kappa P_R\underline{\beta} + G_\kappa H^T\underline{\Delta B} \tag{5.24}$$

The variance of the ridge estimator is

$$VAR[\hat{\underline{\beta}}_R] = \sigma^2 TRACE[G_\kappa^2 H^TH] \tag{5.25}$$

where the TRACE operator computes the sum of the diagonal terms of a matrix.

It can be shown that the bias term is a monotonically increasing function of κ while the variance term is a monotonically decreasing function of κ (see reference [35]). This implies that a κ value exists which will give a minimum MSE for the ridge estimator. (Recall that the MSE is defined as the sum of the variance term and the bias term squared.) Similar to the derivation of the MSE for the OLS estimator in Section 4.5, the MSE of $\hat{\underline{\beta}}_R$ is given by

$$MSE[\hat{\underline{\beta}}_R] = E[(\hat{\underline{\beta}}_R - \underline{\beta})^T(\hat{\underline{\beta}}_R - \underline{\beta})]$$
$$MSE[\hat{\underline{\beta}}_R] = E[(-G_\kappa P_R\underline{\beta} + G_\kappa H^T\underline{\Delta B} + G_\kappa H^T\underline{e})^T(-G_\kappa P_R\underline{\beta} + G_\kappa H^T\underline{\Delta B} + G_\kappa H^T\underline{e})]$$
$$MSE[\hat{\underline{\beta}}_R] = \underline{\beta}^T P_R^T G_\kappa^T G_\kappa P_R\underline{\beta} + \underline{\Delta B}^T H G_\kappa^T G_\kappa H^T\underline{\Delta B} - \underline{\beta}^T P_R^T G_\kappa^T G_\kappa H^T\underline{\Delta B} - \underline{\Delta B}^T H G_\kappa^T G_\kappa P_R\underline{\beta} + \sigma^2 TRACE[G_\kappa^T G_\kappa H^T H]$$

Since G_κ and P_R are symmetric matrices, their inner products are squares (i.e. $G_\kappa^T G_\kappa = G_\kappa^2$ and $P_R^T P_R = P_R^2$). This yields the following equation for the MSE

$$MSE[\hat{\underline{\beta}}_R] = \underline{\beta}^T G_\kappa^2 P_R^2\underline{\beta} - 2\underline{\beta}^T G_\kappa^2 P_R H^T\underline{\Delta B} + \underline{\Delta B}^T H G_\kappa^2 H^T\underline{\Delta B} + \sigma^2 TRACE[G_\kappa^2 H^TH] \tag{5.26}$$

Reference [35] proves that the MSE[$\hat{\underline{\beta}}_R$] is less than or equal to the MSE[$\hat{\underline{\beta}}_{OLS}$] based on a "slope argument": The slope of the above MSE equation can be shown to be negative at $\kappa = 0$. This implies that as κ becomes greater than zero, the MSE will decrease.

5.2.4 Selection of the Ridge Biasing Parameter Based on Geometry Conditions

The problem is to determine the range of κ_i values for which the MSE of the ridge estimator is smaller than the MSE of the OLS estimator [50]

$$MSE[\hat{\underline{\beta}}_R] - MSE[\hat{\underline{\beta}}_{OLS}] < 0 \tag{5.27}$$

The idea is to transform equation 5.27 into its canonical coordinates such that the proper selection of the κ_i parameters can clearly be seen. Canonical coordinates are obtained by implementing a singular value decomposition (SVD) of H

$$H^{nxp} = U^{nxn}\,\Sigma^{nxp}\,(V^T)^{pxp} \tag{5.28}$$

where U and V^T are defined as orthogonal transformation matrices that diagonalize H (i.e. make the measurements independent), and Σ is a diagonal matrix whose elements are the singular values of H, which are given by $\sqrt{\lambda_i}$. Also, $H^TH = V\Sigma^T\Sigma V^T$ where $\Sigma^T\Sigma$ is a p x p diagonal matrix with elements λ_i (the eigenvalues). Additionally, the relations $\underline{\alpha} = V^T\underline{\beta}$ and $\underline{\Delta\alpha} = U^T\underline{\Delta B}$ exist where V^T and U^T are used to transform the system state vector and measurement bias vector into their corresponding canonical vectors. The ridge parameter matrix is also expressed in terms of its canonical coordinates given by

$$P_R^c = V^TP_RV = \begin{bmatrix} \kappa_1 & & & 0 \\ & \kappa_2 & & \\ & & \ddots & \\ 0 & & & \kappa_p \end{bmatrix} \tag{5.29}$$

where P_R^c is a p x p diagonal matrix which permits a different ridge biasing parameter (κ_i) to be selected for each element of the canonical system state vector $\underline{\alpha}$.

In order to perform the transformation and rewrite equation 5.27 in terms of its canonical coordinates, first replace H with Σ, $\underline{\beta}$ with $V\underline{\alpha}$, $\underline{\Delta B}$ with $U\underline{\Delta\alpha}$, and P_R with P_R^c in the ridge estimator's MSE equation (equation 5.26)

$$\begin{aligned} MSE[\hat{\underline{\beta}}_R] &= (V\underline{\alpha})^T(\Sigma^T\Sigma + P_R^c)^{-2}P_R^{c2}(V\underline{\alpha}) - 2(V\underline{\alpha})^T(\Sigma^T\Sigma + P_R^c)^{-2}P_R^{c2}\Sigma^T(U\underline{\Delta\alpha}) \\ &\quad + (U\underline{\Delta\alpha})^T\Sigma(\Sigma^T\Sigma + P_R^c)^{-2}\Sigma^T(U\underline{\Delta\alpha}) + \sigma^2TRACE[(\Sigma^T\Sigma + P_R^c)^{-2}\Sigma^T\Sigma] \end{aligned}$$

Since Σ is diagonal, $\Sigma^T\Sigma = \Sigma^2$ and $\Sigma^T = \Sigma$. Since V and U are orthogonal matrices, then $V^TV = I$ and $U^TU = I$. This reduces the previous equation to

$$\begin{aligned} MSE[\hat{\underline{\beta}}_R] &= \underline{\alpha}^T(\Sigma^2 + P_R^c)^{-2}P_R^{c2}\underline{\alpha} - 2\underline{\alpha}^T(\Sigma^2 + P_R^c)^{-2}P_R^c\Sigma\underline{\Delta\alpha} \\ &\quad + \underline{\Delta\alpha}^T\Sigma(\Sigma^2 + P_R^c)^{-2}\Sigma\underline{\Delta\alpha} + \sigma^2TRACE[(\Sigma^2 + P_R^c)^{-2}\Sigma^2] \end{aligned}$$

Now, rewrite the above equation from its matrix form to its subscript form, given the fact that the diagonal elements of Σ^2 are given by λ_i and P_R^c are given by κ_i for i=1,p

$$MSE[\hat{\underline{\beta}}_R] = \sum_{i=1}^{p} \left[\frac{\kappa_i^2 \alpha_i^2}{(\lambda_i + \kappa_i)^2} - \frac{2\kappa_i \alpha_i \sqrt{\lambda_i} \Delta\alpha_i}{(\lambda_i + \kappa_i)^2} + \frac{\Delta\alpha_i^2 \lambda_i}{(\lambda_i + \kappa_i)^2} + \frac{\sigma^2 \lambda_i}{(\lambda_i + \kappa_i)^2} \right] \quad (5.30)$$

Similarly, perform the same manipulation on the MSE of $\hat{\underline{\beta}}_{OLS}$ given in Section 4.5

$$MSE[\hat{\underline{\beta}}_{OLS}] = \underline{\Delta B}^T H (H^T H)^{-2} H^T \underline{\Delta B} + \sigma^2 TRACE[(H^T H)^{-1}]$$
$$MSE[\hat{\underline{\beta}}_{OLS}] = (U\underline{\Delta\alpha})^T \Sigma (\Sigma^T \Sigma)^{-2} \Sigma^T (U\underline{\Delta\alpha}) + \sigma^2 TRACE[(\Sigma^T \Sigma)^{-1}]$$
$$MSE[\hat{\underline{\beta}}_{OLS}] = \underline{\Delta\alpha}^T \Sigma (\Sigma^2)^{-2} \Sigma \underline{\Delta\alpha} + \sigma^2 TRACE[(\Sigma^2)^{-1}]$$
$$MSE[\hat{\underline{\beta}}_{OLS}] = \underline{\Delta\alpha}^T \Sigma^{-2} \underline{\Delta\alpha} + \sigma^2 TRACE[\Sigma^{-2}]$$

$$MSE[\hat{\underline{\beta}}_{OLS}] = \sum_{i=1}^{p} \left[\frac{\Delta\alpha_i^2}{\lambda_i} + \frac{\sigma^2}{\lambda_i} \right] \quad (5.31)$$

Now, combining equations 5.30 and 5.31 into inequality 5.27 gives

$$\sum_{i=1}^{p} \left[\frac{\sigma^2 \lambda_i}{(\lambda_i + \kappa_i)^2} + \frac{\kappa_i^2 \alpha_i^2}{(\lambda_i + \kappa_i)^2} + \frac{\Delta\alpha_i^2 \lambda_i}{(\lambda_i + \kappa_i)^2} - \frac{2\kappa_i \alpha_i \sqrt{\lambda_i} \Delta\alpha_i}{(\lambda_i + \kappa_i)^2} - \frac{\Delta\alpha_i^2}{\lambda_i} - \frac{\sigma^2}{\lambda_i} \right] < 0 \quad (5.32)$$

Inequality 5.32 will be satisfied for each i if

$$\frac{\sigma^2 \lambda_i}{(\lambda_i + \kappa_i)^2} + \frac{(\kappa_i \alpha_i - \Delta\alpha_i \sqrt{\lambda_i})^2}{(\lambda_i + \kappa_i)^2} < \frac{\Delta\alpha_i^2}{\lambda_i} + \frac{\sigma^2}{\lambda_i} \quad (5.33)$$

Simplifying equation 5.33

$$\lambda_i(\sigma^2\lambda_i) + \lambda_i(\kappa_i\alpha_i - \Delta\alpha_i\sqrt{\lambda_i})^2 < (\lambda_i + \kappa_i)^2\Delta\alpha_i^2 + (\lambda_i + \kappa_i)^2)\sigma^2$$

$$\sigma^2\lambda_i^2 + \lambda_i(\kappa_i^2\alpha_i^2 - 2\kappa_i\alpha_i\sqrt{\lambda_i}\Delta\alpha_i + \Delta\alpha_i^2\lambda_i) - (\lambda_i^2 + 2\kappa_i\lambda_i + \kappa_i^2)\Delta\alpha_i^2$$
$$- (\lambda_i^2 + 2\kappa_i\lambda_i + \kappa_i^2)\sigma^2 < 0$$

$$\sigma^2\lambda_i^2 + \kappa_i^2\alpha_i^2\lambda_i - 2\kappa_i\alpha_i\sqrt{\lambda_i}\lambda_i\Delta\alpha_i + \Delta\alpha_i^2\lambda_i^2 - \Delta\alpha_i^2\lambda_i^2 - 2\kappa_i\lambda_i\Delta\alpha_i^2 - \kappa_i^2\Delta\alpha_i^2$$
$$- \sigma^2\lambda_i^2 - 2\kappa_i\lambda_i\sigma^2 - \kappa_i^2\sigma^2 < 0$$

$$\kappa_i^2\alpha_i^2\lambda_i - 2\kappa_i\alpha_i\sqrt{\lambda_i}\lambda_i\Delta\alpha_i - 2\kappa_i\lambda_i\Delta\alpha_i^2 - \kappa_i^2\Delta\alpha_i^2 - 2\kappa_i\lambda_i\sigma^2 - \kappa_i^2\sigma^2 < 0$$

$$\kappa_i(\lambda_i\alpha_i^2 - \Delta\alpha_i^2 - \sigma^2) - 2(\lambda_i\alpha_i\Delta\alpha_i\sqrt{\lambda_i} + \lambda_i(\Delta\alpha_i^2 + \sigma^2)) < 0$$

$$\downarrow \qquad\qquad\qquad \downarrow$$
$$a_1 \qquad\qquad\qquad a_2$$

Therefore,

$$a_1\kappa_i - 2a_2 < 0 \tag{5.34}$$

Thus for $\kappa_i > 0$

1. If $a_2 < 0$, $a_1 > 0$, there is no $\kappa_i > 0$ which satisfies 5.34 and $\kappa_i = 0$, the value for the OLS estimate.
2. If $a_2 > 0$, $a_1 < 0$, then 5.34 is satisfied for all $\kappa_i > 0$.
3. If $a_2 < 0$, $a_1 < 0$, then a "large" κ_i satisfies 5.34.
4. If $a_2 > 0$, $a_1 > 0$, then a "small" κ_i satisfies 5.34.

These restrictions on κ_i must be satisfied if the ridge estimator is to have a smaller MSE than the OLS estimator whenever a bias component $\underline{\Delta B}$, as well as a variance component σ^2 is inflated by near collinearity.

In practice, the vector $\underline{\alpha} = V^T\underline{\beta}$, which is unknown, is replaced by its estimate $\underline{\alpha}_{OLS} = V^T\hat{\underline{\beta}}_{OLS}$ in equation 5.34. Also required is some information about the vector $\underline{\Delta\alpha} = U^T\underline{\Delta B}$. Normally, for the position fixing problem, only nominal values of $\Delta\alpha_i$ are necessary because the selection of κ_i using 5.34 is not a strong function of $\Delta\alpha_i$ [49].

A procedure has been developed to properly choose the values of κ_i based on the geometry condition. The geometry condition is represented by the eigenvalues (λ_i) of $\bar{H}^T\bar{H}$. Poor geometry exists when the eigenvalues are small. As the eigenvalues become small, a biasing parameter (κ_i) is added. This limits the minimum value that the eigenvalues can obtain. But another restriction exists on the selection of the κ_i parameters. This is called a convergence criterion.

5.2.5 Selection of the Ridge Biasing Parameter Based on a Convergence Criterion

The selection of the ridge biasing parameter also depends on a convergence criterion. This convergence criterion becomes important when bias errors exist on the range measurements or when there is a large offset in the initial estimate of position.

5.2.5.1 Convergence Criterion when Range Measurement Bias Errors Exist

Given the fact that a poor geometry condition exists, the ridge estimator instantaneously reduces the variance inflation when noise errors exist on the range measurements. Additionally, when bias errors are on the range measurements, the ridge estimator initially reduces the bias inflation, but then grows with a certain time constant of convergence to the OLS inflated solution bias. This can be seen by performing the following analysis.

Recall that the bias of the ridge estimator is given by

$$\text{BIAS}[\hat{\underline{\beta}}_R] = -(H^TH + P_R)^{-1}P_R\underline{\beta} + (H^TH + P_R)^{-1}H^T\underline{\Delta B} \qquad (5.35)$$

Transforming this term into its canonical coordinates yields

$$\text{BIAS}[\hat{\underline{\beta}}_R]_i = -\frac{\kappa_i}{\lambda_i + \kappa_i}\alpha_i + \frac{\sqrt{\lambda_i}}{\lambda_i + \kappa_i}\Delta\alpha_i \qquad (5.36)$$

The second term of equation 5.36 counteracts the inflation of the measurement bias errors caused by poor geometry. By inserting a positive κ_i value, there is an initial shrinking of the solution bias. This can be seen more clearly by looking at the following example.

For $\lambda_i = 0.012$:

$$\text{OLS solution } (\kappa_i = 0): \quad \frac{\sqrt{\lambda_i}}{\lambda_i}\Delta\alpha_i = 9.13\Delta\alpha_i$$

$$\text{Ridge solution with } \kappa_i = 0.05: \quad \frac{\sqrt{\lambda_i}}{\lambda_i + \kappa_i} = 1.76\Delta\alpha_i$$

About a factor of 5 improvement in the solution bias can be expected <u>initially</u> by using the ridge estimator in this example. However, the ridge solution bias exponentially converges to the OLS solution bias as shown below.

Start with equation 5.36. Replace the two coefficients in equation 5.36 with C and D

$$\text{BIAS}[\hat{\underline{\beta}}_R]_i = -C\alpha_i + D\Delta\alpha_i \tag{5.37}$$

where $C = \dfrac{\kappa_i}{\lambda_i + \kappa_i}$ $\qquad D = \dfrac{\sqrt{\lambda_i}}{\lambda_i + \kappa_i}$

Now, assume only measurement bias errors exist, and propagate the bias errors ($\Delta\alpha_i$) into the position solution (α_i). Note that as a consequence of the ridge estimator, truth = - estimate (see equation 5.24 or 5.36). Perform iterations (n):

n=1: $\alpha_i = 0$, $\quad \text{BIAS}[\hat{\underline{\beta}}_R]_i = -C(0) + D\Delta\alpha_i = D\Delta\alpha_i$

n=2: $\alpha_i = -D\Delta\alpha_i$, $\quad \text{BIAS}[\hat{\underline{\beta}}_R]_i = -C(-D\Delta\alpha_i) + D\Delta\alpha_i = (C+1)D\Delta\alpha_i$

n=3: $\alpha_i = -(C+1)D\Delta\alpha_i$, $\quad \text{BIAS}[\hat{\underline{\beta}}_R]_i = -C(-(C+1)D\Delta\alpha_i) + D\Delta\alpha_i = (C^2+C+1)D\Delta\alpha_i$

$$n\to\infty: \qquad \text{BIAS}[\hat{\underline{\beta}}_R]_i = \frac{D}{1 - C}\,\Delta\alpha_i \tag{5.38}$$

where the $(1 - C)^{-1}$ term is the result of the geometric series given by $(C^{n-1} + C^{n-2} + \cdots + 1)$ as n goes to ∞. Now substituting the canonical terms back in for C and D in equation 5.38 yields

$$\text{BIAS}[\hat{\underline{\beta}}_R]_i = \frac{\dfrac{\sqrt{\lambda_i}}{\lambda_i + \kappa_i}}{1 - \dfrac{\kappa_i}{\lambda_i + \kappa_i}}\,\Delta\alpha_i$$

$$\text{BIAS}[\hat{\underline{\beta}}_R]_i = \frac{1}{\sqrt{\lambda_i}}\,\Delta\alpha_i \quad \rightarrow \text{ "final value"} \tag{5.39}$$

Note that κ_i drops out. Therefore, when measurement bias errors exist, the ridge solution bias converges to the OLS solution bias as the number of iterations goes to ∞. The associated time constant of convergence will be derived below.

Again looking at the iterative process that formed equation 5.38, it can be seen that the ridge estimator's solution bias exponentially increases to the OLS estimator's bias. This is portrayed in Figure 5.3. Figure 5.3 shows that after 1 iteration (1n), the ridge solution bias converges to within about 37% of the OLS solution bias. (After 2 iterations the ridge solution bias is within 14% of the OLS solution bias.) For the ridge estimator, a time constant (τ) can be defined as the time it takes to converge within about e^{-1} or 37% of the "final value", which in this case is the OLS solution bias. To find the time constant of convergence, consider iteration n

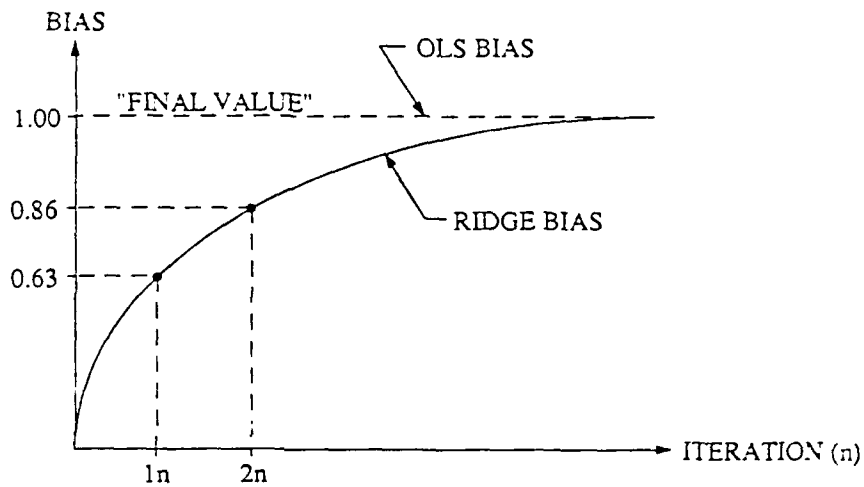

$$(1 - e^{-1}) = 0.63$$

$$(1 - e^{-2}) = 0.86$$

$$(1 - e^{-\infty}) = 1.00$$

02X 029 / 008 E38

Figure 5.3 Exponential increase of the ridge estimator's solution bias to the OLS estimator's solution bias.

$$\text{BIAS}[\hat{\beta}_R]_i = \frac{1 - C^n}{1 - C} D\Delta\alpha_i \tag{5.40}$$

Let the $\text{BIAS}[\hat{\beta}_R]_i$ given by equation 5.40 be called an "initial value". Determine for which n will

$$\frac{\text{"initial value"}}{\text{"final value"}} = 1 - e^{-1} = 0.63 \tag{5.41}$$

$$\frac{\left[\frac{1 - C^n}{1 - C} D\Delta\alpha_i\right]}{\left[\frac{1}{1 - C} D\Delta\alpha_i\right]} = 0.63$$

$$1 - C^n = 0.63$$

$$C^n = 0.37$$

$$\ln[C^n] = \ln[0.37]$$

$$n(\ln[C]) = -1$$

$$n = -(\ln[C])^{-1} \tag{5.42}$$

Replacing C in equation 5.42 with the canonical term it represents

$$n = -\left[\ln\left[\frac{\kappa_i}{\lambda_i + \kappa_i}\right]\right]^{-1} \tag{5.43}$$

Then, the time constant of the ridge solution bias convergence to the OLS solution is given by

$$\tau_{BC} = \Delta T_m \left[-\ln \left[\frac{\kappa_i}{\lambda_i + \kappa_i} \right] \right]^{-1} \qquad (5.44)$$

where ΔT_m is the update interval time. As a special note, reference [35] shows that even increasing the number of range measurements available for determining a position fix will not decrease the solution bias inflation caused by poor geometry.

5.2.5.2 Convergence Criterion when a Large Initial Offset Exists

In order to define a convergence criterion for the selection of κ_i values when a large initial offset is present, again consider the bias term of the ridge estimator

$$\text{BIAS}[\hat{\underline{\beta}}_R] = -(H^TH + P_R)^{-1}P_R\underline{\beta} + (H^TH + P_R)^{-1}H^T\underline{\Delta B} \qquad (5.45)$$

To simplify the analysis, assume that no measurement bias errors exist, ($\underline{\Delta B}$ = 0), therefore

$$\text{BIAS}[\hat{\underline{\beta}}_R] = -(H^TH + P_R)^{-1}P_R\underline{\beta} \qquad (5.46)$$

Transforming this term into its canonical coordinates yields

$$\text{BIAS}[\hat{\underline{\beta}}_R]_i = - \frac{\kappa_i}{\lambda_i + \kappa_i} \alpha_i \qquad (5.47)$$

Based on equation 5.47, a system response time constant (τ_{SR}) may be defined by implementing a similar procedure to the one given in Section 5.2.5.1. The result is identical.

5.2.6 Ridge Recursive Filter Development

So far, ridge regression has been presented using batch processing, whose exposition is easier to follow than a recursive presentation. Section 5.1.1 points out that the performance of the batch and recursive presentation is equivalent. A procedure for using ridge regression to explain the behavior of the Kalman filter will now be discussed.

Similar to the derivation of the recursive Kalman filter in Section 5.1.2, obtain the state update equation (equation 5.7) in ridge form [51]

$$\hat{\underline{\beta}}_{Rk} = (P^{-1}_{k/k-1} + P_{Rk} + H_k^TR^{-1}H_k)^{-1}(P^{-1}_{k/k-1}\hat{\underline{\beta}}_{Rk/k-1} + H_k^TR^{-1}\underline{y}_k) \qquad (5.48)$$

where the ridge parameter matrix, P_{Rk}, has been added to counteract the effects of an ill-conditioned ($H_k^TR^{-1}H_k$) term (which is caused by poor geometry).

Extending the work done by Kelly [51], equation 5.48 can be linearized using equation 5.13 from Section 5.1.3 to obtain the linearized state update

equation

$$\hat{\underline{\beta}}_{Rk} = \hat{\underline{\beta}}_{Rk/k-1} + (P^{-1}_{k/k-1} + P_{Rk} + H_k^T R^{-1} H_k)^{-1}(H_k^T R^{-1} \delta \underline{Y}_k) \qquad (5.49)$$

where P_{Rk} has been added to the $(P^{-1}_{k/k-1} + H_k^T R^{-1} H_k)$ term in order to reduce the effects of near collinearity. Equation 5.49 forms the basis for the extended Ridge/Kalman filter. Also, the update equation for the error covariance matrix is given by

$$P_k = (P^{-1}_{k/k-1} + P_{Rk} + H_k^T R^{-1} H_k)^{-1} \qquad (5.50)$$

Two cases may now be defined in which ridge regression can explain the behavior of the Kalman filter. First, in the absence of system dynamics, the ridge parameter matrix, P_{Rk}, is functionally equivalent to the state error covariance matrix, $P_{k/k-1}$. Therefore, the EKF has similar convergence properties (equation 5.44) when the model incorrectly represents the system and $P_{k/k-1}$ is small. Second, if dynamics exist, P_{Rk} is related to both $P_{k/k-1}$ and the system error covariance matrix, Q, given by the following relation

$$(\Phi P_k \Phi^T + Q)^{-1} \text{ - } (\Phi P_k \Phi^T + Q)^{-1} + P_{Rk} \qquad (5.51)$$

where in this case, the - symbol means "relating to". Again, the EKF has similar convergence properties when the model incorrectly represents the system and $(\Phi P_k \Phi^T + Q)^{-1}$ is small.

Usually P_k is small, which means that the $P^{-1}_{k/k-1}$ term in equation 5.49 is large; therefore, there is no collinearity problem. Note that P_k varies as the Kalman filter is updated, but normally a constant Q is added which "limits" it (i.e. puts uncertainty in the model). As seen in the above equation, P_k will be large when Q is large. Q is chosen large for dynamic situations (i.e. turn-induced accelerations). When a poor geometry condition exists in addition to the dynamic situation, P_{Rk} may be added to counteract the large Q. Therefore, a proper P_{Rk} can be chosen to incorporate ridge regression into the Kalman filter.

The procedure recommended for implementing ridge regression theory into the Kalman filter depends upon three different situations [49]:

(1) The GDOP is small, therefore $H_k^T R^{-1} H_k$ is well-conditioned. $Q_{k/k-1}$ is chosen to match the model's process noise covariance in the usual way. $\hat{\underline{\beta}}_k$ is unbiased.

(2) The GDOP is large, therefore $H_k^T R^{-1} H_k$ is ill-conditioned. But $(P^{-1}_{k/k-1} + H_k^T R^{-1} H_k)$ is well-conditioned. Do nothing. The estimator is matched to the model and $\hat{\underline{\beta}}_k$ is unbiased.

(3) The GDOP is large and $H_k^T R^{-1} H_k$ is ill-conditioned. $P_{k/k-1}$ is identified in the usual way and $(P^{-1}_{k/k-1} + H_k^T R^{-1} H_k)$ is also ill-conditioned because the elements of $P^{-1}_{k/k-1}$ are not large enough to remove the near collinearity. The ridge parameter matrix, P_{Rk}, is chosen to reduce the near collinearity of $(P^{-1}_{k/k-1} + H_k^T R^{-1} H_k)$ using the selection rules given by equation 5.34.

Situations (1) and (2) are optimized in the usual way, i.e. choosing $P_{k/k-1}$ in the filter such that the innovations are white. Situation (3), on the other hand, minimizes the MSE by applying equation 5.34 to determine P_{Rk}.

When situation (3) occurs, only the values of $P^{-1}_{k/k-1}$ are adjusted by adding P_{Rk}. In summary, the optimization procedure for situation (3) is:

1. Identify $P_{k/k-1}$ and determine $\hat{\underline{\beta}}_{OLS}$.

2. Calculate $\hat{\underline{\alpha}}_{OLS} = V^T\hat{\underline{\beta}}_{OLS}$ and $\underline{\Delta\alpha} = U^T\underline{\Delta B}$. Note that since the measurement bias error $\underline{\Delta B}$ is unknown, it must be approximated.

3. Insert the calculation results from step 2 into equation 5.34 to obtain κ_i for i = 1,2, ... p. (This gives P^c_{Rk}.)

4. Using V^T, form P_{Rk} from P^c_{Rk} using equation 5.34 and add P_{Rk} to $(P^{-1}_{k/k-1} + H^T_k R^{-1} H_k)$ to make it well-conditioned.

The key idea in developing the ridge recursive filter is the following: Each step in the recursive process is viewed as a new prior linear model wherein the last estimate $\hat{\underline{\beta}}_{Rk/k-1}$ is the prior equation for the next iteration. The ridge solution is recomputed at each step using the above selection rules to determine a proper P_{Rk}.

6. MULTISENSOR NAVIGATION SOLUTION AND INTEGRITY

6.1 Multisensor Navigation Solution

Navigation measurement data can be expressed in terms of range or bearing with respect to a reference station, as discussed in Chapter 2. The relation between the measurement data and the user position is nonlinear, as shown by the following two measurement equations:

$$\text{Range:} \quad R_i = ((X-X_i)^2 + (Y-Y_i)^2)^{1/2} \tag{6.1}$$

$$\text{Bearing:} \quad \theta_i = \arctan\{(X-X_i)/(Y-Y_i)\} \tag{6.2}$$

where (X,Y) is the user position, (X_i,Y_i) is the location of reference station i, R_i is the range between the user and reference station i, and θ_i is the bearing of the user with respect to reference station i measured clockwise with respect to North, see also Figure 2.2. Another widely used measurement is the time difference (TD) between the time of arrivals of signals from two different reference stations. The TD defines a hyperbolic line-of-position and the measurement equation is given by:

$$\text{TD:} \quad TD_{ij} = b - R_i + R_j \tag{6.3}$$

where b is the length of the baseline between station i and j, and R_i, R_j are given by equation 6.1.

To obtain a position solutions, equations 6.1 through 6.3 are usually linearized with respect to some reference point $(\hat{X},\hat{Y})$, the *a priori* estimate. Following the linearization procedure presented in Section 4.4.1, equations 6.1 through 6.3 can be linearized as follows.

$$\delta R_i = \begin{bmatrix} \dfrac{\hat{X} - X_i}{R_i} & \dfrac{\hat{Y} - Y_i}{R_i} \end{bmatrix} \begin{bmatrix} \delta X \\ \delta Y \end{bmatrix} \tag{6.4}$$

$$\delta\theta_i = \begin{bmatrix} \dfrac{\hat{Y} - Y_i}{R_i^2} & \dfrac{X_i - \hat{X}}{R_i^2} \end{bmatrix} \begin{bmatrix} \delta X \\ \delta Y \end{bmatrix} \tag{6.5}$$

$$\delta TD_{ij} = \begin{bmatrix} \dfrac{\hat{X} - X_j}{R_j} - \dfrac{\hat{X} - X_i}{R_i} & \dfrac{\hat{Y} - Y_j}{R_j} - \dfrac{\hat{Y} - Y_i}{R_i} \end{bmatrix} \begin{bmatrix} \delta X \\ \delta Y \end{bmatrix} \tag{6.6}$$

Equations 6.4 through 6.6 relate a change in the user position to a change in the range, bearing, and time difference measurements, respectively. In general, each of these equations is of the form:

$$\delta y_i = h_i \, [\delta X \; \delta Y]^T \tag{6.7}$$

where h_i is the row vector corresponding to measurement number i, given by y_i. Equation 6.7 can be written to include all the different measurements as follows.

$$\delta \underline{Y} = H \, \delta \underline{\beta} \tag{6.8}$$

where $\underline{Y}$ is the measurement vector, $\underline{\beta}$ is the user state vector, and H is the matrix containing the row vectors given by h_i. Equation 6.8 can be used directly in a recursive estimator such as the least squares estimator or an extended Kalman filter, as discussed in Section 5.1.3.

The presence of an unknown variable in either of the above measurement equations adds another variable to the user state vector $\underline{\beta}$. For instance, if a range measurement contains an unknown clock phase offset, then the corresponding pseudorange measurement equation is given by:

$$\text{Pseudorange:} \qquad R_i = ((X-X_i)^2 + (Y-Y_i)^2)^{1/2} + B \tag{6.9}$$

where B is the unknown clock phase offset. The linearized measurement equation is then given by:

$$\delta PR_i = \begin{bmatrix} \dfrac{\hat{X} - X_i}{R_i} & \dfrac{\hat{Y} - Y_i}{R_i} & 1 \end{bmatrix} \begin{bmatrix} \delta X \\ \delta Y \\ \delta B \end{bmatrix} \tag{6.10}$$

Similar expansions can be developed for other unknowns, e.g. velocity and acceleration, which are to be determined simultaneously with the position solution. This concludes the development of a unified solution for a multisensor position solution.

6.2 Multisensor Integrity

A multisensor navigation system has many redundant measurements available to perform fault detection and isolation (FDI), which is also referred to as receiver autonomous integrity monitoring (RAIM). The basic idea is to use the inconsistency in the measurement data to derive failure detection and isolation parameters. The next section presents a derivation of the least squares residual vector which is commonly used for FDI. The least squares residual method does not rely on the history of the measurement data; it is based on a "snapshot" least squares solution. The use of this method is justified for several reasons:

1. The main purpose of the least squares residual method is to detect slowly growing measurement errors which do not grow rapidly enough to be detected by an input data editor. (An input data editor would simply reject measurement data which gives rise to large residuals).

2. Filtering of the measurement data could reduce the false alarm rate; however, for GPS, the measurement errors are dominated by Selective Availability which has a correlation time on the order of minutes. Also, the least squares solution still allows for some variance reduction by averaging over several measurements.

3. No matter what kind of estimator is used, the position bias error caused by measurement bias errors will always converge to the position bias error of the least squares estimator as shown in Chapter 5. In almost all cases, the time constant of convergence is short compared to the slow error growth of a difficult to detect measurement error.

4. Integrity information must be available soon after receiver start-up or re-start.

5. The integrity performance of filtered data is difficult to guarantee under dynamic conditions.

6.2.1 The Least Squares Residual Vector

With reference to Section 4.2 and Figure 4.1, the Projection Theorem yields the ordinary least squares (OLS) estimator given by

$$\hat{\underline{\beta}} = (H^T H)^{-1} H^T \underline{Y} = \hat{\underline{\beta}}_{OLS} \tag{6.11}$$

Multiplying equation 6.11 by H yields

$$H\hat{\underline{\beta}} = H(H^T H)^{-1} H^T \underline{Y} \tag{6.12}$$

$$\hat{\underline{Y}} = P\underline{Y} \tag{6.13}$$

where the projection matrix $P = H(H^T H)^{-1} H^T$ projects the measurement vector $\underline{Y}$ onto the estimation space defined by the column space of H. Therefore, the rank of P for an overdetermined system is equal to the number of unknowns in the user state vector $\underline{\beta}$. This projection finds the closest point on the estimation space with respect to $\underline{Y}$ by constructing a perpendicular line from $\underline{Y}$ to the column space of H, see Figure 4.1.

The least squares residual vector $\underline{e}_R$, also referred to as the error vector, is given by

$$\underline{e}_R = \underline{Y} - \hat{\underline{Y}} = \underline{Y} - P\underline{Y} = (I - P)\underline{Y} \tag{6.14}$$

where (I - P) is also a projection matrix, it projects any vector $\underline{Y}$ onto the orthogonal complement of the estimation space. The rank of (I - P) is equal to the degrees of freedom of the overdetermined system. For instance, consider the GPS solution which requires 4 measurements. If 6 measurements are available, then the rank of (I - P) is equal to 2. This also means that the number of rows of the (I - P) matrix can be reduced to 2.

The expected value of $\underline{e}_R$ is

$$E[\underline{e}_R] = (I - P)\, E[\underline{Y}] = (I - P)\underline{\Delta B} \tag{6.15}$$

where $\underline{\Delta B}$ is a vector containing bias errors present in the measurements. The covariance matrix of $\underline{e}_R$ is

$$\begin{aligned} COV[\underline{e}_R] &= E[\underline{e}_R \underline{e}_R^T] = E[(I - P)\underline{e}\underline{e}^T (I - P)^T] \\ &= (I - P)\, COV[\underline{e}]\, (I - P) \end{aligned} \tag{6.16}$$

where $\underline{e}$ is a vector which represents zero-mean measurement noise. Note that

$(I - P)^T = (I - P)$, which is one of the basic properties of a projection matrix. The second property of a projection matrix is that $(I - P)^2 = (I - P)$; a projection followed by the same projection does not change the result from the first projection. If the measurement noise is uncorrelated and normally distributed with equal variances, then the covariance of the measurement noise is

$$COV[\underline{e}] = \sigma^2 I \tag{6.17}$$

where σ is the standard deviation of the measurement noise. It then follows that the covariance of the error vector is

$$COV[\underline{e}_R] = \sigma^2(I - P) \tag{6.18}$$

Using the Projection Theorem, the error vector $\underline{e}_R$ is easily obtained, as given by equation 6.14. This error vector is widely used for failure detection and isolation, see for instance references [52, 53, 54].

Following reference [55], the above general solution can be expanded to include a weighting matrix W to represent the relative importance of the measurements. The weighted least squares estimate is obtained by

$$\hat{\underline{\beta}}_W = (H^T W H)^{-1} H^T W \underline{Y} \tag{6.19}$$

where W is a positive definite weighting matrix. The best unbiased weighting matrix is given by the inverse of the covariance matrix of the measurement vector [55]

$$W = (COV[\underline{Y}])^{-1} \tag{6.20}$$

Again, the projection $H\hat{\underline{\beta}}_W$ onto the estimation space and the error $(\underline{Y} - H\hat{\underline{\beta}}_W)$ are perpendicular. It then follows that the new projection matrix is given by

$$P_W = H(H^T W H)^{-1} H^T W \tag{6.21}$$

and the weighted error vector is given by

$$\underline{e}_{RW} = (I - P_W)\underline{Y} \tag{6.22}$$

6.2.2 Fault Detection and Isolation Using the Least Squares Residual Vector

Once the least squares residual vector or error vector has been obtained, several methods are available to perform the failure detection and isolation. References by Parkinson and Axelrad [52] and by Sturza [53] use the square of the magnitude of the error vector as the basis for the decision variable

$$D = \underline{e}_R^T \underline{e}_R \tag{6.23}$$

If the measurements are normally distributed with the same variance σ^2, then the normalized decision variable

$$D_n = D/\sigma^2 \tag{6.24}$$

has a chi-square distribution with rank(I - P) degrees of freedom. If the

measurements have nonzero means, then D_n has a noncentral chi-square distribution. The noncentral chi-square distribution and calculation methods for this distribution are documented in references [52, 53].

If the degrees of freedom, m, is greater than one, the decision variable, D, could be scaled by the degrees of freedom. Reference [52] suggests the use of the range residual parameter r for the test statistic or integrity parameter:

$$r = \sqrt{(D/m)} = \sqrt{(\underline{e}_R^T \underline{e}_R/m)} \qquad (6.25)$$

This particular integrity parameter has also been adopted for the baseline scheme contained in the document "Minimum Operational Performance Standards for Supplemental Airborne Navigation Equipment Using GPS" [15]. Other integrity parameters have been suggested, see for instance references [54, 56, 57, 58, 59, 60].

Next, the integrity parameter must be compared with a threshold, T. If the threshold is exceeded, a fault is detected, otherwise, no fault is detected. The performance of the integrity algorithm can be expressed in terms of two probabilities:

Probability of a false alarm: $P_{FA} = P(r>T \mid \text{no fault})$
Probability of a missed detection: $P_{MD} = P(r<T \mid \text{fault})$

Chapter 3 lists the preliminary requirements for supplemental navigation using GPS for these probabilities: $P_{FA} < 0.002/Hr$; and $P_{MD} < 0.001$ on a per sample basis. For GPS, it is generally assumed that independent samples are available every 2 minutes (correlation time of Selective Availability). It then follows that the $P_{FA} < 0.000067$ on a per sample basis. From reference [53], the threshold T must be set at approximately $\sqrt{(16.6\sigma^2)}$ for the case of one degree of freedom. Assuming a standard deviation of approximately 30 meters, the threshold T = 122 meters. If the standard deviation of the measurement noise is 100 meters, the threshold T = 407 meters.

To satisfy the probability of a missed detection for GPS, it follows from reference [53] that the radial protection error has to be increased to approximately 1500 meters, rather than the 550 meters required for nonprecision approaches. It should be noted that the performance of the integrity algorithm would improve if more measurements are available. However, not all these measurements are required for positioning and FDI, the question remains if all measurements have to be included in the FDI process. Also, other detection techniques have been proposed which claim to perform better than the above method [54]. Further studies are recommended to analyze the performance of several integrity techniques, and to quantify the performance of specific multisensor systems, such as GPS/LORAN.

In addition to fault detection, several techniques have been proposed to perform fault isolation, such as the maximum likelihood estimation approach [53], comparison of detection thresholds based on different subsets [52], and coordinate changes to maximize the visibility of a certain measurement error [54]. A detailed study of these techniques is outside the scope of this report, but is required to address the issue of sole means navigation. Therefore, further studies are also recommended in this area.

7. PROTOTYPE HYBRID GPS/LORAN RECEIVER

7.1 Hardware Configuration

The block diagram of the hardware configuration for the prototype hybrid GPS/LORAN receiver is shown in Figure 7.1. A four-channel GPS receiver (Motorola, model Eagle) and an eight-channel LORAN-C receiver (Advanced Navigation, Inc., Model 5300), both employing continuous tracking, are used to collect GPS and LORAN-C data. Only the raw measurement data from both receivers is used to determine the position solution. The two receivers are interfaced to a microcomputer (model AT) through two serial communication ports. The microcomputer is also interfaced to a course deviation indicator (CDI, model KI 206), through a parallel port, to display the guidance data to the pilot. All of the hardware used is commercially available equipment, except for the interface between the microcomputer parallel port and the CDI instrument, which was designed and implemented at Ohio University.

7.2 Software Algorithms

The software modules implemented on the hybrid GPS/LORAN receiver are executed in realtime. The algorithm is given by:

```
initialization
WHILE in operation
      DO once per second
            check for keyboard input data
            IF keyboard input data
                  process keyboard data
            END
            check for GPS and LORAN-C measurement data, and
                  request LORAN-C data
            IF sufficient data
                  calculate position
                  determine integrity
            END
            update CDI and status screen
            store all relevant data
      END
END
system shut-down
```

7.2.1 Initialization

During initialization, the following tasks are performed:

1. Open the GPS/LORAN initialization data file.
2. Read the following data from the initialization data file:
   a. GPS ephemerides
   b. LORAN-C transmitter locations
   c. LORAN-C propagation data
   d. Waypoints
   e. Position estimate
   f. Integrity threshold

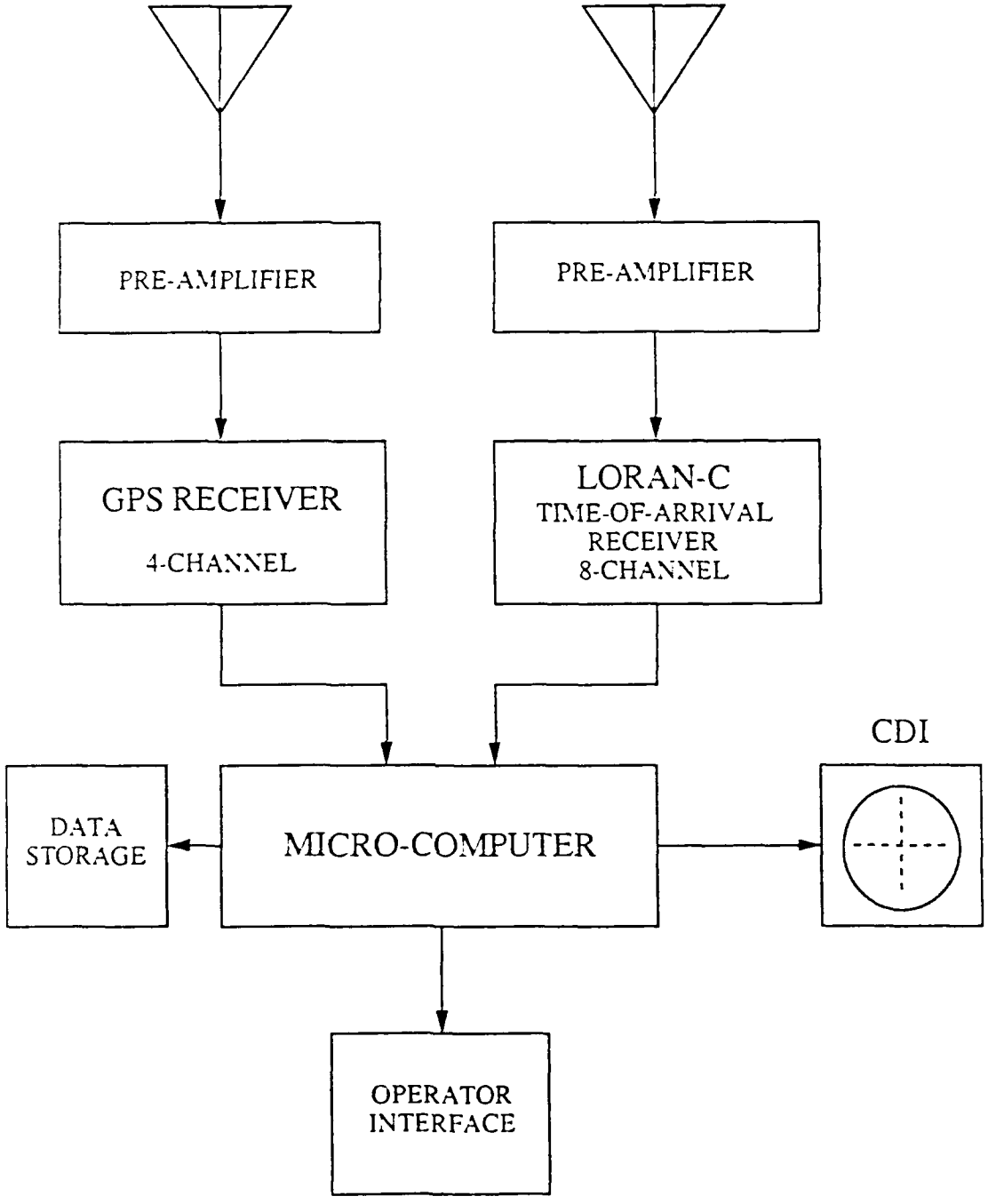

Figure 7.1 Hardware configuration of the prototype hybrid GPS/LORAN receiver.

g. CDI centering and offset corrections
h. Ephemeris threshold (for comparison of old and new ephemeris data)

3. Close the GPS/LORAN initialization data file.
4. Open the GPS/LORAN output file.
5. Install serial communication interrupt service routines.
6. Output the status screen.

7.2.2 Check For and Process Keyboard Input Data

The keyboard input buffer is checked for input data. If input data is present, the data is read and processed according to the list of possible commands given in Table 7.1.

Command	Action
Q	Initiate receiver shut-down.
Wxy	Waypoint, from x to y, where x,y = 0,1, ... ,9.
Fmx	Inject failure into signal number m; x is the failure type
	x = A, a 100 meter step failure
	x = B, a 1,000 meter step failure
	x = C, a 10,000 meter step failure
	x = D, a 1 m/s ramp failure
	x = E, a 2 m/s ramp failure
	x = F, a 3 m/s ramp failure
	x = G, a 4 m/s ramp failure
	x = H, a 5 m/s ramp failure
	x = I, a 10 m/s ramp failure
	x = J, a 25 m/s ramp failure
	x = K, a 50 m/s ramp failure
	x = L, a 100 m/s ramp failure
R	Reset injected failure to zero.
A	Set CDI scale to ±1.25 nmi (approach mode).
E	Set CDI scale to ±5.00 nmi (enroute mode).
C	Clear the display.

Table 7.1 List of keyboard commands for the GPS/LORAN receiver.

7.2.3 Check for GPS and LORAN-C Measurement Data, and Request LORAN-C Data

During system initialization, the GPS receiver is commanded to send measurement date at a rate of once per second. As soon as GPS data is received, a LORAN-C measurement trigger command must be sent to ensure that the LORAN-C data is valid at the same time as the GPS data. Following the measurement trigger command, LORAN-C data is requested and collected for up to eight receiver channels. All data is verified for validity as indicated by the receivers. If at least five measurements are valid, sufficient data is available for the position calculation. The five measurements are used to solve for three-dimensional position, clock offset with respect to GPS time, and clock offset with respect to LORAN-C time. The number of required measurements could be reduced to four if the GPS and LORAN-C receivers measure

the time-of-arrivals with respect to the same clock, and if the hardware delays of both receivers are known. A minimum of six valid measurements are required to execute the integrity algorithm.

7.2.4 Calculate Position

The hybrid position solution is based on a least-squares solution. The GPS and LORAN-C measurements are equally weighted. Reference [4] contains a detailed description of the algorithm used. Since the measurements from GPS and LORAN-C are equally weighted, the accuracy of the hybrid system will be mostly determined by the LORAN measurements. For this effort, standard LORAN propagation models are used such that the achieved accuracies are representative for current LORAN receivers. Because of this, the accuracy of the hybrid system will not be as good as that provided by GPS; however, the availability and integrity of the hybrid system exceeds that of GPS by several orders of magnitude [4]. At the same time, the hybrid system accuracies are still well within the current requirements. The accuracy of the hybrid GPS/LORAN system can be improved upon significantly through one or more of the following methods:

1. Use of a weighting matrix W to incorporate the statistical knowledge of the measurements (see Section 6.1);

2. Calibration of LORAN using validated GPS positions;

3. Use of improved LORAN propagation models which could contain seasonal correction data based on the LORAN-C monitor network.

Especially the latter two methods are very promising, these methods have the potential to achieve LORAN measurement accuracies very close to those provided by GPS [4, 8, 61, 62, 63]. The effects on the integrity performance of the first method is not well understood at this time. Further efforts are recommended with respect to each of the above methods to improve the accuracy of hybrid GPS/LORAN.

7.2.5 Determine Integrity

Integrity is calculated using the range residual parameter given by equation 6.25 in Chapter 6. It should be noted that the performance of this particular integrity scheme does not fully demonstrate the integrity capabilities of a hybrid GPS/LORAN system. For instance, the LORAN-C system will have its own integrity monitor (also known as aviation blink), which is anticipated to be fully operational by 1992. At that time, the main function of the receiver autonomous integrity monitor for LORAN would be to detect rare occurrences of receiver cycle slip. One of the purposes of this effort, however, is to evaluate the range residual parameter technique, which is the baseline RAIM scheme proposed in reference [15].

7.2.6 Update CDI and Status Screen

The current "from" and "to" waypoints are used to calculate the course deviation to be displayed to the pilot. The CDI needle deviation is scaled according to the phase of flight; ±1.25 nmi for the nonprecision approach, and

±5 nmi for enroute navigation. The results of the integrity calculation are used to drive the CDI flag. The status screen is used to monitor the performance of the GPS/LORAN receiver, and to observe the numerical effects of the injection of signal failures. Parameters of interest include: current time, position estimate, GPS satellites and LORAN transmitters being used, current waypoints, injected failure type and magnitude, CDI value, integrity parameter and integrity flag.

7.2.7 Store all Relevant Data

All data collected from the GPS and the LORAN-C receiver is recorded on a flexible disk. This data allows for a complete flight evaluation in the laboratory environment, see also Chapter 8.

7.2.8 System Shut-Down

During system shut-down, the following tasks are performed:

1. Close the GPS/LORAN output file.
2. Save all new ephemeris data collected during the run.
3. Remove serial communication interrupt service routines.

7.3 Prototype GPS/LORAN Receiver Installation

The prototype GPS/LORAN receiver is installed in a Piper Saratoga PA-32-301, N8238C, which is owned by Ohio University. The N8238C is a 1980 model aircraft with a fixed landing-gear, and a useful load capacity of 1,537 pounds. The aircraft is equipped as a flying laboratory.

The GPS antenna/pre-amplifier is mounted on top of the fuselage at a distance of approximately 4 feet from the front windshield. The antenna/pre-amplifier is 4.5 inches square, and 2.5 inches high. Located in the top of the pre-amplifier is a micro-strip antenna. A one-foot slanted LORAN antenna is also mounted on top of the fuselage, approximately 8 feet back from the GPS antenna. Both antennas are connected to the corresponding receivers which are located in an equipment rack together with the microcomputer. This equipment rack replaces one of the passenger seats in the back of the airplane. The microcomputer is also connected to a KI 206 course deviation indicator mounted in the primary view of the pilot. The equipment is connected to the aircraft power system, which provides 14 Volts and 28 Volts DC; and 110 Volts AC through a solid state power invertor. The prototype receiver can be installed in less than one hour.

8. POST-FLIGHT REAL TIME GPS/LORAN SIMULATOR

A post-flight real time simulator has been developed to support the design and evaluation of the GPS/LORAN receiver. The simulator consists of a microcomputer which simulates the GPS and LORAN receivers based on previously collected flight data. Figure 8.1 shows the block diagram of the simulator configuration. The flight data is read by the simulator computer program and transmitted over two serial ports following the same protocols as those employed by the GPS and LORAN receivers. Initially, the simulator used data which was collected in September of 1988 [4]. This data includes several turns and data outages. Based on this data, the real time software could be fully exercised in the laboratory environment. This proved to be a very powerful approach, since several potential problems were corrected before the actual flight tests. These problems ranged from incorrect ephemeris information obtained from the GPS receiver to numerical problems due to the injection of large signal failures.

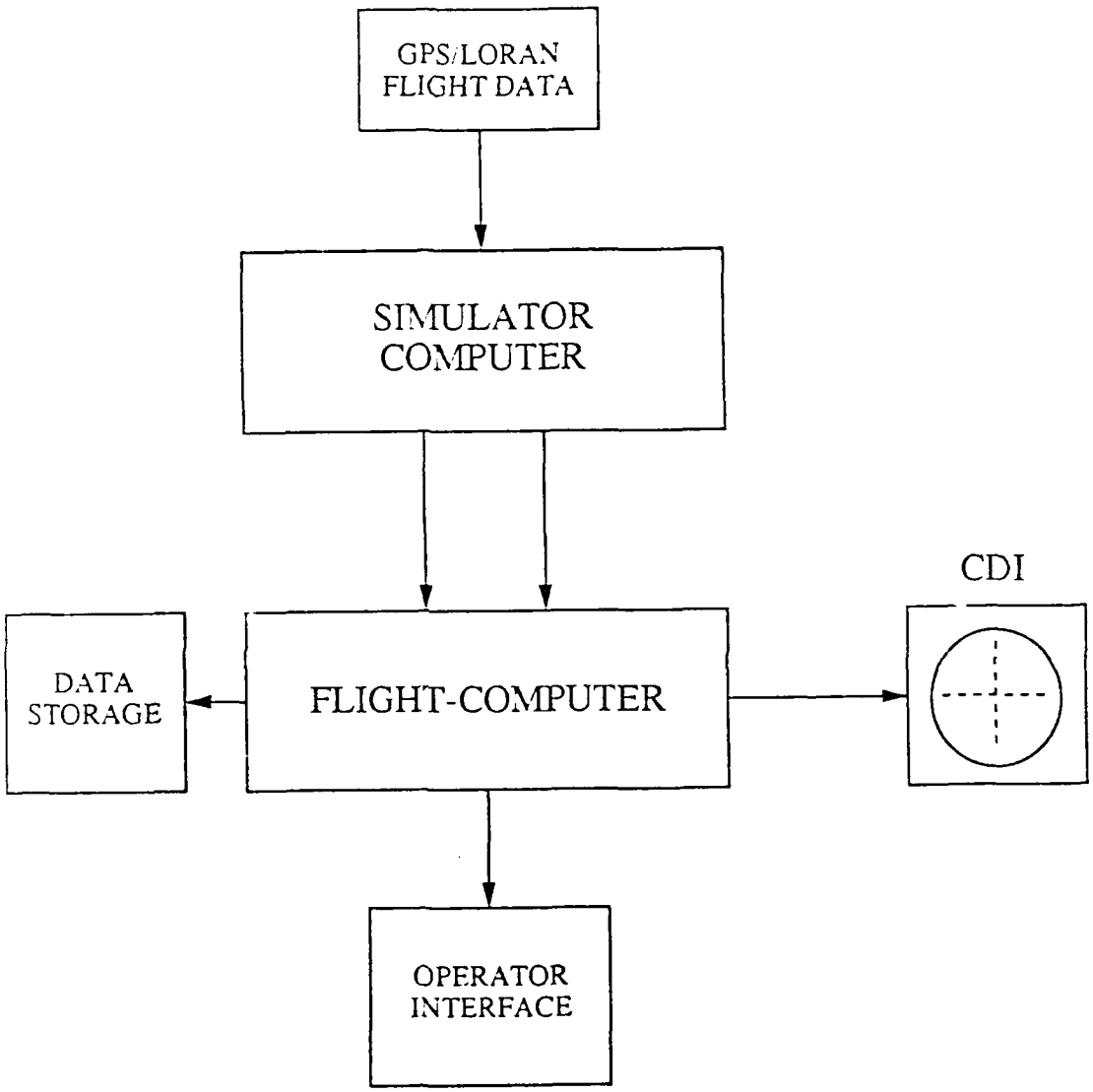

Figure 8.1 Post-flight real time GPS/LORAN simulator block diagram.

9. LABORATORY TESTING OF THE GPS/LORAN RECEIVER USING FLIGHT DATA

GPS/LORAN flight data collected on September 16, 1988 was used to evaluate the realtime hybrid GPS/LORAN software. This particular set of flight data was chosen because a differential GPS (DGPS) reference trajectory is available. The DGPS trajectory is based on GPS flight data corrected for known GPS errors as determined by a GPS reference station. This reference station consists of a GPS receiver and processing equipment. The accuracy of the DGPS system is better than 10 meters (2 drms) [4]. This level of accuracy qualifies DGPS very well for a truth reference system for the evaluation of navigation results where the highest accuracy requirement is 100 m (2 drms). Reference [4] describes the DGPS system used for this study in detail.

Figure 9.1 shows the two-dimensional position errors as a function of time, and Figure 9.2 shows the corresponding scatter plot. The flight lasted for approximately 70 minutes. Two relatively large discontinuities in the data are caused by the exchange of flexible disks and by a system restart. The system was restarted to evaluate the re-acquisition of the navigation signals during operational conditions. A few smaller discontinuities are the result of satellite switching by the airborne GPS receiver. During satellite switching, the receiver temporarily enters an altitude-hold mode. The accuracy of the resulting differential reference trajectory is then no longer determined, and consequently, the trajectory cannot be used for the evaluation of the hybrid GPS/LORAN receiver. Note that the hybrid receiver can still continue to provide a solution based on the three remaining satellites and two or more LORAN-C transmitters.

The largest position errors occur during the middle of the flight. These deviations are caused be a relatively poor GPS geometry. Also, all sudden changes in the magnitude of the two-dimensional error are caused by transitions to different sets of four GPS satellites. The horizontal position accuracy for the hybrid system, based on all measurements (785 data points), is 210 meters (2 drms), with respect to the DGPS trajectory. The mean position errors in the North and East directions were found to be -52 meters and 30 meters, respectively. The 2 drms positioning accuracy is well within all current requirements for enroute navigation (2778 m), terminal navigation (2037 m), and nonprecision approaches (556 m).

Next, the performance of the integrity algorithm was addressed. A straight-line section of the flight data was used which lasted for approximately 400 seconds. During this time, a 50 meters per second ramp error was simulated on one of the measurements, as depicted in Figure 9.3. The actual value of the ramp is not important for the performance of the detection algorithm, since the algorithm takes "snapshots" of the measurement data. The ramp error was repeated for all seven measurements, which consisted of four GPS satellites: SV6, SV9, SV11, and SV12; and three LORAN stations: Carolina Beach, Dana, and Seneca. Figures 9.4 and 9.5 show the resulting horizontal radial position errors and the integrity or range residual parameters. The integrity parameter corresponds to $\underline{e}_R$ in Figure 4.1.

In the absence of malfunctions, both the integrity parameter and the horizontal radial position error are well below 200 m. In the case of GPS or Dana malfunctions, the integrity parameter grows faster than the corresponding radial position error. However, both Seneca and Carolina Beach malfunctions cause the radial position error to grow rather rapidly. Detection of these malfunctions is still possible as indicated by Figure 9.4,

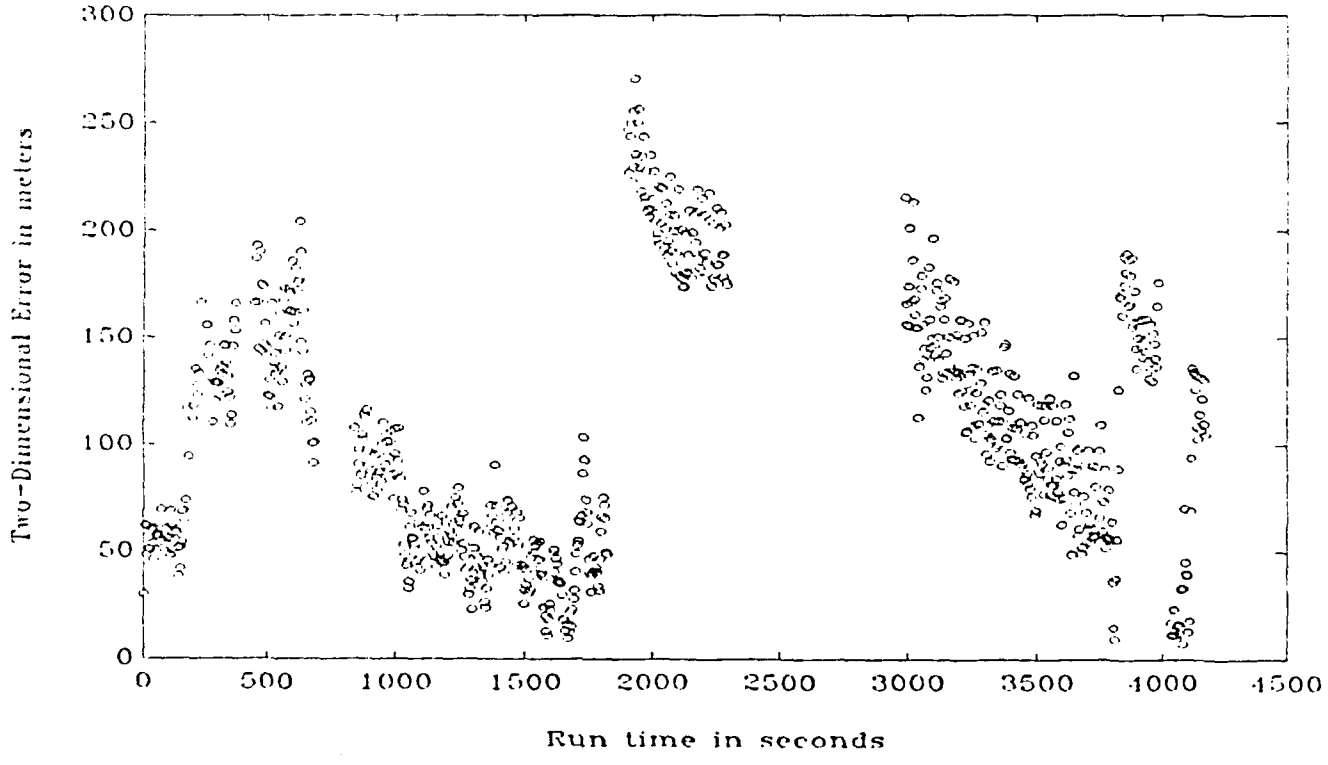

Figure 9.1 Hybrid GPS/LORAN two-dimensional position errors.

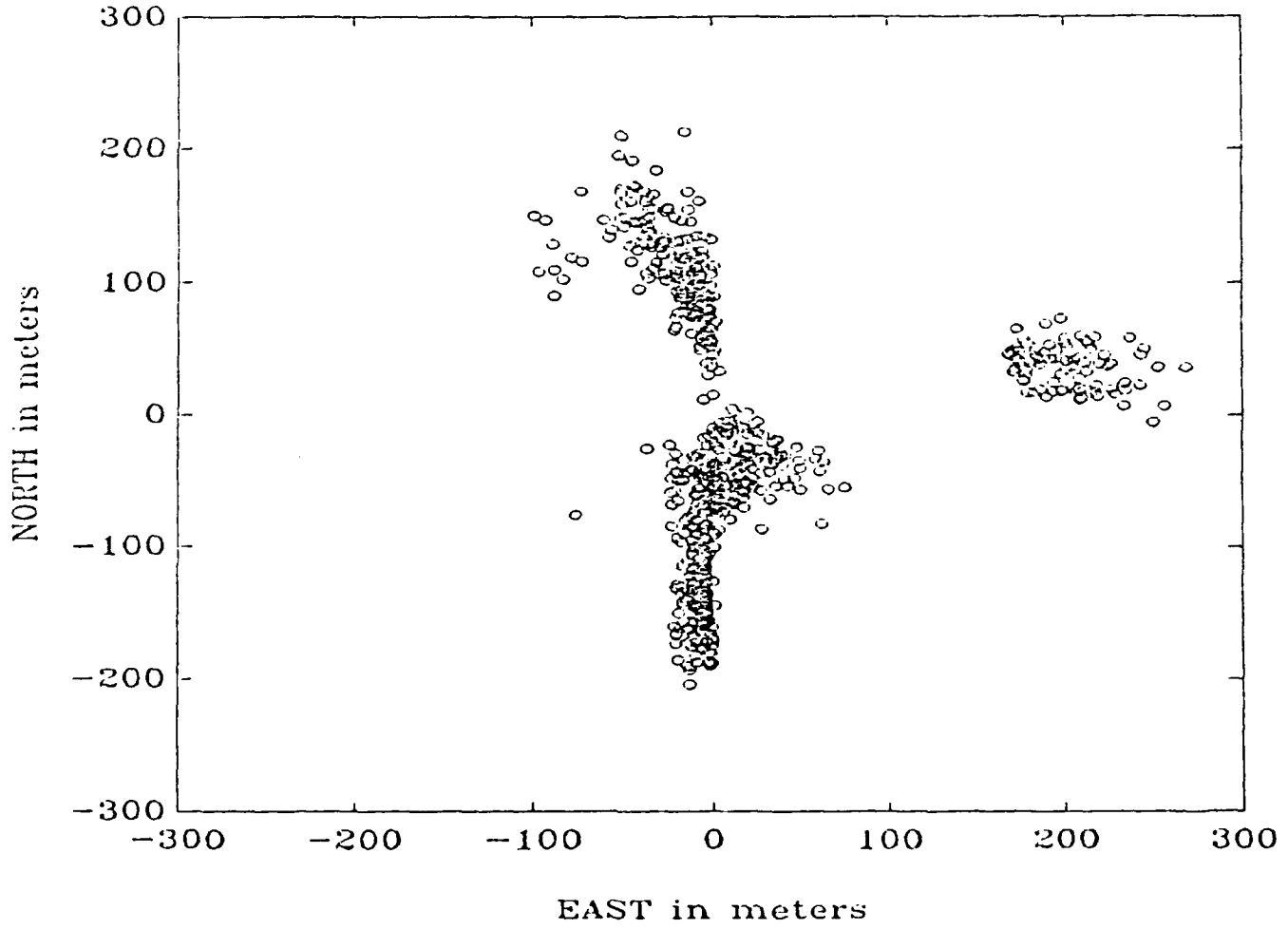

Figure 9.2 Scatter plot of hybrid GPS/LORAN two-dimensional position errors.

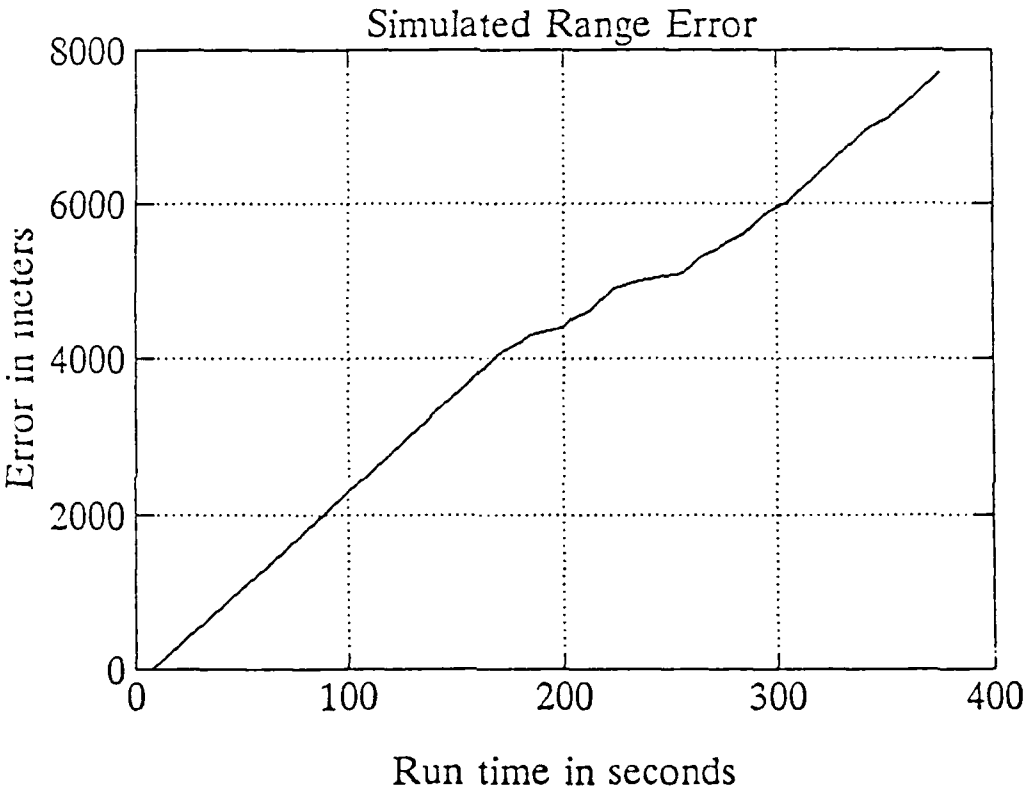

Figure 9.3 Simulated 50 meters per second ramp failure.

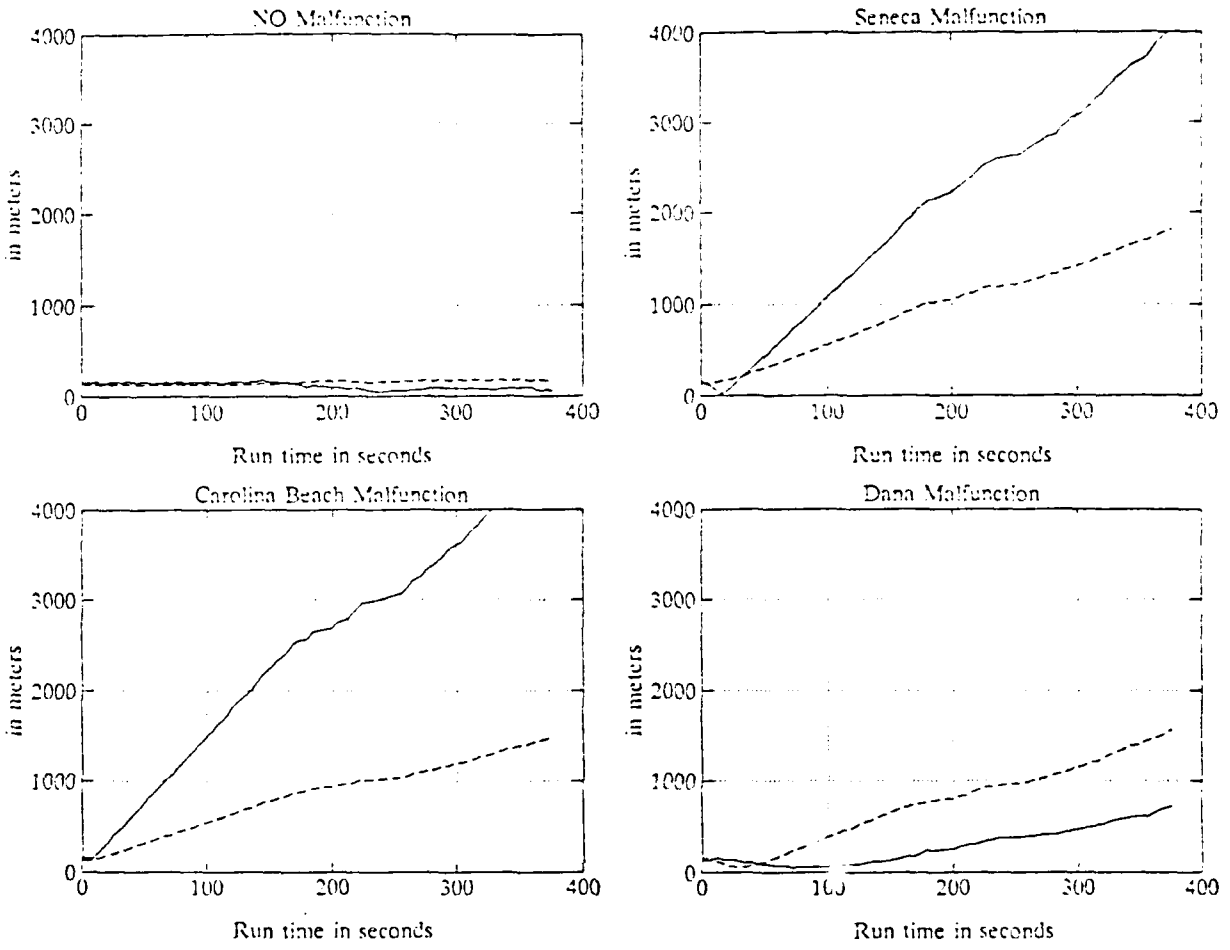

——— Horizontal Radial Position Error

– – – Integrity Parameter (range residuals)

Figure 9.4 Horizontal radial position error and integrity parameter for a simulated 50 meters per second ramp failure.

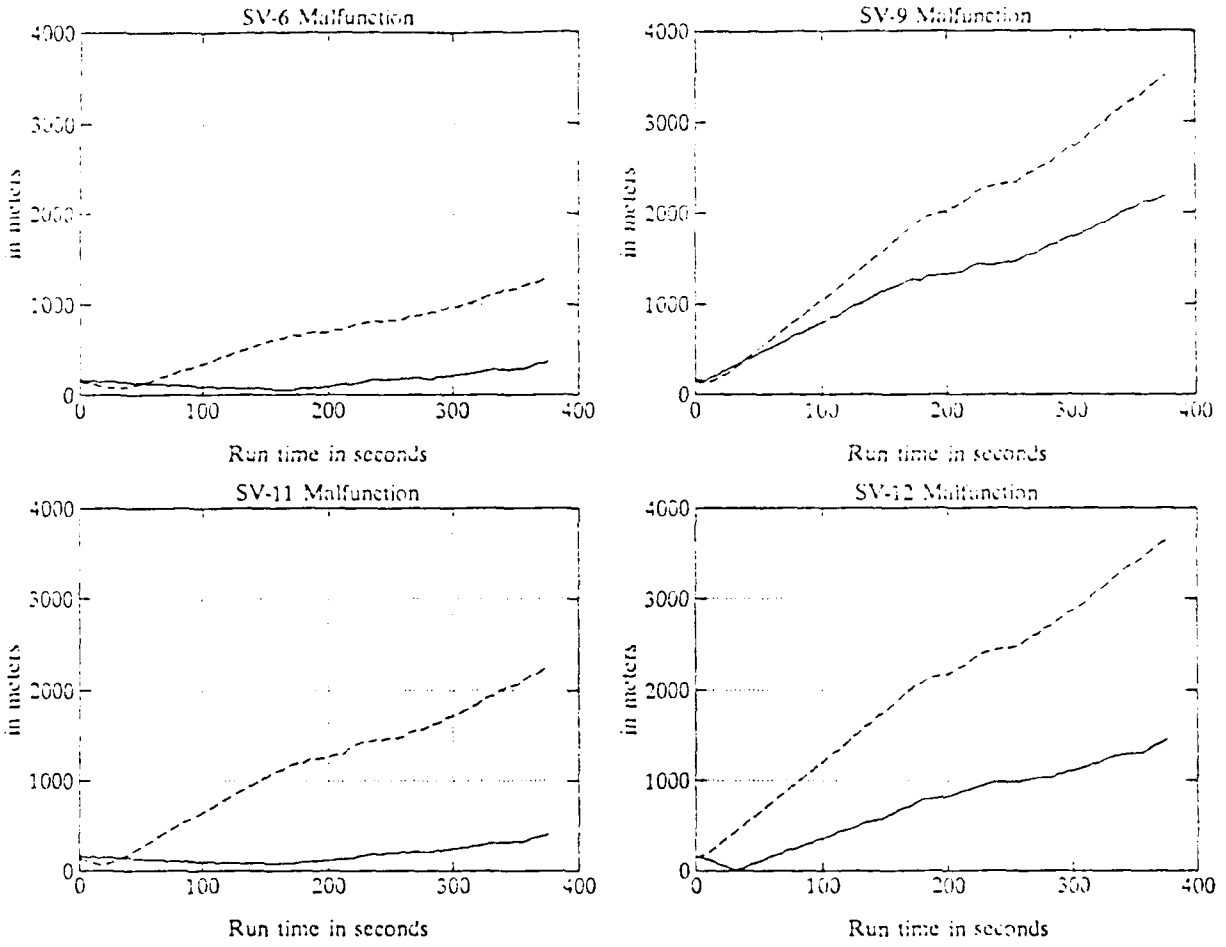

——— Horizontal Radial Position Error

– – – Integrity Parameter (range residuals)

Figure 9.5 Horizontal radial position error and integrity parameter for a simulated 50 meters per second ramp failure.

but the threshold for the integrity parameter must be set much lower than for all other cases.

Further analysis of the measurement geometries for all the cases depicted in Figures 9.4 and 9.5 explains the larger sensitivity to Seneca and Carolina Beach malfunctions. The measurement geometry is shown in Figure 9.6, where the arrows represent the line-of-sight vectors to the GPS satellites and the LORAN transmitters projected onto the horizontal plane and normalized. The horizontal dilutions of precision (HDOP) for the all-in-view solution and for each of the sub-sets are given in Table 9.1.

Solution	HDOP
All-in-view	1.08
Sub-set without Seneca	1.94
Sub-set without Carolina Beach	2.17
Sub-set without Dana	1.65
Sub-set without Satellite 6	1.14
Sub-set without Satellite 9	1.15
Sub-set without Satellite 11	1.14
Sub-set without Satellite 12	1.13

Table 9.1 Horizontal dilutions of precision (HDOP) for the all-in-view solution and for each of the sub-sets.

From Figure 9.6 and Table 9.1 it can be seen that the solutions without Seneca and Carolina Beach significantly affect the remaining geometry. For both cases, the HDOP without either Seneca or Carolina Beach is approximately twice as large as the all-in-view solution. This means that a measurement error in either of these signals has a much larger effect on the horizontal radial position error than any of the other five signals, which is clearly shown by Figures 9.4 and 9.5.

In addition to the effects of geometry, Figures 9.4 and 9.5 also show the effects of initial bias errors in the measurements. In some of the cases, the integrity parameter initially decreases, which indicates that the injected failure compensates for the measurement error. As expected, this also corresponds to a smaller radial position error. After 10 to 20 seconds, however, all measurement error has been compensated for by the injected error, and the integrity parameter will steadily grow.

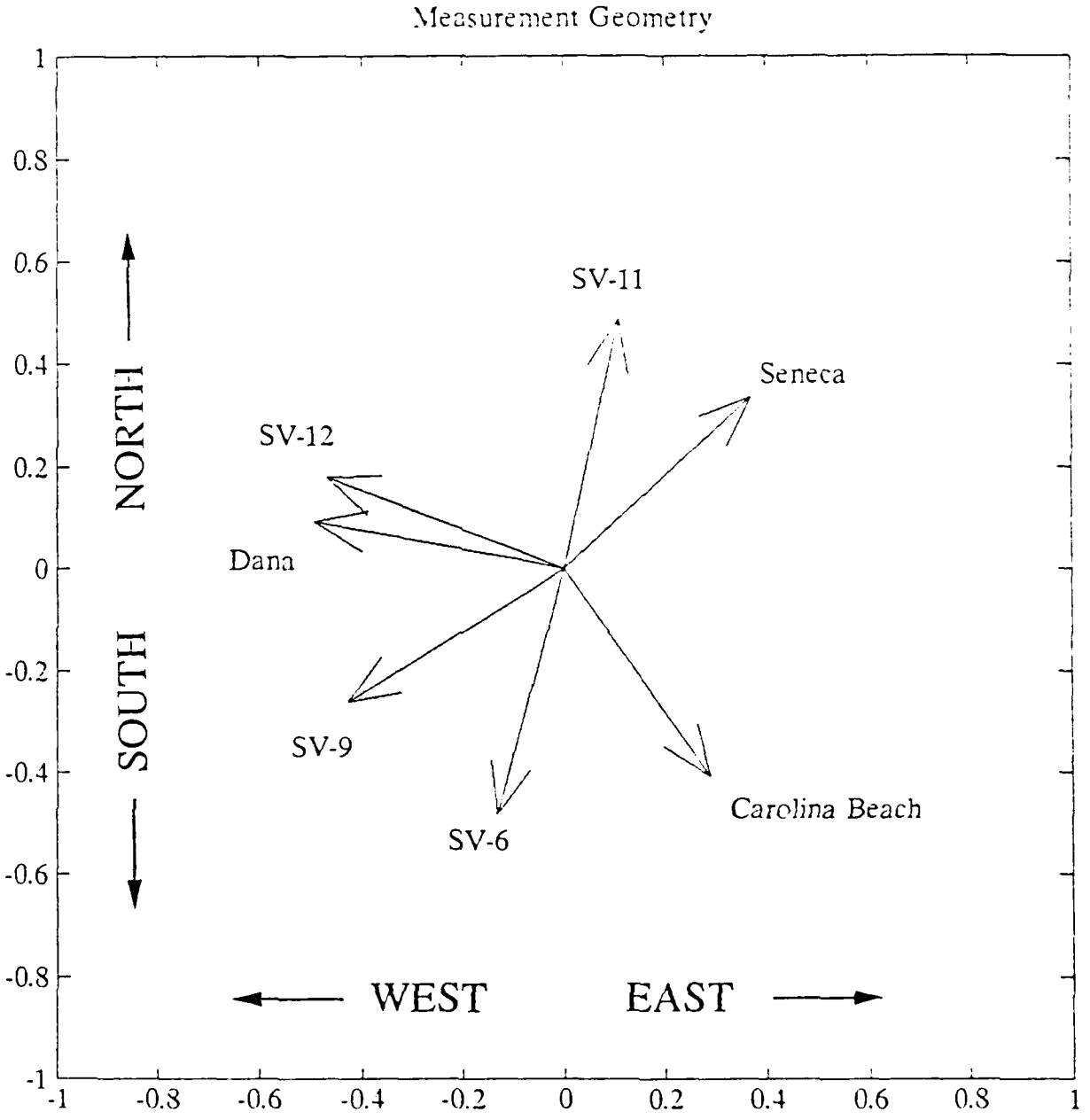

Figure 9.6 GPS/LORAN measurement geometry.

10. FLIGHT TESTING OF THE GPS/LORAN RECEIVER

The prototype hybrid GPS/LORAN receiver has been flight tested on two occasions at the time of this writing. The first flight test occurred on August 21, 1990; and the second flight test took place on August 23, 1990. Both flight tests were performed in the vicinity of the Ohio University airport at Albany, Ohio. The duration of flight number one was approximately 34 minutes, and the duration of flight number two was approximately 52 minutes. Figures 10.1 and 10.2 show the ground tracks for the two flight tests. The ground tracks reflect the simulated signal malfunctions; both flight tracks contain many flight path deviations caused by the injection of simulated signal malfunctions. Tables 10.1 and 10.2 list the sequence of events for each of the flight tests. The emphasis of the flight tests was on the following two items:

1. Operational verification of a realtime hybrid GPS/LORAN receiver.

2. Preliminary assessment of the flight technical error and the impact of failure modes.

Based on the flight tests, it was apparent that the hybrid GPS/LORAN receiver performed in accordance with its design. Both test pilots noted that the course deviation indicator is very responsive and that the indicated course compares favorably with other area navigation equipment. Also, cross-checks with DME, VOR, NDB, and the ILS localizer indicated that the GPS/LORAN horizontal accuracy is on the order of 0.1 nmi. This compares well with the laboratory results provided in Chapter 8, which are based on flight data collected under similar circumstances.

The flight technical error is the accuracy with which the aircraft is controlled as measured by the indicated aircraft position with respect to the indicated command or desired position. Only the cross-track portion of the flight technical error is used for analysis purposes. (The cross-track error is identical to the signal send to the course deviation indicator). The analysis of the flight technical error is very preliminary. Because of instrument meteorological conditions (IMC) during take-off and landing, the GPS/LORAN course could not be flown. Also, both pilots were briefed about the nature of the flight experiment and they were specifically instructed to fly the CDI as closely as possible. Nevertheless, the FTE error traces in terms of the CDI deviations for both flights are shown in Figures 10.3 and 10.4. Note that for flight number one, the full-scale CDI deflection is ±5 nmi (enroute guidance) or ±1.25 nmi (approach). Both test pilots found a smaller full-scale CDI deflection nmi desireable for the enroute mode. Therefore, flight number two used ±2.5 nmi for the enroute guidance and ±1.25 for the approach mode. Both pilots utilized an ILS localizer approach to runway 25 at the end of the mission. As a result, the latter part of the FTE traces is not representative for the GPS/LORAN FTE; however, it is a good indication of the GPS/LORAN cross-track error. For both flights, the GPS/LORAN cross-track error is of the order of 0.1 nmi. Since the offset is the same for both flights, it is most likely caused by uncorrected LORAN propagation delays and secondary station clock offsets. The spikes in the FTE traces are either caused by waypoint switching or by the injection of step failures. These do not reflect the ability of the pilot to fly the indicated GPS/LORAN course. Because of the capability of the GPS receiver to always know the exact value of the FTE, a study is recommended to investigate the effects of flagging a nonprecision approach based on a FTE of such magnitude that the approach

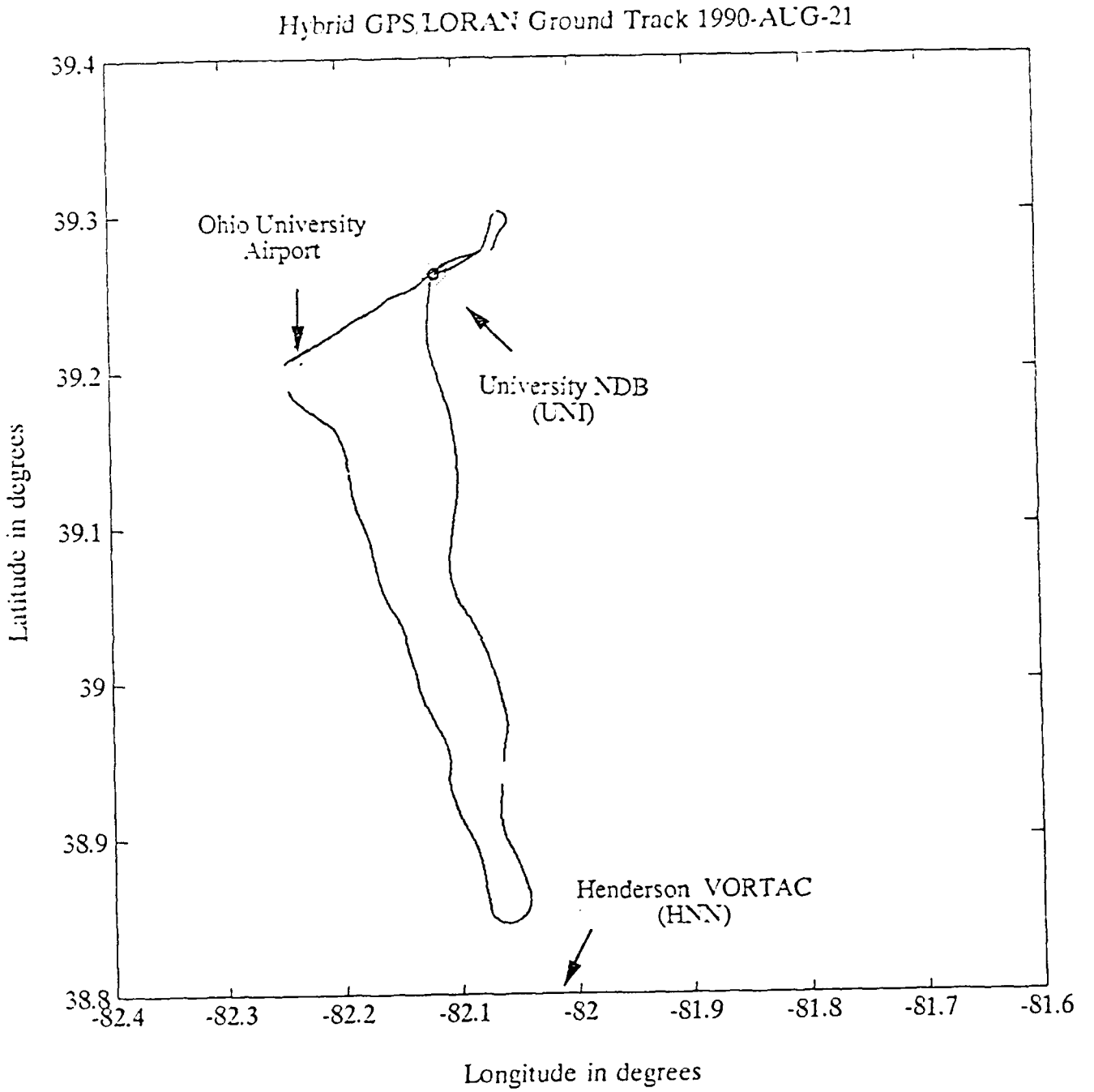

Figure 10.1 Hybrid GPS/LORAN ground track for flight one, August 21, 1990.

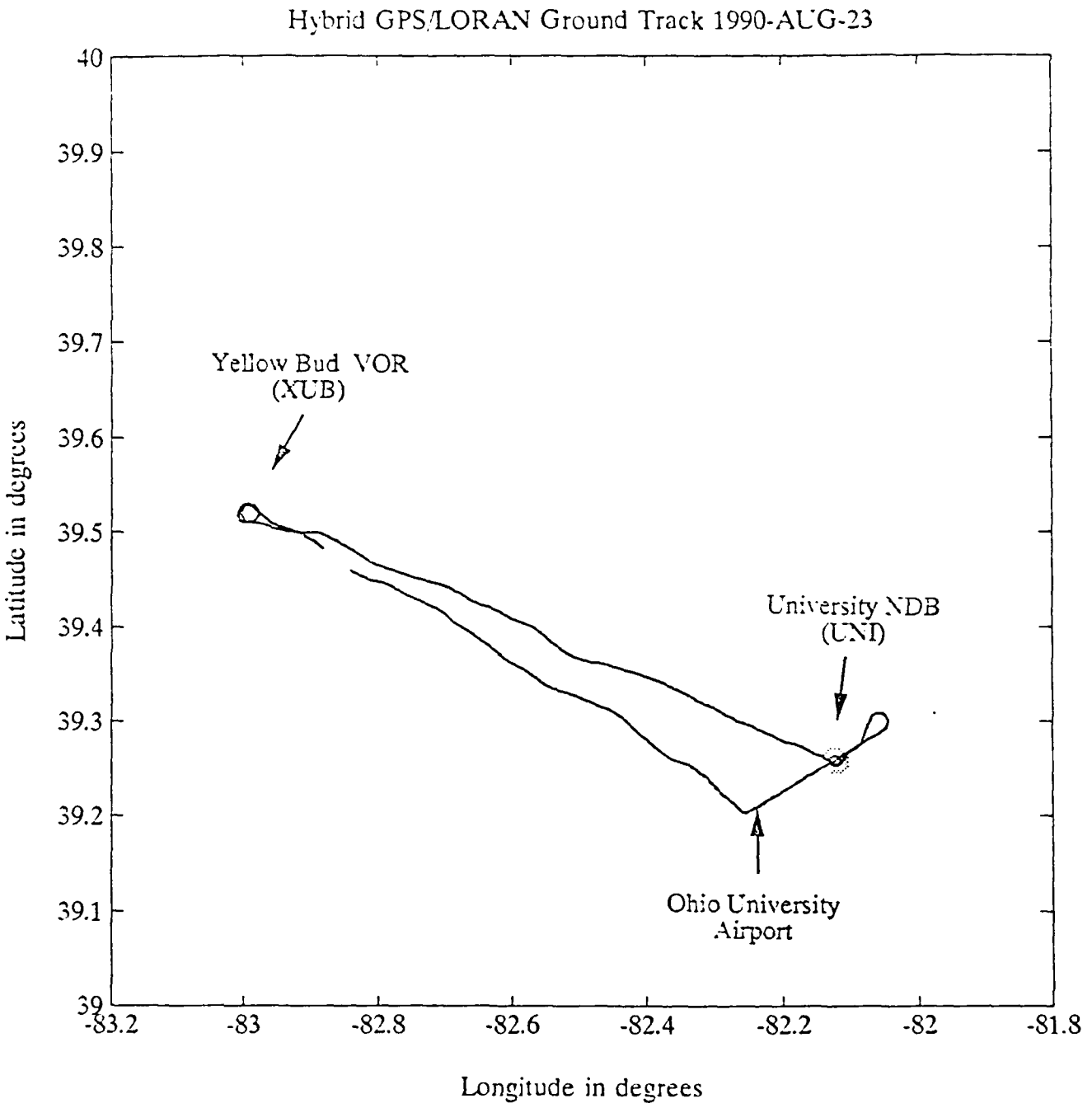

Figure 10.2 Hybrid GPS/LORAN ground track for flight two, August 23, 1990.

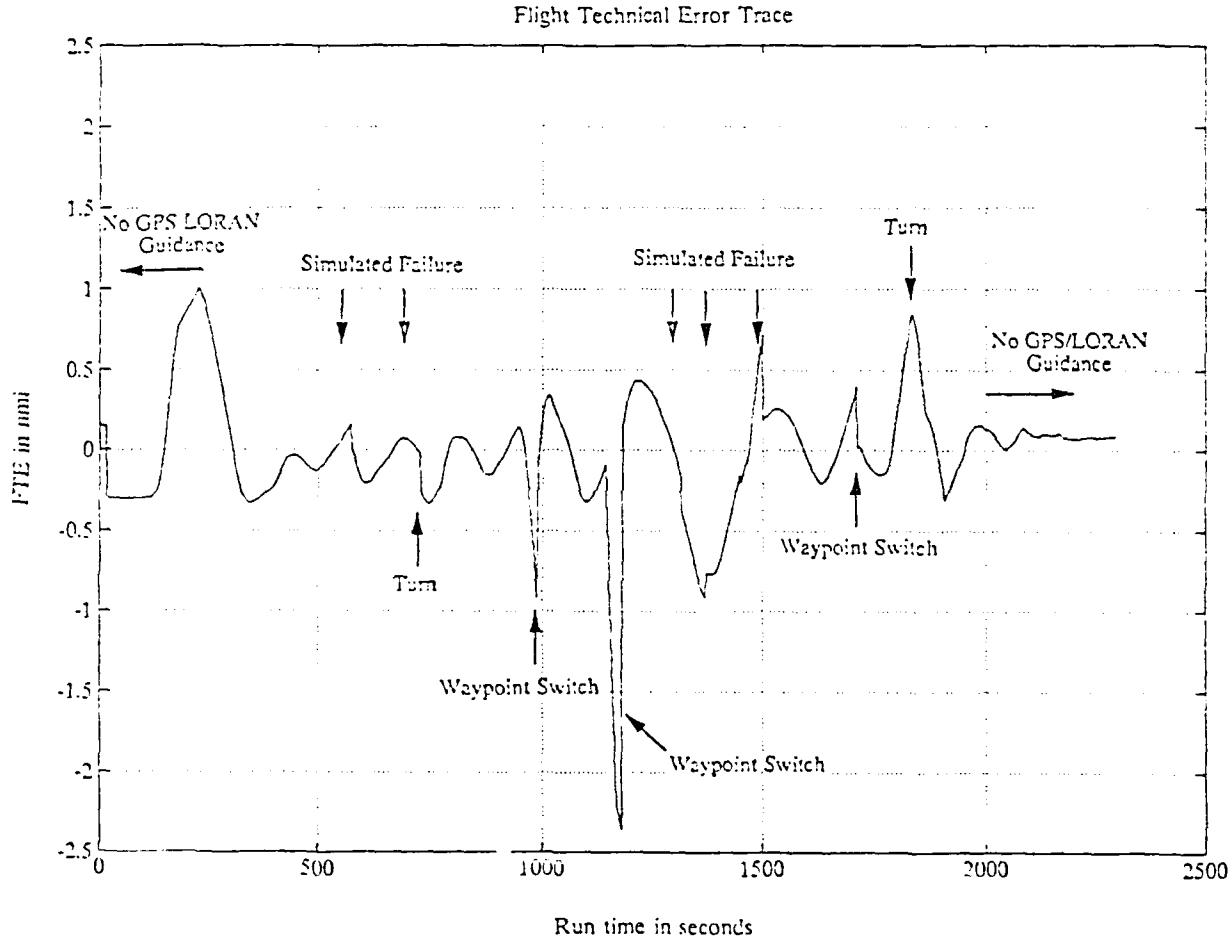

Figure 10.3 Flight technical error trace for flight one.

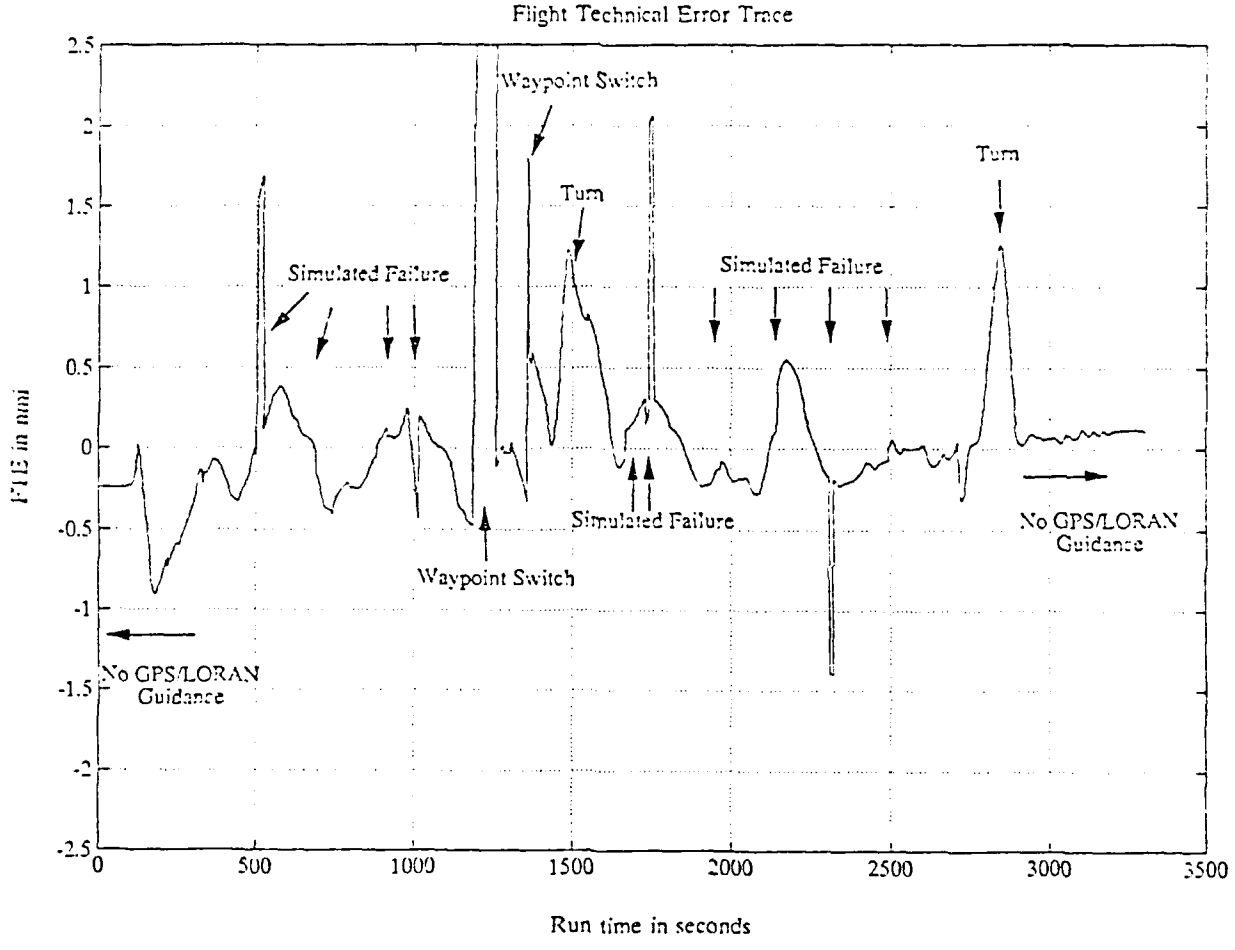

Figure 10.4 Flight technical error trace for flight two.

Time (GMT)	Event
17:09:00	Take-off from UNI, to Henderson VOR.
17:09:30	GPS/LORAN program stopped and restarted to verify correct operation of the data collection.
17:10:37	Receiver is tracking SV2, SV11, SV13, SV14, Seneca, Dana, and Carolina Beach.
17:12:00	CDI switched to expanded scale per pilot request.
17:14:47	Failure 1: SV2 100 m/s ramp.
17:15:00	Integrity threshold of 300 m exceeded, CDI is flagged.
17:15:05	Reset failure 1.
17:15:57	Failure 2: SV2 25 m/s ramp.
17:17:33	Range error has grown to 2400 m, integrity parameter = 316.
17:17:45	Reset failure 2.
	DME cross-check, Henderson DME agrees to within 0.1 nmi with range indicated by GPS/LORAN; baro-altitude = 4,000 ft.
17:21:13	Standard left turn towards the University NDB.
17:24:35	GPS/LORAN program stopped and restarted to save collected data to flexible disk.
17:25:05	GPS/LORAN receiver operational, waypoints: from Henderson VOR to University NDB, CDI in enroute mode.
17:27:35	Failure 3: Carolina Beach 10,000 m step.
17:28:30	Reset failure 3.
17:29:00	Failure 4: SV14 50 m/s ramp.
17:30:00	Reset failure 4.
17:30:10	Failure 5: Dana 100 m/s ramp.
17:31:10	Reset failure 5.
17:31:23	Initiation of descend.
17:32:30	CDI switched to expanded scale (approach mode).
17:34:15	Waypoint changed to threshold of RW 25.
17:38:20	6.6 nmi from runway threshold, baro-altitude = 2,500 ft
17:38:50	Cross-check: good agreement with ILS localizer.
17:39:40	Passing university NDB, 4.76 nmi from threshold of RW 25.
17:41:15	Cross-check on final: GPS/LORAN needle shows a slight deflection to the left.
17:42:00	Visual to RW 25, preparing for a full stop.
17:43:00	Touch-down.
17:43:53	GPS/LORAN receiver program stopped.

Table 10.1 Sequence of events for flight test one, August 21, 1990.

Time (GMT)	Event
20:01:50	Take-off from UNI, to Yellow Bud VOR.
20:04:00	At 2,500 ft and climbing. Receiver is tracking SV9, SV13, SV14, SV20, Seneca, Dana, and Carolina Beach.
20:06:25	Level at 4,000 ft, difficulty tracking SV20
20:08:03	Failure 6: SV9 10,000 m step.
20:08:20	Reset failure 6.
20:10:30	Failure 7: Dana 25 m/s ramp.
20:11:07	CDI is flagged, reset of failure 6.
20:14:17	Failure 8: Carolina Beach 1,000 m step, little effect. Difficulty tracking SV9. Reset failure 8.
20:16:00	Failure 9: SV20, 50 m/s ramp.
20:16:09	CDI is flagged, still difficulties tracking SV9. Reset failure 9.
20:20:00	GPS/LORAN program stopped and restarted to save collected data to flexible disk.
20:20:37	GPS/LORAN receiver operational, waypoints from University NDB to Henderson VOR. Tracking SV16, SV13, SV14, SV20.
20:22:23	Waypoints from Henderson VOR to University NDB.
20:24:57	Passing Yellow Bud VOR
20:27:25	Failure 10: SV14, 1,000 m step. GPS/LORAN altitude changed by +3,000 ft.
20:28:29	Reset failure 10.
20:28:40	Failure 11: Seneca 10,000 m step, CDI is flagged, reset failure 11.
20:31:29	Failure 12: SV16, 5 m/s ramp.
20:32:25	Reset failure 12, error is growing too slowly.
20:32:50	Failure 13: SV16, 10 m/s ramp.
20:35:10	CDI is flagged, reset failure 13, CDI changes by -30.
20:36:00	Descend to 3,000 ft per ATC request, 16 nmi to beacon.
20:38:07	Failure 14: Dana, 10,000 m step, CDI is flagged.
20:38:17	Reset failure 14.
20:40:01	Failure 15: SV13, 100 m/s ramp.
20:41:01	CDI is flagged. Reset failure 15.
20:43:43	8.3 nmi to NDB
20:44:45	Switched to approach mode, waypoint from University NDB to threshold of RW 25.
20:46:30	Procedure turn around NDB.
20:48:23	On course, Range 8.5 nmi to RW 25, GPS/LORAN CDI needle slightly to the left compared to the ILS localizer.
20:49:11	At 2,500 ft, crossed over NDB.
20:53:43	Touch-down.
20:54:43	GPS/LORAN receiver program stopped.

Table 10.2 Sequence of events for flight test two, August 23, 1990.

cannot be safely completed. Potential benefits are increased safety and a possible reduction in the size of obstacle clearance surfaces. Furthermore, this would also accomodate the development of generic approach procedures for earth referenced navigation systems.

To analyze the impact of signal malfunctions, a total of fifteen simulated failures were injected into the measurement data during the two test flights. Both sudden errors (step failures) and slowly increasing errors (ramp failures) were simulated. Figures 10.5 and 10.6 show the horizontal radial differences between the unperturbed GPS/LORAN flight trajectory and the trajectory with the simulated signal failures, as well as the integrity parameter (range residual parameter). Also indicated in these two figures are the numbers corresponding to each of the failures. Flight number one used an integrity parameter threshold of 300 m, flight number two used an integrity parameter threshold of 400 m. All signal malfunctions which would have caused unacceptable course deviations were detected by the integrity algorithm.

Most failures increase the integrity parameter and the radial position error as expected, except for failure number 8. This failure is a 1,000 m. step on the Carolina Beach LORAN measurement. The integrity parameter reduces from 300 meters to approximately 40 meters, while the radial position difference grows to 410 meters. This type of error could easily be detected by a time-history filter on each of the measurements. Moreover, the Carolina Beach transmitter would probably have "blinked" under the simulated condition. However, if this error would be slowly increasing, detection would be much harder. Closer observation of the data showed that the GPS receiver experienced difficulties tracking satellite number 9. As a result, the Carolina Beach malfunction is expected to have a large impact on the position error (see also Chapter 8). Although this error might not be detected at the time the radial error threshold is exceeded, the least squares residual method would eventually raise the flag.

Although the test pilots knew of our capability to inject signal failures, relevant pilot remarks with respect to each of the fifteen failure scenarios are given in Table 10.3. It is interesting to note that both test pilots detected significant failures before the integrity threshold was surpassed. As expected, sudden failures are easy to detect by the pilot; however, this is only true if the pilot almost continuously monitors the CDI, otherwise, small step failures go undetected by the pilot.

In the presence of strong winds, it is difficult to tell the difference between a heading correction to compensate for a cross wind, or a heading correction caused by a malfunctioning navigation signal, especially if the net effect is in the same direction. It also became evident that the pilots were using the change in the indicated magnetic course to detect the small ramp failures. In addition to the pilot remarks, the GPS/LORAN system operators in the back of the aircraft also noticed large climb/descend rates and large negative altitudes on the status screen as a result of the injected failures. In some of the cases, the unreasonableness of the GPS/LORAN altitude was apparent long before the integrity parameter would exceed the threshold.

Based on the results of the flight experiments, the following is recommended for further investigations: evaluation of integrity and failure isolation schemes which are not just based on the inconsistency of the

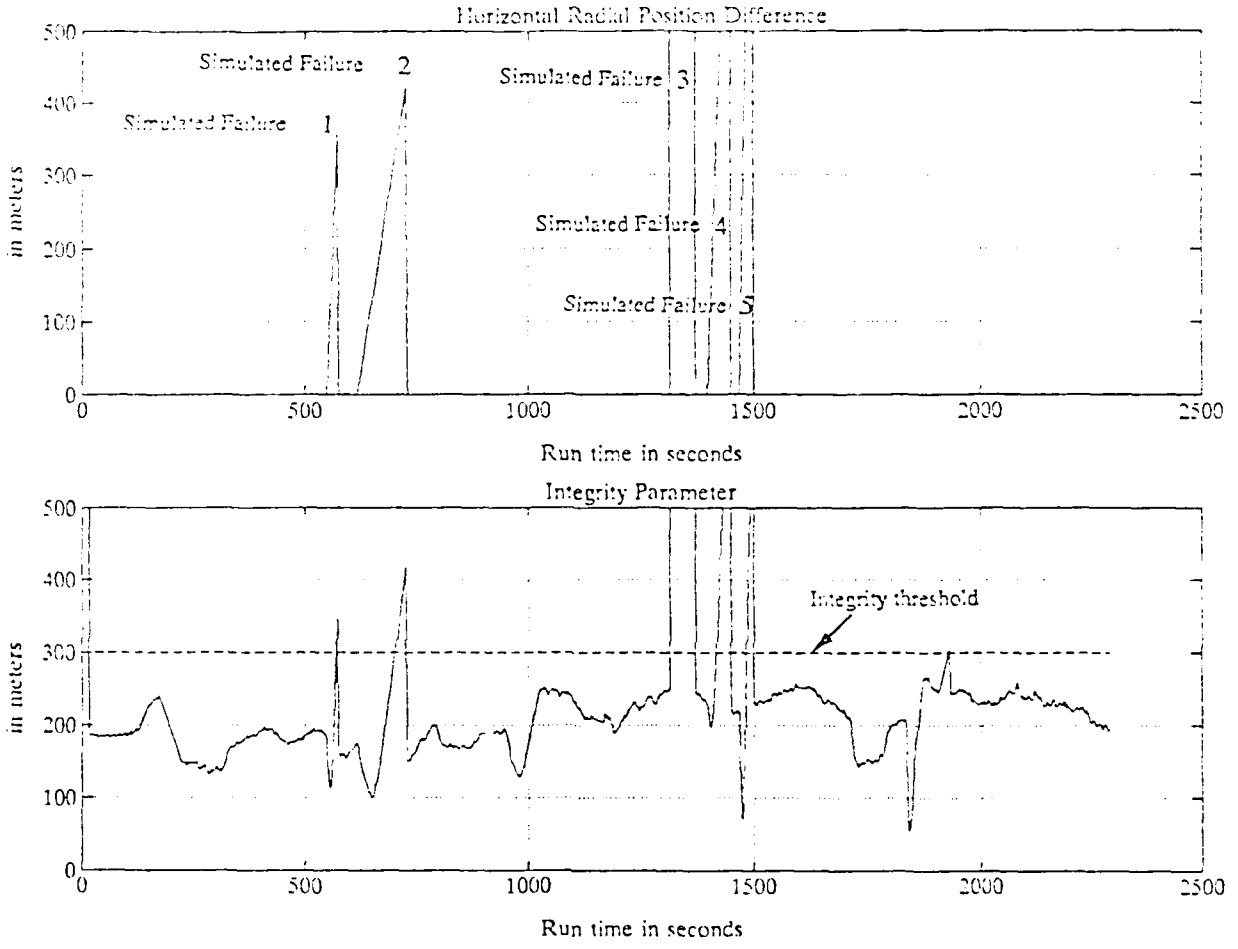

Figure 10.5 Horizontal radial difference between the unperturbed GPS/LORAN flight trajectory and the trajectory with simulated signal failures; and the integrity parameter for flight one.

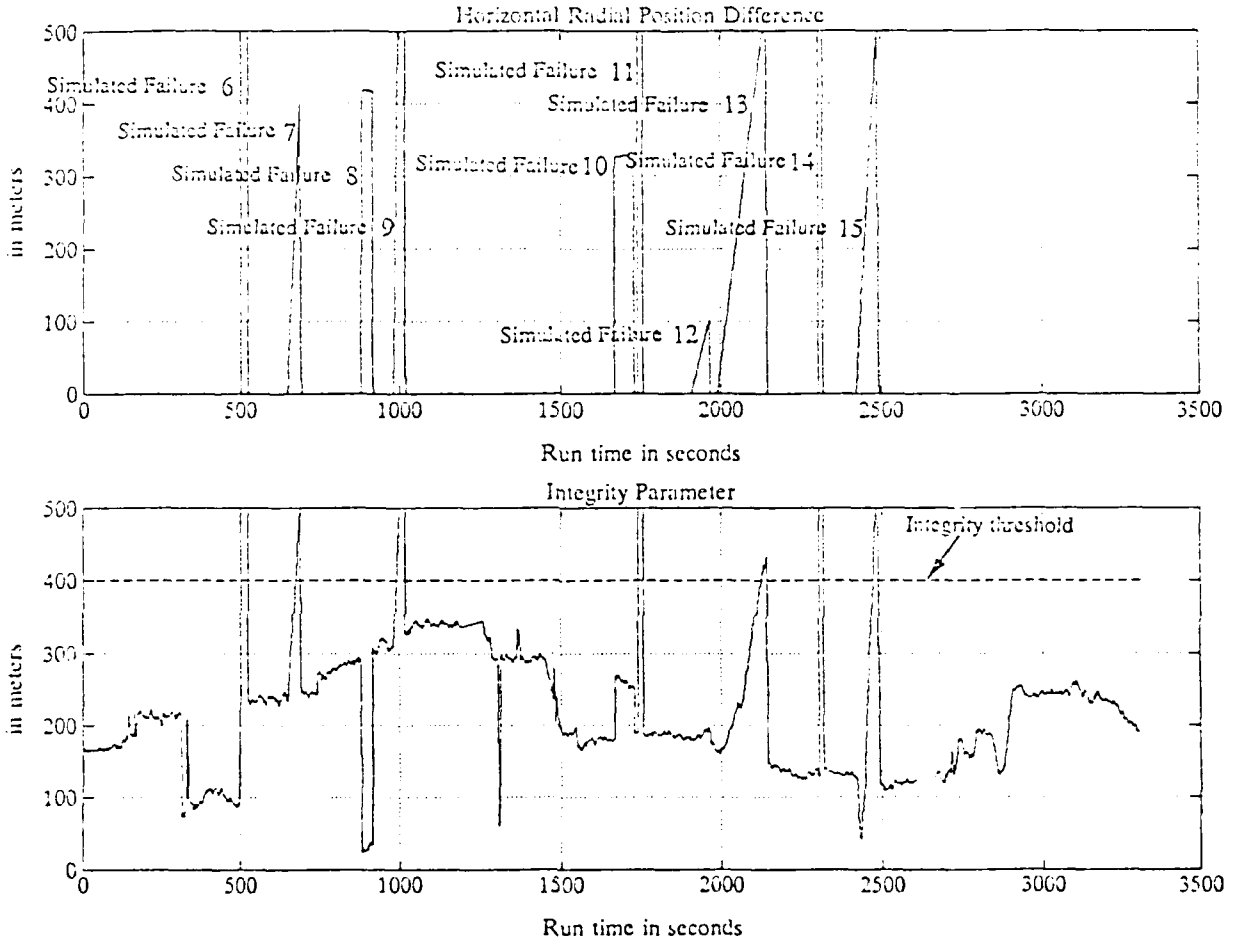

Figure 10.6 Horizontal radial difference between the unperturbed GPS/LORAN flight trajectory and the trajectory with simulated signal failures; and the integrity parameter for flight two.

Failure Description	Test Pilot Remark
1. SV2 100 m/s ramp	After a few seconds, pilot notices a deviation to the left, pilot reports that he is correcting for the wind. Just before the flag appears, pilot confirms a definite command to fly left. Flag is noticed immediately by pilot.
2. SV2 25 m/s ramp	After approx. 30 seconds, pilot notices a slow deviation to the left. Flag is noticed by the pilot within one second. Pilot reports a heading change of 10 degrees.
3. Carolina 10,000 m step	Pilot notices flag immediately, CDI deviation is not significant.
4. SV14 50 m/s ramp	Error discarded, pilot workload did not allow for monitoring/flying the GPS/LORAN CDI.
5. Dana 100 m/s ramp	Error discarded because of pilot workload.
6. SV9 10,000 m step	Pilot notices immediately a major error.
7. Dana 25 m/s ramp	Error not noticed by pilot until several seconds after CDI flag. Pilot remarks that strong winds are present, he thought that he was correcting for a cross wind.
8. Carolina 1,000 m step	Not much effect on the navigation, not noticed by pilot.
9. SV20 50 m/s ramp	CDI flag detected by pilot within a few sec.
10. SV14 1,000 m step	No flag, but pilots notices wrong CDI track.
11. Seneca 10,000 m step	CDI flagged, pilot notices error.
12. SV16 5 m/s ramp	Malfunction not noticed by pilot, error injection aborted, it would take too long before CDI would be flagged.
13. SV16 10 m/s ramp	Pilot starts noticing malfunction when the integrity parameter is 340 m. CDI flag is detected quickly.
14. Dana 10,000 m step	Error discarded because of pilot workload. CDI was flagged.
15. SV13 100 m/s ramp	Pilot notices slight jerk to the right, which he notices because the correction is in a direction opposite the wind.

Table 10.3 GPS/LORAN simulated failure scenarios with test pilots' remarks.

GPS/LORAN measurements, but which also take the following information into account:

- reasonableress of the climb/descend rate and altitude as indicated by GPS/LORAN;

- rate of change and magnitude of the differences between the indicated GPS/LORAN heading, and the calculated heading and/or indicated magnetic heading.

11. CONCLUSIONS

The first part of this report shows the derivation of the ordinary least squares (OLS) estimator from the linear model using the Projection Theorem. The performance of the OLS is subjected to a detailed error analysis which includes the effects of geometry and measurement errors, both bias and noise. Using similar procedures, the extended Ridge and Kalman filters are derived which are representative for the classes of biased and unbiased estimators, respectively. It is shown that in the presence of measurement bias errors, both estimators converge to the OLS inflation of the position error. It is therefore concluded that in the case of dominant measurement bias errors (e.g. GPS or LORAN), the integrity monitoring performance offered by the OLS estimator cannot be improved upon. It was also found that the Ridge estimator can be used to explain/optimize the performance of a mismatched Kalman filter. This provides a very helpful insight into the performance of the Kalman filter in the presence of unmodeled dynamics.

Based on the conclusion that the OLS estimator is sufficient to perform integrity monitoring, a general solution methodology is presented for a multisensor navigation system. The range residual integrity parameter was derived, again using the Projection Theorem.

The above results have been applied to a realtime prototype hybrid GPS/LORAN receiver. Two flight tests revealed that the hybrid GPS/LORAN receiver performs in accordance with its design. The course deviation indicator is responsive and the indicated course compares favorably with other area navigation equipment. Out of a total of fifteen simulated signal malfunctions, twelve malfunctions which would have caused unacceptable course deviations were detected by the range residual integrity algorithm.

Equal weighting of GPS and LORAN measurements is used for the flight tests. Therefore, the accuracy of the hybrid system will be mostly determined by the LORAN measurements. Standard LORAN propagation models are used such that the achieved accuracies are representative for current LORAN receivers. Because of this, the accuracy of the hybrid system will not be as good as that provided by GPS; however, the availability and integrity of the hybrid system exceeds that of GPS by several orders of magnitude [4]. At the same time, the hybrid system accuracies were still found to be well within all current requirements as listed in Chapter 3. It is also concluded that the accuracy of hybrid GPS/LORAN can be improved upon significantly through LORAN calibration or by using a weighting matrix in the hybrid solution, see Section 6.1.

In summary, hybrid GPS/LORAN is a successful case study of fully hybrid, multisensor navigation. Similar performance characteristics may be anticipated for other multisensor systems based on sensors such as GPS, LORAN, GLONASS, Omega, and baro-altimeter.

12. RECOMMENDATIONS

Based on the findings presented in this report, the following recommendations are made for further efforts in the areas of multisensor navigation and GPS/LORAN:

1. Development of a generic approach procedure for earth referenced navigation systems.

2. Study of the effects of flagging a nonprecision approach based on a flight technical error of such magnitude that the approach cannot be safely completed. Potential benefits are increased safety and a possible reduction in the size of obstacle clearance surfaces.

3. Continued integration of hybrid GPS/LORAN into the National Airspace System. The results of this study can also be applied to multisensor navigation systems in general. It is recommended that this effort takes place along the following avenues:

- Continued flight testing of the prototype hybrid GPS/LORAN receiver to address the flight technical error and the impact of failure modes on enroute navigation and nonprecision approach operations;

- Detailed study of failure isolation schemes, which is required for sole means navigation;

- Development and evaluation of criteria to be used for the certification of hybrid GPS/LORAN receivers;

- Development and evaluation of criteria to be used for the definition of sole means of navigation systems.

4. Specific efforts to further integrate GPS and LORAN should also address promising accuracy improvement techniques, which have the potential to achieve LORAN measurement accuracies comparable to those provided by GPS [4, 8, 61-63]:

- Use of a weighting matrix W to incorporate the statistical knowledge of the measurements (see Section 6.1);

- Calibration of LORAN using validated GPS positions;

- Use of improved LORAN propagation models which could contain seasonal correction data based on the LORAN-C monitor network.

5. Evaluation of integrity and failure isolation schemes which are not just based on the inconsistency of the GPS/LORAN measurements, but which also take the following information into account:

- reasonableness of the climb/descend rate and altitude as indicated by GPS/LORAN;

- rate of change and magnitude of the differences between the indicated GPS/LORAN heading, and the calculated heading and/or indicated magnetic heading.

13. REFERENCES

[1] The Federal Aviation Administration Plan for Research, Engineering, and Development, Volume I, Draft, November 28, 1988.

[2] Kelly, R. J., Cusick, D. R., "Distance Measuring Equipment and its Evolving Role in Aviation," Advances in Electronics and Electron Physics, Academic Press, Vol. 68, 1986.

[3] Vicks [illegible] F. B., Goddard, R. B., "Implementation and Performance of the TOT Control [illegible] French LORAN Chain," Proceedings of the 15th Annual Technical Symposium of the Wild Goose Association, New Orleans, Louisiana, October 21-24, 1986.

[4] Van Graas, F., "Hybrid GPS/LORAN-C: A Next-Generation of Sole Means Air Navigation," Ph. D. Dissertation, Ohio University, Department of Electrical and Computer Engineering, November 1988.

[5] DOT/FAA Advisory Circular No. 20-130, "Airworthiness Approval of Multi-Sensor Navigation Systems for Use in the U.S. National Airspace System (NAS) and Alaska," September 12, 1988.

[6] Radio Technical Commission for Aeronautics, Special Committee 137, "Minimum Operational Performance Standards for Airborne Area Navigation Equipment Using Multi-Sensor Inputs," Report No. RTCA/DO-187, Washington, D.C., November 1984.

[7] Code of the Federal Regulations Title 14, Aeronautics and Space (revised January 1, 1987).

[8] Van Graas, F., "Sole Means Navigation Through Hybrid LORAN-C and GPS," Navigation: Journal of the Institute of Navigation, Vol. 35, No. 2, Summer 1988.

[9] Sharma, S., "Error Sources Affecting Differential or Ground Monitoring Operation of the NAVSTAR Global Positioning System," Avionics Engineering Center, Ohio University, Report No. OU/AEC 15-87TMNASATRI-U/X-3, June 1987.

[10] Braasch, M., "A Signal Model for the NAVSTAR Global Positioning System," The Second International Satellite Division Meeting of The Institute of Navigation, Colorado Springs, CO, September 25-29, 1989.

[11] Federal Radionavigation Plan (FRP), 1990. DOD-4650.4 and DOT-VNTSC-RSPA-90-3, U.S. Department of Defense and U.S. Department of Transportation, Washington, D.C., 1990.

[12] Chin, G. Y., "Two Dimensional Measures of Accuracy in Navigational Systems," DOT-TSC-RSPA-87-1, Transportation System Center, Cambridge, MA, 1987.

[13] DOT/FAA Federal Register, "Sole Radio Navigation System; Minimum Standards for Certification; Advance Notice of Proposed Rulemaking," Part III, 14 CFR Part 91, January 22, 1990.

[14] Department of Transportation, Federal Aviation Administration, Advisory Cicular AC 90-45A, "Approval of Area Navigation Systems for Use in the U.S. National Airspace System, February 1975.

[15] Radio Technical Commission for Aeronautics, Special Committee 159, "Minimum Operational Performance Standards for Airborne Supplemental Navigation Equipment Using the Global Positioning System (GPS)," Third Draft, RTCA Paper No. 12-91/SC159-263, Washington, D.C., March 27, 1991.

[16] Draper, N., Smith, H., *Applied Regression Analysis*, Second Edition, John Wiley and Sons, New York, 1981.

[17] Foy, W. H., "Position-Location Solutions by Taylor-Series Estimation," IEEE Transactions on Aerospace and Electronic Systems, Vol. AES-12, No. 2, March 1984.

[18] Orfanidis, S. J., *Optimum Signal Processing: An Introduction*, Second Edition, McGraw-Hill, New York, 1988.

[19] Kelly, R. J., "MLS System Error Identification and MLS Signal Models," Seminar at Ohio University, Avionics Engineering Center, Department of Electrical and Computer Engineering, Part 3, Athens, OH, April 6, 1989.

[20] Lawson, C. L., Hanson, Richard J., *Solving Least Squares Problems*, Prentice-Hall, Englewood Cliffs, New Jersey, 1974.

[21] Torrieri, D. J., "Statistical Theory of Passive Location Systems," IEEE Transactions on Aerospace and Electronic Systems, Vol. AES-20, No. 2, March 1984

[22] Belsley, D. A., Kuh E., Welsch, R., *Regression Diagnostics: Identifying Influential Data and Sources of Collinearity*, John Wiley and Sons, 1980.

[23] Jorgensen, P., "NAVSTAR/Global Positioning System 18-Satellite Constellations," Global Positioning System, Volume III, The Institute of Navigation (ION), 1986

[24] Kuhl, M. R., "Implementation of the Geometrical Determination of PDOP," Avionics Engineering Center, Ohio University, Report No. OU/AEC 86-88TM FE706083/2-2, August 1988.

[25] Diderrich, G. T., "The Kalman Filter From the Perspective of Goldberger-Theil Estimators," The American Statistician, Vol. 39, No. 3, August 1985.

[26] Duncan, D., Horn, S., "Linear Dynamic Recursive Estimation From the Viewpoint of Regression Analysis," Journal American Statistical Association, Vol. 67, December 1972.

[27] Toutenburg, H., *Prior Information in Linear Models*, John Wiley, New York, 1982.

[28] Kalman, R. E., "A New Approach to Linear Filtering and Prediction Problems," Transactions of the ASME, Series D, Journal of Basic Engineering, Vol. 82, 1960.

[29] Stengel, R. F., *Stochastic Optimal Control - Theory and Application*, John Wiley and Sons, New York, 1986.

[30] Kelly, R. J., "Global Positioning System Accuracy Improvement Using Ridge Regression," AIAA Guidance, Navigation and Control Conference, Boston, MA, August 14-16, 1989.

[31] Brown, R. G., *Introduction to Random Signal Analysis and Kalman Filtering*, John Wiley and Sons, New York, 1983.

[32] Ewing, P. L., "The Design and Implementation of Tracking and Filtering Algorithms for an Aircraft Beacon Collision Warning System," Master's Thesis, Ohio University, Department of Electrical and Computer Engineering, March 1989.

[33] Chui, C. K., Chen, G., "Kalman Filtering with Real-Time Applications," Springer-Verlag, 1987.

[34] Sorenson, Harold W., *Kalman Filtering: Theory and Applications*, IEEE Press, New York, 1985

[35] Kuhl, M. R., "Ridge Regression Signal Processing Applied to Multisensor Position Fixing," Master's thesis, Department of Electrical and Computer Engineering, Ohio University, June 1990.

[36] Hoerl, A. E., Kennard, R. W., "Ridge Regression: Applications to Nonorthogonal Problems," Technometrics, Vol. 12, No. 7, February 1970.

[37] Hoerl, A. E., "Optimum Solution of Many Variables Equations," Chemical Engineering Progress, Vol. 55, 1959.

[38] Hoerl, A. E., Kennard R. W., Baldwin, K. F., "Ridge Regression: Some Simulations," Communications in Statistics, Vol. 4, Marcel Dekker, 1975.

[39] Hoerl, A. E., Kennard R. W., "Ridge Regression Iterative Estimation of the Biasing Parameter," Communications in Statistics, Vol. 4, Marcel Dekker, 1975.

[40] Golub, G. H., Heath, M., Wahba, G., "Generalized Cross-Validation as a Method for Choosing a Good Ridge Parameter," Technometrics, Vol. 21, No. 2, May 1979.

[41] Oman, S. A., "A Confidence Bound Approach to Choosing the Biasing Parameter in Ridge Regression," Journal of the American Statistical Association, Vol. 76, No. 374, June 1981.

[42] Efron, B., "Biased Versus Unbiased Estimation," Advances in Math, Vol. 16, 1975.

[43] Vinod, H. D., Ullah, Aman, *Recent Advances in Regression Methods*, Vol. 41, Marcel Dekker, New York, 1981.

[44] Hoerl, A. E., Kennard, R. W., "Ridge Regression and Biased Estimation for Nonorthogonal Problems," Technometrics, Vol. 12, No. 1, February 1970.

[45] Marquardt, D. W., "Generalized Inverses, Ridge Regression, Biased Linear Estimation, and Nonlinear Estimation," Technometrics, Vol. 12, No. 3, August 1970.

[46] Kelly, R. J., "Reducing Geometric Dilution of Precision Using Ridge Regression Signal Processing," IEEE Position Location and Navigation Symposium, 1988, Orlando, FL, November 29 - December 2, 1988.

[47] Kelly, R. J., "OMEGA Accuracy Improvement Using Ridge Regression," OMEGA: International and Economic, Proceedings of the Fourteenth Annual Meeting, Long Beach, CA, 1989.

[48] Kelly, R. J., "Reducing Geometric Dilution of Precision Using Ridge Regression Processing," IEEE Transactions on Aerospace and Electronic Systems, Vol. 26, No. 1, January 1990.

[49] Kelly, R. J., Van Graas, F., Kuhl, M. R., "Improved Effectiveness of GPS RAIM Through Ridge Regression Signal Processing," The Second International Satellite Division Meeting of The Institute of Navigation, Colorado Springs, CO, September 27-29, 1989.

[50] Theobold, C. M., "Generalization of Mean Square Error Applied to Ridge Regression," Applied Statistics, Vol. 36, 1974.

[51] Kelly, R. J., "Additional Results on Reducing Geometric Dilution of Precision Using Ridge Regression," IEEE Transactions on Aerospace and Electronic Systems Correspondence, Vol. 26, July 1990.

[52] Parkinson, B. W., Axelrad, P., "Autonomous GPS Integrity Monitoring Using the Pseudorange Residual," Navigation: Journal of the Institute of Navigation, Vol. 35, No. 2, Summer 1988.

[53] Sturza, M. A., "Navigation System Integrity Monitoring Using Redundant Measurements," Navigation: Journal of the Institute of Navigation, Vol. 35, No. 4, Winter 1988-89.

[54] Brenner, M., "Implementation of a RAIM Monitor in a GPS Receiver and an Integrated GPS/IRS," Proceedings of the Third International Technical Meeting of the ION Satellite Division, Colorado Springs, CO, September 1990.

[55] Strang, G., *Linear Algebra and its Applications*, Third Edition, Harcourt Brace Jovanovich, Publishers, San Diego, 1988.

[56] Kalafus, R. M., Chin, G. Y., "Performance Measures of Receiver Autonomous GPS Integrity Monitoring," Proceedings of the Fifth National Technical Meeting of the ION, Santa Barbara, CA, January 1988.

[57] Lee, Y. C., "Analysis of Range and Position Comparison Methods as a Means to Provide GPS Integrity in the User Receiver," Proceedings of the Annual Meeting of the ION, Seatle, WA, June 24-26, 1986.

[58] Brown, R. G., Hwang, P. Y. C., "GPS Failure Detection by Autonomous Means Within the Cockpit," Proceedings of the Annual Meeting of the ION, Seatle, WA, June 24-26, 1986.

[59] Brown, R. G., "Self-contained GPS Integrity Check Using Maximum Solution Separation," Navigation: Journal of the Institute of Navigation, Vol. 35, No. 1, Spring 1988.

[60] Parkinson, B. W., Axelrad, P., "Receiver Autonomous Integrity Monitoring of the Navigation Service Provided by the Global Positioning System," Submitted to the U.S. DOT/Transportation Systems Center, Contract No. 88-P-82289, May 1989.

[61] Lachapelle, G., Towsend, B., "En Route Calibration of Loran-C with GPS," Proceedings of the Third International Technical Meeting of the ION Satellite Division, Colorado Springs, CO, September 1990.

[62] Pisano, J., Levin, P., Enge, P., "Using GPS-Aided Tomography to Calibrate Loran-C," Proceedings of the Third International Technical Meeting of the ION Satellite Division, Colorado Springs, CO, September 1990.

[63] Comparato, C. P., MacKenzie, F. D., Arneson, D., "A Comparative Study of LORAN-C Forecasting Algorithms," U.S. DOT, Transportation Systems Center, Cambridge, MA, 1988.